SANDIA REPORT
SAND2010-4683
Unlimited Release
Printed July 2010

Transient PVT Measurements and Model Predictions for Vessel Heat Transfer—Part II

William S. Winters, Gregory H. Evans
Thermal/Fluid Science and Engineering

Steven F. Rice, Nicholas J. Paradiso, Todd G. Felver
Gas Transfer Systems

Prepared by
Sandia National Laboratories
Albuquerque, New Mexico 87185 and Livermore, California 94550

Sandia National Laboratories is a multi-program laboratory managed and operated by Sandia Corporation, a wholly owned subsidiary of Lockheed Martin Corporation, for the U.S. Department of Energy's National Nuclear Security Administration under contract DE-AC04-94AL85000.

Issued by Sandia National Laboratories, operated for the United States Department of Energy by Sandia Corporation.

Available to DOE and DOE contractors from
U.S. Department of Energy
Office of Scientific and Technical Information
P.O. Box 62
Oak Ridge, TN 37831

Telephone: (865) 576-8401
Facsimile: (865) 576-5728
E-Mail: reports@adonis.osti.gov
Online ordering: http://www.osti.gov/bridge

Available to the public from
U.S. Department of Commerce
National Technical Information Service
5285 Port Royal Rd.
Springfield, VA 22161

Telephone: (800) 553-6847
Facsimile: (703) 605-6900
E-Mail: orders@ntis.fedworld.gov
Online order: http://www.ntis.gov/help/ordermethods.asp?loc=7-4-0#online

SAND2010-4683
Unlimited Release
Printed July 2010

TRANSIENT PVT MEASUREMENTS AND MODEL PREDICTIONS FOR VESSEL HEAT TRANSFER—PART II

William S. Winters, Gregory H. Evans
Thermal/Fluid Science and Engineering

Steven F. Rice, Nicholas J. Paradiso, Todd G. Felver
Gas Transfer Systems

Sandia National Laboratories
P.O. Box 969
Livermore, CA 94550

ABSTRACT

Part I of this report focused on the acquisition and presentation of transient PVT data sets that can be used to validate gas transfer models. Here in Part II we focus primarily on describing models and validating these models using the data sets. Our models are intended to describe the high speed transport of compressible gases in arbitrary arrangements of vessels, tubing, valving and flow branches. Our models fall into three categories: (1) network flow models in which flow paths are modeled as one-dimensional flow and vessels are modeled as single control volumes, (2) CFD (Computational Fluid Dynamics) models in which flow in and between vessels is modeled in three dimensions and (3) coupled network/CFD models in which vessels are modeled using CFD and flows between vessels are modeled using a network flow code. In our work we utilized NETFLOW as our network flow code and FUEGO for our CFD code. Since network flow models lack three-dimensional resolution, correlations for heat transfer and tube frictional pressure drop are required to resolve important physics not being captured by the model. Here we describe how vessel heat transfer correlations were improved using the data and present direct model-data comparisons for all tests documented in Part I. Our results show that our network flow models have been substantially improved. The CFD modeling presented here describes the complex nature of vessel heat transfer and for the first time demonstrates that flow and heat transfer in vessels can be modeled directly without the need for correlations.

ACKNOWLEDGMENTS

The authors would like to acknowledge our colleague Ralph Greif, Professor of Mechanical Engineering at the University of California, Berkeley for his help and insight which added to our understanding of this problem. We would also like to acknowledge the contributions of the FUEGO development team Stefan Domino, Greg Wagner, Jeremy Templeton and David Glaze for the timely code additions that enabled us to perform compressible flow calculations with FUEGO and coupled FUEGO/NETFLOW.

TABLE OF CONTENTS

FIGURES

TABLES

1. INTRODUCTION

This is the second in a series of two reports documenting a multiyear effort to improve Sandia's modeling tools for predicting gas transport in gas transfer systems (GTS). This effort was divided into three tasks:

- The acquisition of high quality data sets that could be used to validate network flow models and multi-dimensional CFD (Computational Fluid-Dynamic) models of gas transfer systems.

- The development of vessel heat transfer correlations and network flow models that replicate the validation data sets.

- The development of validated multidimensional CFD models that do not rely on vessel heat transfer correlations.

The first of these tasks, the acquisition of validation data sets, was performed by personnel in the Gas Transfer Systems Department, 8224. Their work is documented in the first report [1]. The second task, development of vessel heat transfer correlations and network flow models, was performed by personnel in the Thermal/Fluid Science & Engineering Department 8365. The third task, also performed by 8365 personnel, was performed as part of a multiyear ASC V&V project entitled "GTS Multidimensional Fluid Flow & Heat Transfer." Results from Tasks 2 and 3 are documented here.

When flow losses in gas transfer systems are properly characterized, Sandia's network flow codes (e.g. NETFLOW [2] and TOPAZ [3]) do an adequate job predicting times to pressure equilibrium. Accurate prediction of masses delivered depends on the code's ability to account for vessel heat transfer. Network flow codes rely on experimentally validated correlations to account for vessel heat transfer. This report focuses on correlations for two of the most important situations in GTS: (1) heat transfer during the monotonic blow down of a supply vessel and (2) heat transfer during the monotonic fill up of a receiver.
Unfortunately it is nearly impossible to develop correlations for each and every vessel heat transfer situation encountered in GTS. For example the two correlations documented here may not apply to vessels undergoing non monotonic blow down or fill up. Furthermore, it may prove difficult to extend these correlations to arbitrary tank geometries.

We can eliminate the need to rely on correlations for vessel heat transfer by directly modeling the physics of transient multidimensional flow in vessels. For this we must rely on CFD. The highly compressible/high Mach number flows that are common to GTS are a challenge for any commercially available code (*e.g.* CFX, FLUENT, FIDAP, etc.) since problems with stability and long computational times are often difficult to overcome. In this effort we have attempted to utilize Sandia's massively parallel computing platforms and the computer codes FUEGO and NETFLOW to model the important features of flow in gas transfer systems. This has required tight coordination with ASC and 8365 code

developers to implement needed features. Although we have demonstrated the feasibility of applying CFD to gas transfer analysis, additional code development is necessary to advance this new modeling capability.

Chapter 2 of this report describes the technique of network flow modeling and its application to gas transfer systems. It is pointed out that network flow models rely heavily on correlations for pressure drop and heat transfer. The importance of understanding vessel heat transfer is discussed in some detail.

Chapter 3 contains a survey of the literature on vessel heat transfer. Surprising little research has been performed to understand and quantify heat transfer in vessels.

Chapter 4 discusses the nature of heat transfer in vessels. Results from qualitative CFD simulations of supply (reservoir) blow down and receiver fill up are used to describe the modes of heat transfer in vessels. This is done by showing the development of time evolving temperature and velocity fields in multi dimensional modeling of vessels during transfer.

Chapter 5 discusses improvements in NETFLOW modeling that were required to validate network flow models of the GTS supply/receiver experiments. These improvements have resulted in more accurate models than those documented previously in reference [1], particularly for receivers. Results from NETFLOW models are directly compared to the data sets obtained by Department 8224 as part of Task 1. Comparisons for supply and receiver transient pressure and mass-averaged temperature are presented. The implications for predicting mass transfer are also discussed.

Chapter 6 documents the effort to utilize CFD for modeling gas transfer flows. The approach used to overcome problems related to high Mach number flows is discussed and results are shown comparing CFD predictions to the data sets in Task 1. Areas for improvement are also discussed.

Chapter 7 provides a brief summary and states several conclusions. Recommendations for future work are also provided.

2. NETWORK FLOW MODELING AND THE IMPORTANCE OF HEAT TRANSFER

In this chapter we describe the technique of network flow modeling as it applies to predicting flows in gas transfer systems and other plumbing networks. We also discuss the importance of being able to accurately compute vessel heat transfer. We show that inaccurate prediction of heat transfer leads to errors in predicting mass inventories in gas transfer systems.

2.1 History and Description of Network Flow Modeling

Network flow models have been used for many years to simulate fluid and gas flows in piping networks. This modeling technique first became popular in the early 1970s as means of predicting off-design flow transient behavior in nuclear power plants. Comprehensive network flow modeling codes like RELAP [4] and RETRAN [5] were used to simulate plant response to the loss of coolant accident (LOCA) and other system emergencies. Historically these models have been zero-dimensional and one-dimensional transient network flow models in which vessels are modeled using single control volumes. The tubing that connects these vessels is modeled using a series or string of control volumes. Solving the tube flow problem in a network flow modeling code is equivalent to solving the one-dimensional transient flow conservation equations. For high speed compressible flow with large pressure differences between vessels, network flow codes must be able to identify locations where flow choking occurs and properly limit flow velocity to the local sonic value.

In the early 1980s, Sandia made use of network flow models to simulate coolant flow through solar central receiver systems, see *e.g.* [6,7]. Sandia's first network flow modeling tool dedicated to the solution of gas transfer problems was the computer code TOPAZ (Transient One-dimensional Pipe flow AnalyZer). TOPAZ has been extensively documented in References [8-11]. TOPAZ has been recently replaced by NETFLOW (see *e.g.* [2,12]) which utilizes an improved stiff differential-algebraic equation solver DASKR [13] for the solution of high speed compressible network flows.

Since the solution of the flow conservation equations in network flow modeling is restricted to zero or one dimension, locally applied quasi-steady correlations are often used to account for multi-dimensional effects. For example, frictional pressure-drop in tubing, an inherently multi-dimensional effect, is modeled using a quasi-steady correlation such as the one first proposed by Moody [14]. Similarly, multi-dimensional heat transfer effects in tube flow are modeled using a quasi-steady heat transfer correlation (see, *e.g.* Dittus and Boelter [15]). In vessels, correlations must be used to describe the multi-dimensional, transient effects of heat transfer. Unfortunately, existing correlations are very limited which is why network flow models that accurately predict transfer times (times to pressure equilibrium) often over-predict or under predict transient vessel temperatures and hence masses delivered. This point is demonstrated in the next sub chapter by predicting and comparing mass deliveries for the two extremes of vessel

heat transfer, i.e. no heat transfer and infinite heat transfer. By infinite heat transfer we mean that that heat transfer coefficient that describes heat transfer between the gas and the interior containment wall is infinite.

2.2 The Influence of Vessel Heat Transfer

Figure 1 shows a schematic for a simple helium gas transfer system consisting of a high pressure (2.079×10^7 Pa) supply (200 cc nominal volume) connected to a low pressure (9.997×10^4 Pa) receiver (700 cc nominal volume). The initial temperature of the system is assumed to be ambient (296.4 K). The line connecting the supply to the receiver contains an orifice (0.0508 cm diameter) where most of the pressure drop between supply and receiver takes place. At time zero the valve in the line connecting the supply and receiver is opened and the gas is permitted to flow from the supply to the receiver until pressure and temperature equilibrium is achieved in the system. The initial supply-to-receiver pressure ratio results in choked flow at the orifice for most of the transfer. The objective is to use NETFLOW to predict helium mass in the supply and receiver as a function of time. The geometry and initial conditions for this simulation are identical to one of the high-precision transient PVT tests (Test 700-3000PSI) documented in Part I of this report [1].

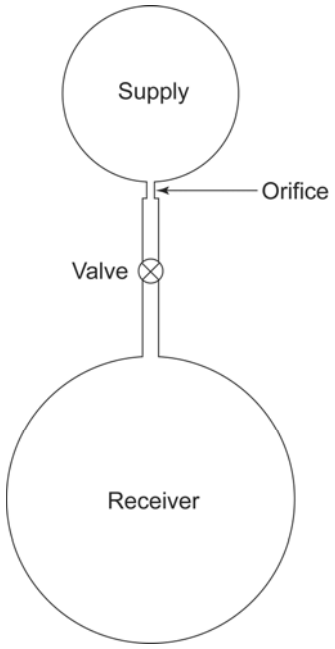

Figure 1. Simple helium gas transfer system.

During the gas transfer process the pressure in the supply falls rapidly causing a corresponding drop in temperature. In the receiver the pressure rises causing a corresponding rise in temperature. As time proceeds heat exchange between the vessel walls and the gas cause the supply and receiver gas temperatures to return to ambient

levels. Figures 2 and 3 show the measured supply and receiver mass averaged temperature for the helium in Test 700-3000PSI. The method used to obtain these measurements is documented in Reference [1] and briefly described here in Chapter 5.

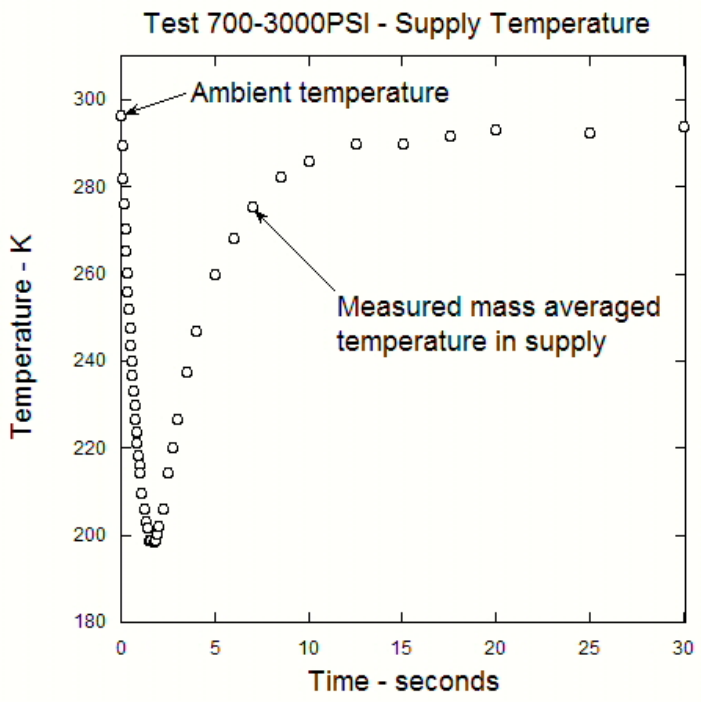

Figure 2. Measured supply mass averaged temperature.

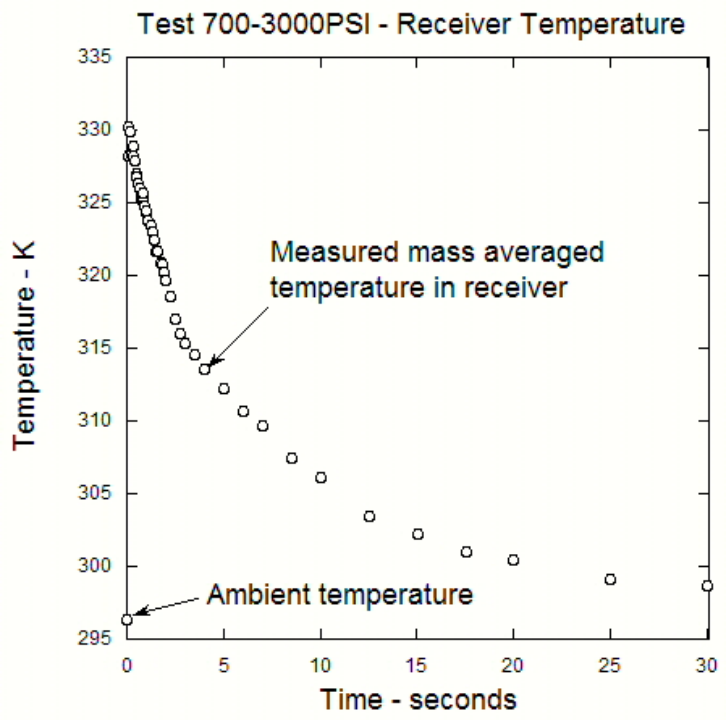

Figure 3. Measured receiver mass averaged temperature.

NETFLOW was used to compute the mass distribution in the supply/receiver system for the two extremes of heat transfer, *i.e.* no heat transfer in which the gas undergoes adiabatic temperature changes and infinite heat transfer in which the heat transfer is so high that the gas stays at ambient temperature during transfer. A third case was also examined, the case of nominal heat transfer in which the predicted mass transfer was within approximately 1% of the measured mass transfer in Test 700-3000PSI. In all cases the time to achieve pressure equilibrium was less than three seconds. Here we refer to the time to achieve pressure equilibrium as the time at which pressure-driven flow stops. When heat transfer is present this time may not be precisely identified since the period of pressure driven flow is followed by a period of thermally driven flow often referred to as the "thermal pumping" time period. During thermal pumping the cold gas in the supply at the time of "near" pressure equilibrium begins to heat up and return to ambient temperature as the vessel wall transfers heat to the supply gas. At the same time, the hot gas in the receiver begins to cool down to ambient temperature as receiver gas transfers heat to the vessel wall. The increasing and decreasing temperatures cause corresponding increases and decreases in supply and receiver pressures resulting in thermal pumping. If the transfer is interrupted during thermal pumping, it may be difficult to predict the mass distribution in the system without properly accounting for the heat transfer. This is particularly true of systems in which the supply and receiver vessels are of similar sizes. In the present case the receiver volume is approximately 3.5 times the supply volume.

We have simplified the explanation of thermal pumping here by saying that "it follows" the period of pressure-driven flow. In some cases thermal pumping may in fact take place

in parallel with pressure-driven flow, *i.e.* the influence of vessel wall heat transfer may be present even before near pressure equilibrium has been achieved.

The predicted supply and receiver helium mass inventories are shown in Figures 4 and 5 respectively. In both figures it can be seen that the mass levels predicted with the nominal heat transfer model are between the zero and infinite heat transfer extremes. This is to be expected. The “no heat transfer” prediction badly over estimates the final supply mass inventory and under estimates the final receiver mass inventory. The “infinite heat transfer” and “nominal heat transfer” predictions produce the same final mass inventories but during the period of thermal pumping the mass inventories predicted by infinite heat transfer are in considerable error. For example, at three seconds, the time of “near” pressure equilibrium, the mass inventory in the supply is approximately 70% of the correct value while the mass inventory in the receiver is approximately 10% greater than the correct value.

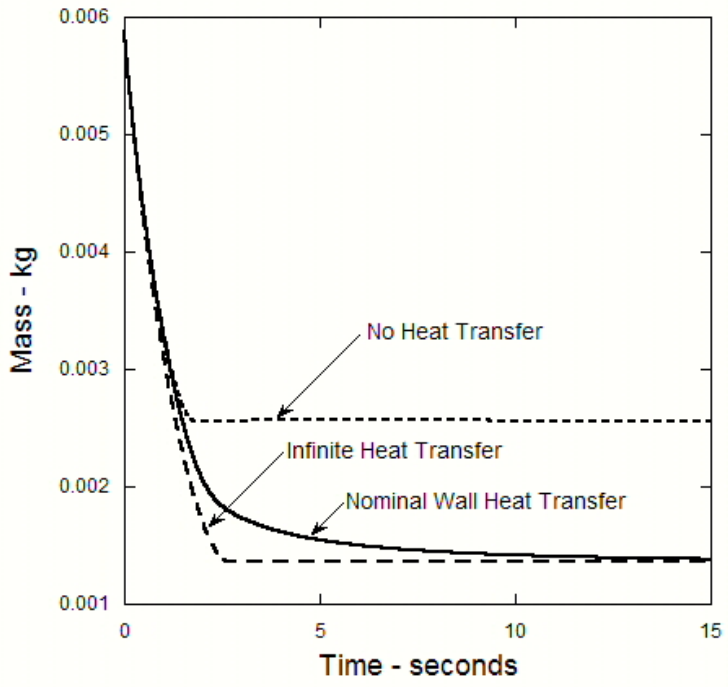

Figure 4. Transient supply mass inventory.

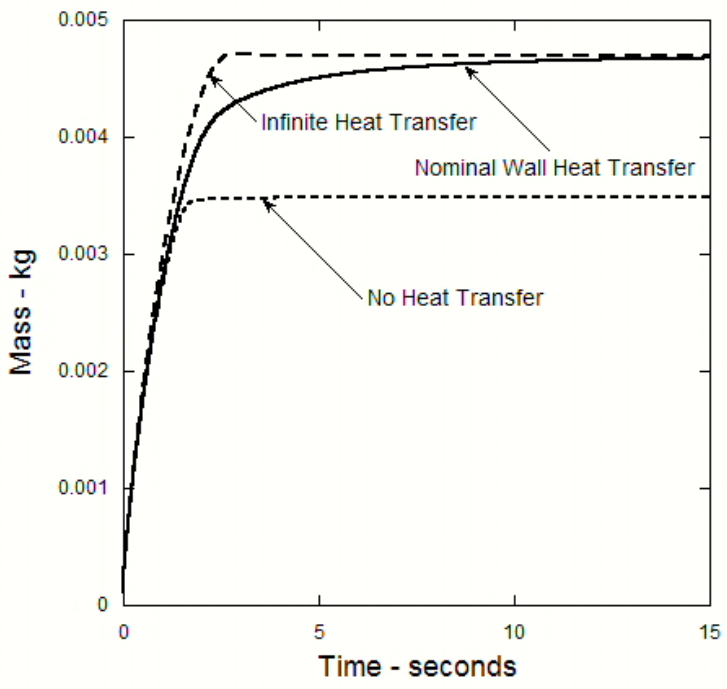

Figure 5. Transient receiver mass inventory.

3. SURVEY OF THE VESSEL HEAT TRANSFER LITERATURE

Surprising little research has been published on heat transfer during filling and discharge of compressible gases from tanks. The controlling heat transfer mechanisms often change over the course of the fill or discharge and the entire process is transient in nature. Heat transfer is influenced by tank geometry, the number and location of inlet and outlet holes, the orientation of the tank with respect to gravity and in some cases the thermal properties and dimensions of the tank wall. Because of this vessel heat transfer is not easily described with a single correlation.

Landram [16] modeled the discharge of a compressible gas from a supply vessel. His model included convective heat transfer at the outer wall surface, the heat conduction in the vessel wall, and convective heat transfer from the inner wall surface to discharging gas. A quasi-steady turbulent free-convection heat transfer coefficient was used to model the interior wall heat transfer. Landram compared his model predictions for gas supply temperature to transient thermocouple data. He also predicted times for the onset of free convection in the vessel.

Johnston and Dwyer [17] developed a model to describe heat transfer in a discharging vessel prior to the time when thermal instabilities form leading to free convection. Their model assumes a conduction layer exists adjacent to the walls at early time. Measurements were also made to quantify the onset time of thermal instabilities that occur when the mode of heat transfer transitions from pure heat conduction to free convection.

Paolucci [18] developed an analytical solution for heat transfer during the early expansion of gas during vessel discharge. The solution is valid for early times when lateral forced convection and buoyantly driven free convection are not present. Heat transfer is influenced by convection normal to the wall during decompression. Greif, *et al*. [19] developed a similar solution for heat transfer from the sidewalls of a channel in which gas is compressed by a piston.

The very high heat transfer during the initial filling of a receiver from a high pressure storage tank or immediately upon close of the filling valve was noted by Ulrich *et al*. [20] to be a factor of two higher than predicted by turbulent free convection theory. Reynolds [21] noted this increased heat transfer was probably due to the stirring effect of inlet jets during injection; however, Reynolds assumed a heat transfer coefficient of free convection for a vertical plate in his analysis of receivers. Experimental validation of Reynolds' analysis was performed by Lyons [22] who recommended that additional work be performed to determine a convective heat transfer coefficient during charging.

Perhaps the most extensive work to date on vessel heat transfer was conducted by Means and Ulrich [23]. They performed experiments and analyzed the transient convective heat transfer during and after the sonic filling of a receiving vessel with gas from a high

pressure source. Since the form for their forced and free convection correlations were adapted for this study, it is worthwhile to discuss their work in some detail.

During injection of an ideal gas into an otherwise closed vessel, Means and Ulrich provide the following energy equation:

$$\frac{d\left(mc_vT\right)}{dt} = \dot{m}c_pT_o - hA\left(T - T_w\right) \tag{3.1}$$

where T_o and T_w are the upstream stagnation temperature of the gas and the vessel wall temperature, respectively. Note that $\dot{m}$ and T, the mass flow rate and average receiver temperature, are functions of time. Using the ideal gas equation of state, the energy equation can be rearranged to solve for the spatial averaged heat transfer coefficient, given as

$$h = \frac{\dot{m}c_pT_o - \dfrac{\dot{P}V}{\gamma - 1}}{A\left(\dfrac{PV}{mR} - T_w\right)} \tag{3.2}$$

where V and A are the receiving vessel volume and surface area, respectively, and γ is the specific heat ratio, c_p/c_v, of the gas. Means and Ulrich write the following dimensionless form of the energy equation:

$$\mathrm{Nu} = \frac{hD}{k} = \frac{\dfrac{\mathrm{Re}\,\mathrm{Pr}\left(\dfrac{P_n}{P_o}\right)^{-\frac{(\gamma-1)}{\gamma}}}{4\dfrac{L}{D}\left(\dfrac{D}{d}\right)^2} - \dfrac{V}{\gamma AD}\dfrac{dp}{d\tau}}{\phi - \phi_w} \tag{3.3}$$

where $\dot{m} = \rho_n u_n A_n$, $\mathrm{Re} = \left(\rho_n u_n D\right)/\mu$, $A_n/A = \left(d/D\right)^2\left(D/L\right)/4$; $\phi = T/T_n$; $p = P/P_n$; $\tau = \alpha t/D^2$; subscripts *n* and *o* designate conditions at the nozzle and stagnation upstream of the nozzle. The signs on the terms in the numerator of Equation (3.3) are reversed in Means and Ulrich's work, apparently a mistake in their paper. Means and Ulrich used this equation as a guide for the form of a heat transfer correlation during the time that gas is entering the vessel. They argue that the term involving the time derivative of pressure can be neglected because V/AD is insignificant in their experiments. However, the term might not be negligible because during the initial period of receiver filling $dp/d\tau$ may be large. Furthermore the use of a heat conduction time scale in the non-dimensionalization of the pressure-time derivative ($t_{\mathrm{char}} = D^2/\alpha$) seems to be inappropriate, given that the pressure transient is rapid compared with the heat

conduction time based on the receiver dimension. For instance, in one of the recent Sandia tests, the receiver vessel volume was 700 cc and the gas was helium. Evaluating thermal diffusivity ($\alpha = k/\rho c_p$) at 1 atm, 300 K, yields a characteristic heat conduction time of $t_{\text{char}} = 65$ s, whereas the time to pressure equilibrium for a transfer of gas from a 200 cc supply initially at 3000 psi to a 700 cc receiver initially at 1 atm is approximately 5 s. For this Sandia test the coefficient of the pressure-time derivative term in Equation (3.3) is $V/\gamma AD = 0.1$. The resulting correlation given in Means and Ulrich for the receiver during filling is given by

$$\text{Nu} = 22\left[\text{Re}\,\text{Pr}/\left(L/D\right)\left(D/d\right)^2\right]^{0.635}. \tag{3.4}$$

There is a major difference between the Means and Ulrich study and our work in that Means and Ulrich used a constant pressure and temperature supply and the receiver inlet condition was always choked, until the valve was closed; thus, in their work the mass flow rate and the properties of the jet entering the receiver were constant. We have a supply vessel of fixed initial mass which means the inlet conditions to our receiver change with time as the supply vessel blows down. Thus we should not expect the highly transient early time behavior of the heat transfer in the receiver for our problem to be completely described by a steady heat transfer correlation such as Equation (3.4). For the Means and Ulrich work, the Reynolds number and hence the Nusselt number were fixed during their tests. Our Reynolds number is variable with time because the mass flow rate into the receiver is a decreasing function of time. Another difference (perhaps minor) is that in the Means and Ulrich work, the flow into the receiver is abruptly shut off at some point in time whereas in our problem the mass transfer between supply and receiver is allowed to continue even beyond pressure equilibrium.

Johnston and Dwyer [24] developed an experimental method for determining the bulk gas temperature in a vessel during discharge based on the technique of Clement and Desormes [25]. The method was used to measure the bulk or mass averaged temperature of helium and nitrogen in a vessel as it discharged to the atmosphere. We refer to the Johnston-Dwyer method as the transient PVT method. It forms the basis of the technique used in the experiments documented in Part I [1] of this work and was also used by Clark [26] in his experiments and modeling of vessel heat transfer. Clark's use of this method and his subsequent modeling of vessel heat transfer with the Sandia computer code TRIC, led him to alter the form of the Means and Ulrich correlations for vessel heat transfer. Based on a single transient PVT test for vessel fill up, Clark concluded that the Means and Ulrich correlation in Equation (3.4) over predicted receiver heat transfer. He attempted to rescale the correlation by reducing the leading constant from 22 to 2.2 and by providing a correction to account for the fact that inlet conditions were changing over time. His resulting correlation took the following form:

$$\mathrm{Nu} = 2.2\left[\frac{2}{\gamma+1}\left(\frac{P_{exit}}{P_O}\right)^{\frac{1-\lambda}{\gamma}}\frac{\mathrm{Re}\,\mathrm{Pr}}{(L/D)(D/d)^2}\right]^{0.635}. \qquad (3.5)$$

Clark also made adjustments to the Means and Ulrich correlations used for modeling the heat transfer in the supply. Since velocities are low in the supply during transfer, Clark utilized the following free convection heat transfer correlations:

$$\mathrm{Nu} = c\mathrm{Ra}^n \qquad (3.6)$$

where the constants c and n very depending on whether the flow is laminar or turbulent, i.e.

laminar flow: $(\mathrm{Ra} \prec 1.24\mathrm{x}10^8)$: c =1.15, n=.22 (3.7)

turbulent flow: $(\mathrm{Ra} \succ 1.24\mathrm{x}10^8)$: c =0.14, n=.333. (3.8)

The non-dimensional Rayleigh number, Ra, is defined in Chapter 5.

The transient PVT tests used by Clark to fit his correlations for the supply were subsonic tests. The supply-to-receiver initial pressure ratios were not high enough to cause flow choking.

Charton et al. [27] modeled the discharge of helium and deuterium from a vessel to a vacuum chamber via a long small diameter tube. Their model includes heat transfer in the supply and receiver vessels and frictional pressure drop in the tube. The heat transfer in both vessels was assumed to be dominated by free convection. They utilized correlations identical to those presented in Equations (3.7-3.8) but with different values of c and n. The transition from laminar to turbulent free convection was assumed to take place at a Rayleigh number of 10^9. Their modeling results were compared to transient thermocouple measurements corrected for lags in time response.

Recent interest in developing on-vehicle storage systems for highly compressed (35-70 MPa) hydrogen has generated interest in characterizing heat transfer in vessels with relatively large charge times.

Monde et al. [28] conducted a series of experiments to measure the temperature rise that accompanies the filling of a 1.38 liter tank with hydrogen. The hydrogen temperature distribution was measured along the centerline of the tank. In addition the radial temperature distribution was measured at an axial location that was slightly farther from the inlet than the mid point of the tank. The maximum pressures achieved during filling ranged from 5 to 35 MPa.

Terada et al. [29] conducted a series of tests in which two hydrogen tanks were filled with hydrogen over a period of several minutes. Both tanks were composite wrapped tanks with working pressures of 35 MPa. One of the tanks was a Type 3 tank with an aluminum liner having a volume of 34 liters and the other was a Type 4 tank with a plastic liner having a volume of 65 liters. Tests were conducted with the filling pressure increasing at a constant rate from a starting pressure of 2 MPa. Tank temperature measurements were made at locations on the interior wall, in the gas near the wall and in the center of the vessel.

Winters [38] developed a model for charging high pressure hydrogen vehicle tanks that include the effects of forced and free convection in the tank using correlations similar to Equations (3.4) and (3.6) respectively. The model accounted for free convection at the tank outer surface and transient heat conduction in the tank liner and composite wrap. Modeling results were compared to the measurements of Monde et al. [28] and Terada et al. [29].

4. THE NATURE OF VESSEL HEAT TRANSFER

4.1 Introduction

In network flow models, heat transfer effects must be captured by correlations. The actual form of the correlations and the heat transfer mechanisms they incorporate must be physically motivated. In the past this physical insight has been obtained through experimental measurements of temperature and velocity in charging and discharging vessels. The measurement of "real time" temperature distributions in vessels is difficult using conventional thermocouples since response times are usually inadequate. Furthermore, large temperature gradients exist in the gas so that it is difficult to measure an effective or mass-averaged temperature using a single thermocouple. Optical techniques which normally provide excellent visualization of temperature and velocity fields are difficult to implement. Pressure vessels have thick non-transparent steel walls and even if transparent optical ports are used, it is difficult to visualize the entire velocity and temperature field in the vessel.

With the advent of massively parallel computers it has become increasingly possible to compute velocity and temperature fields in vessels using multi-dimensional CFD codes. These problems are difficult to solve since they are transient, three-dimensional and highly compressible. Pressure ratios in GTS applications (as high as 10,000:1) produce transonic flow and underexpanded jets with complex shock structures in receiver vessels. Modern CFD codes are usually limited to pressure ratios of 20:1 and transonic Mach numbers of 5 or 6.

A multi-year ASC verification and validation project entitled "Multi-Dimensional Modeling of Fluid Flow and Heat Transfer in GTS" was ended in September of 2009. In this chapter computational results from this effort will be used to provide much-needed insight into the nature of supply and receiver flows. The results presented here are qualitative in the sense that they have not been validated against actual data. Some of this validation will be provided in Chapter 6.

4.2 Vessel Wall Temperature Assumption

For GTS applications, tank filling and discharge times are relatively short. As a result, the heat transfer process is not greatly influenced by vessel wall thermal characteristics and dimensions. Hence in this work it is assumed that the interior wall surface temperature remains constant during vessel blow-down or fill-up. The influence of wall temperature will be studied in greater detail in a future publication.

4.3 Nature of Supply Heat Transfer— Qualitative FUEGO/NETFLOW Calculations

Flow in a high pressure gas supply vessel was studied using a coupled FUEGO/NETFLOW model. The model was designed to mimic one of the high precision transient PVT experiments [1] in which helium in a 200 cc (nominal) supply at 300 PSI

(nominal) was transferred to a 700 cc (nominal) receiver. The flow path consisted of a conical transition into 0.020 inch diameter orifice. The test is referred to as Test 700-300PSI in Chapter 5. The supply vessel and conical flow path was modeled using FUEGO. The orifice, downstream tubing and receiver were modeled using NETFLOW. The NETFLOW coupling served to isolate FUEGO from the transonic/choked flow that occurs briefly at the orifice outlet. From a CFD modeling point-of-view, this was a FUEGO fully compressible three-dimensional-transient calculation of the supply flow with a time dependent exit mass flow rate boundary condition that was provided by NETFLOW.

A "snap shot" of the temperature distribution in the supply at 0.9 seconds into the transfer is shown in Figure 6. The figure shows a cutting plane across the mid plane of the spherical supply vessel and conical exit at the bottom. Gravity is acting downward. During the entire transfer the pressure in the supply and conical section (except very near the exit plane) is uniform and time varying. The velocity in the vessel and conical exit is extremely low except in the region just upstream of the exit plane where the Mach number approaches 1. Actual flow choking does not occur in the FUEGO computational space but rather at the orifice which is simulated by NETFLOW. The low velocity in the supply suggests that heat transfer is primarily governed by free convection for which the Rayleigh number (as defined in Chapter 5) is the most important parameter in characterizing the heat transfer.

In Figure 6, the upward flow due to natural convection along the curved wall which is warmer than the gas is evident. At this time, the temperature difference between the vessel wall and the bulk temperature of the gas is 65 K; the Rayleigh number is 7.5×10^6, indicating laminar free convection. Post processing of the computational results at 0.9 seconds can be used to compute the Nusselt number as:

$$\mathrm{Nu} \equiv \frac{hD}{k} = \frac{\int q_{\mathrm{surf}}\, dA}{A_{\mathrm{surf}} \Delta T} \cdot \frac{D}{k} = 42 \tag{4.1}$$

As mentioned previously, a typical correlation for laminar free convection takes the form

$$\mathrm{Nu}=c\mathrm{Ra}^{n}. \tag{4.2}$$

The procedure used to fit c and n to the high precision transient PVT as described in Chapter 5 yielded values of .93 and .25 respectively. For these values we can compute a laminar free convection Nusselt number as follows:

$$\mathrm{Nu}=.93\mathrm{Ra}^{.25} = 48 \tag{4.3}$$

The relatively good agreement demonstrated by the Nusselt number calculations in Equations (4.1) and (4.3) support the conclusion that the dominate heat transfer mechanism in the supply is free convection.

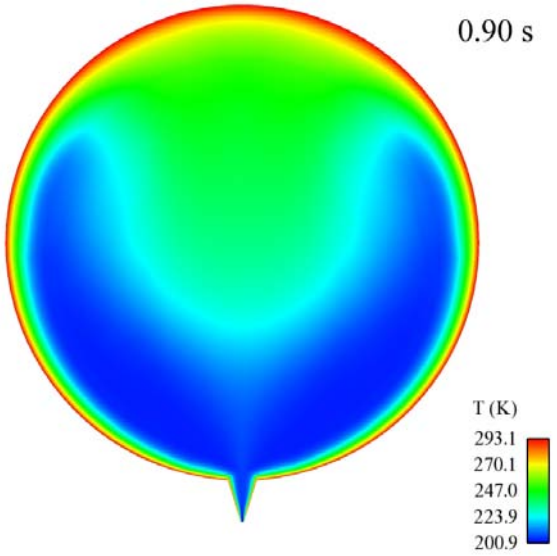

Figure 6. FUEGO computed supply temperature distribution for Test 700-300PSI.

4.4 Nature of Receiver Heat Transfer— Qualitative FUEGO/NETFLOW Calculations

Flow in receiver vessel was studied using a second coupled FUEGO/NETFLOW model. The model was designed to mimic Test 700-300PSI. FUEGO was used to model the receiver space and NETFLOW was used to model the supply blow-down, and flow path between the supply and the receiver. As was the case in the coupled FUEGO/NETFLOW simulation of the supply, NETFLOW coupling served to isolate FUEGO from the transonic/choked flow that occurs briefly at the orifice outlet. From a CFD modeling point-of-view, this was a FUEGO fully compressible three-dimensional-transient calculation of the receiver flow with a time dependent mass flow rate inlet boundary condition that was provided by NETFLOW

A time sequence of the FUEGO-computed temperature field in the receiver is shown in Figure 7 (a-c) and in Figure 8 (a and b). As in Figure 6 the color-contoured temperature distribution is plotted on a cutting plane in the mid-plane of the vessel. Next to each temperature contour plot is a plot of interior wall heat flux along a curve starting and ending at the inlet hole. Also shown on each picture are the bulk (mass averaged) temperature of the gas in the receiver and the spatially averaged Nusselt number. Figure 7(a) shows that at 0.0017 seconds the cold jet has not yet reached the opposite wall of the receiver. Note that the core of this jet (blue) is relatively cold and representative of the supply gas temperature. There is a region of heated gas possibly due to compression surrounding the jet core. This heated gas results in a bulk temperature of 295.8 K, slightly higher than the wall temperature (293.15 K). At this point in time heat is transferred from the gas to the wall with a positive Nusselt number of 376.9. At the slightly later time of

0.0022 seconds shown in Figure 7(b), the cold jet has almost impacted the wall, the bulk temperature has risen to 297 K and the Nusselt number has increased to 1819.6. After the cold gas jet impacts the receiver wall, the spatially averaged heat transfer at 0.0106 seconds as shown in Figure 7(c) is from the wall to the gas. The Nusselt number is negative (Nu=-765.7), even though the bulk temperature continues to increase (300.6 K at this time) due to compression and is greater than the wall temperature. Later, at 0.0221 seconds Figure 8a, the average heat transfer is reversed again (Nu=378.8), even though there is still a region on the wall where the cold jet results in the local heat transfer being negative (from the wall to the gas). In the final picture Figure 8(b) at 0.0598 seconds the cold jet no longer results in a region of negative heat transfer and the Nusselt number has increased to 572.7.

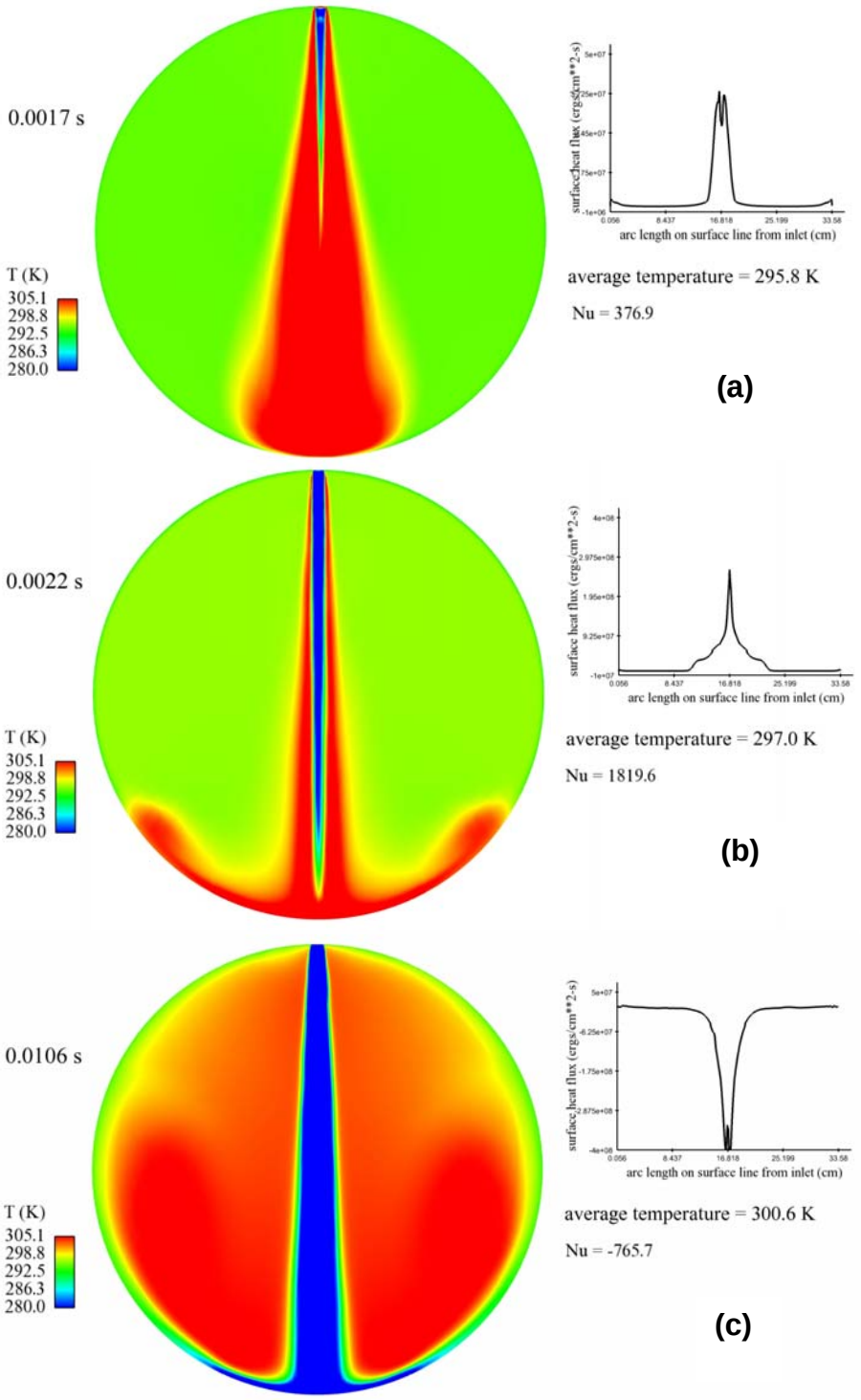

Figure 7. FUEGO-computed receiver temperature distribution and wall heat transfer for Test 700-300PSI at t=.0017, .0022 and .0106 seconds.

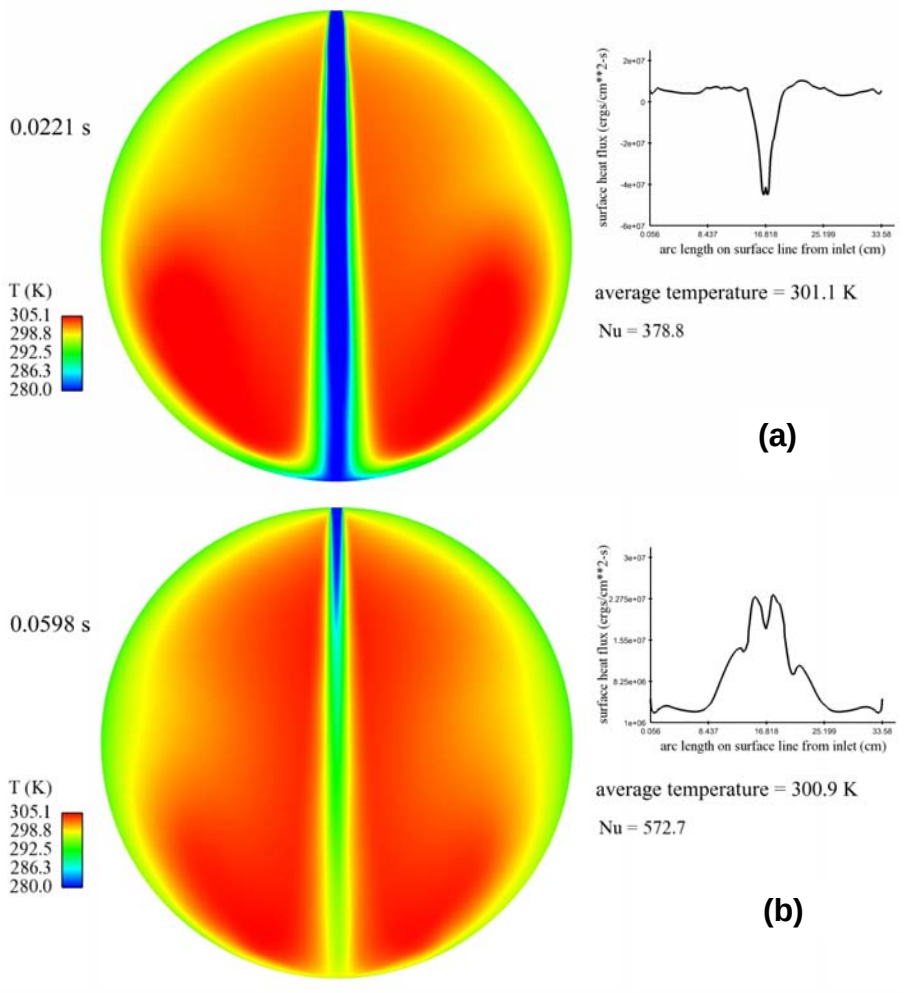

Figure 8. FUEGO-computed receiver temperature distribution and wall heat transfer for Test 700-300PSI at t=.0221 and .0598 seconds.

The phenomena shown in Figures 7 and 8 are complex and transient with gas heating by compression and local gas cooling by the cold incoming fluid resulting in strongly local heat transfer effects that for a brief time cause the spatially averaged heat transfer to be from the wall to the gas even though the bulk gas temperature is higher than the wall temperature at that time.

It is interesting to compare the Nusselt numbers predicted by the NETFLOW correlations for the receiver heat transfer at the early times shown in Figures 7 and 8 with the values computed from the FUEGO solution and shown in the figures. The small temperature differences of less than 10 K between the wall and the FUEGO-computed gas bulk temperature yield laminar Rayleigh numbers of approximately $2x10^4$ and from the correlation a Nusselt number of approximately 12. The forced convection heat transfer correlation in NETFLOW that was optimized from the PVT experiments (see Chapter 5),

$$\mathrm{Nu}=6.7\left[\mathrm{Re}_D\,\mathrm{Pr}\left(\frac{d}{D}\right)^2\right]^{0.632} \tag{4.4}$$

yields Nusselt numbers that vary from approximately 180 to 370 over the range of mass flow rates for the times shown in Figures 7 and 8. In NETFLOW's implementation of the receiver heat transfer correlations, the larger of the natural and forced convection Nusselt numbers is used; thus the forced convection values would be applied over the time range shown in the Figures 7 and 8. Over this time period the correlation predicts positive heat transfer (from the gas to the wall) with the magnitude being within the range of the values calculated with FUEGO and shown in the Figures 7 and 8. However, the rapid swings and the magnitudes of those swings in heat transfer are not captured in the correlations.

The FUEGO calculations demonstrate that unlike supply vessel flows, receiver vessel flows exhibit large and steep velocity and temperature gradients during the time period in which gas is transferred. It is reasonable to assume that fluid inertia will cause continued fluid motion after injection and pressure equilibrium.

Computed results in Figure 7 and 8 simulate a relatively low inlet pressure ratio. For larger pressure ratios (i.e. Tests 700-3000PSI, 700-6000PSI, 90-3000PSI and 90-6000PSI discussed in Chapter 5), the flow entering the receiver will form a highly under-expanded jet with transonic flow upstream of a series of shocks and expansion waves. While this transonic behavior is expected to be confined to the region very near the hole, the downstream subsonic part of the jet can be expected to produce even larger velocity and temperature gradients than those shown in Figures 7 and 8.

It appears unlikely that a single forced convection heat transfer correlation like the one in Equation (4.4) will accurately reproduce the early heat transfer characteristics in all receiver flows. Material presented in Chapter 5 will demonstrate that despite our best efforts to correlate forced and free convection heat transfer for the receiver, measured receiver bulk temperatures from the transient PVT tests were not accurately reproduced by the NETFLOW simulations during most of the time prior to pressure equilibrium.

Our inability to predict receiver heat transfer at early times has no impact on our ability to predict the final mass transferred to a receiver if the transfer continues to thermal equilibrium. The NETFLOW calculations with optimized heat transfer correlations presented in the next chapter show that receiver temperature spikes at early time are routinely over predicted yet the agreement between measured and predicted temperatures at later times is acceptable and leads to a relatively good prediction for the final mass transferred. However as noted early, there can be substantial errors in the predicted mass transfer prior to thermal equilibrium if the heat transfer is not predicted accurately.

5. VALIDATION OF NETFLOW MODELING USING GTS DATA

In Part I [1] of this report NETFLOW predictions were made for each of seven transient PVT experiments. These predictions were made using default heat transfer correlations for supply and receiver heat transfer as they existed at the time of the experiments. In this chapter we describe model improvements and how the data obtained from the transient PVT experiments were used to improve the heat transfer correlations. Finally we demonstrate NETFLOW model validation by comparing the improved predictions of supply and receiver pressure and temperature transients to those measured in the experiments. We also demonstrate how the improved predictions impact our ability to predict the masses transferred in the experiments.

5.1 Description of the Validation Experiments

For the convenience of the reader we will briefly describe the seven transient PVT validation experiments. Five of the validation experiments were high precision tests in which great effort was expended to start the experiment from near identical initial conditions. In these five experiments most masses computed from measured pressures and mass averaged temperatures were within 1% of total system mass over the entire transfer transient (see [1]). The five high precision tests are summarized here in Table 1.

Table 1. Precision tests.

Test Name	Nominal Supply Volume (cc)	Nominal Receiver Volume (cc)	Nominal Initial Supply Pressure (PSIA)	Nominal Initial Receiver Pressure (PSIA)
200-700-300PSI	200	700	300	14.7
200-700-3000PSI	200	700	3000	14.7
200-700-6000PSI	200	700	6000	14.7
200-90-3000PSI	200	90	3000	14.7
200-90-6000PSI	200	90	6000	14.7

Prior to conducting the tests shown in Table 1, two tests were conducted using a relatively large receiver (nominally 13,000 cc). For the most part these tests were conducted for the purpose of developing the transient PVT technique. In some cases the individual experiments used to determine the transient mass averaged supply and receiver temperatures were not started from identical initial conditions. Hence these tests, which are summarized here in Table 2, are more qualitative but nevertheless valuable in contributing to our understanding of vessel heat transfer, especially for large receivers.

Table 2. Qualitative tests.

Test Name	Nominal Supply Volume (cc)	Nominal Receiver Volume (cc)	Nominal Initial Supply Pressure (PSIA)	Nominal Initial Receiver Pressure (PSIA)
200-13K-300PSI	200	13000	300	203
200-13K-6000PSI	200	13000	6000	Vacuum

Exact vessel volumes and initial conditions for the Tests listed in Tables 1 and 2 are documented in Reference [1].

The naming convention used here to identify each test takes on the form:

AAA-BBB-CCCPSI

where AAA represents the nominal volume of the supply in cc, BBB represents the nominal volume of the receiver in cc and CCC represents the nominal initial supply pressure in PSI. For the tests conducted using the 13,000 cc receiver BBB is abbreviated as 13K. Since all tests were conducted using the nominal 200cc supply vessel, the naming convention used here was shortened to BBB-CCCPSI where it is understood that in each case the supply volume was 200cc. Except for Test 13K-300PSI which had an initial receiver pressure of 203 PSI and Test 13K-6000PSI which a vacuum receiver pressure, all initial receiver nominal pressures were 1 ATM.

A detailed schematic for one of the tests, TEST 700-300PSI, is reproduced here in Figure 9. Exact sizes of all vessels and interconnecting plumbing are shown. Except for the size of the receiver volume, the experimental apparatus used for the remaining tests varied only slightly from that shown in Figure 9. The supply and receiver volumes and all the volumes in the interconnecting tubing were simulated in the NETFLOW models. Extra fill/vent tubes and transducer volumes attached to the supply and receiver vessels were not simulated separately but instead their volumes were added to the supply and receiver volumes.

As previously discussed, NETFLOW models treat the supply and receiver vessels as single control volumes with NETFLOW computing a time varying uniform pressure and temperature for each vessel. The discussion in Chapters 2 and 4 supports the observation that pressures in these vessels are nearly uniform in space but large thermal gradients are present as a result of vessel heat transfer. In order to validate a NETFLOW prediction there must be some means to experimentally determine the time varying mass averaged temperature in the vessel since this is the quantity computed by NETFLOW. The transient PVT technique provides the means to do this.

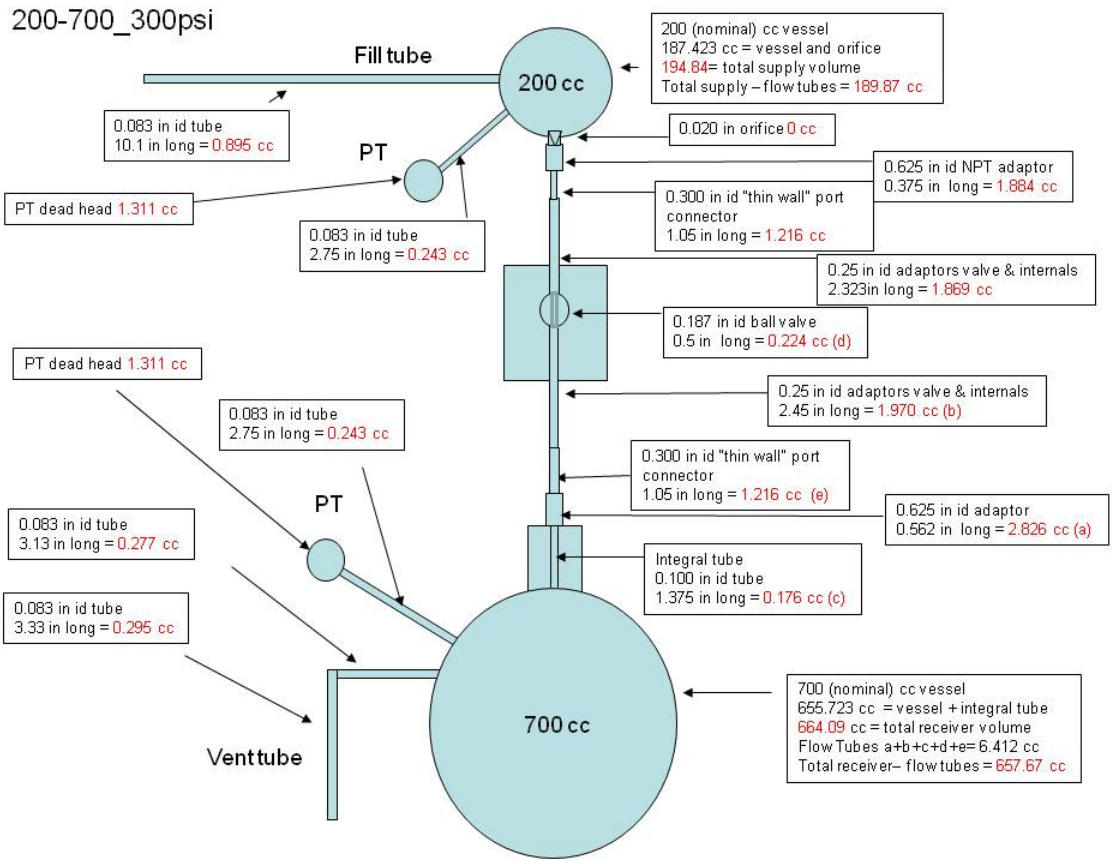

Figure 9. Detailed schematic of the test apparatus.

The transient PVT technique documented by Johnston and Dwyer [24] was employed by the present authors to obtain mass averaged temperature data like that presented in Figures 2 and 3. The data in these figures represents the time varying mass averaged temperature in the supply and the receiver for TEST 700-3000PSI. For each instance in time a single experiment was used to compute a pair of points, one point on the supply curve (Figure 2) and one point on the receiver curve (Figure 3). The procedure outlined below describes the process although the description has been simplified greatly for the purposes of this discussion. The procedure assumes we wish to determine the transient pressure and the mass averaged temperature in the supply and receiver at a time equal to t^*.

1. Charge supply and receiver to desired initial conditions and wait until the temperature in each vessel is uniform.

2. At t=0 open the valve between the supply and the receiver and allow gas to flow.

3. At $t = t^*$ close the valve and record P_S^* and P_R^*, the supply and receiver pressures at t^*.

4. Wait for the temperature and pressure in the supply and receiver to become uniform in space and use these temperatures and pressures together with the equation of state to compute ρ_S^* and ρ_R^*, the supply and reservoir gas densities at $t = t^*$.

5. Use P_S^* and P_R^* with ρ_S^* and ρ_R^* in the equation of state to determine T_S^* and T_R^*, the mass averaged supply and receiver temperatures at $t = t^*$.

6. Repeat steps 1-5 until sufficient data is collected to describe the transient pressure and mass averaged temperatures in the supply and receiver over of the time period of interest.

Time varying values of P_S^*, P_R^* T_S^* and T_R^* were obtained for all 7 test series listed in Tables 1 and 2. This data is compared directly to NETFLOW predictions in Sub Chapters 5.4 and 5.5.

5.2 NETFLOW Model Description

NETFLOW input files for the tests listed in Tables 1 and 2 are presented in Appendices A-G. These input files serve to describe exact geometries and precise initial conditions for each test. The supply and receiver were simulated as single control volumes or NODES. The valve and tubing shown in Figure 9 that connects the two vessels were simulated using a series of PATHS and PIPES (See References [2,12] for an explanation of NETFLOW modeling nomenclature). In addition to the physical components in the flow path, the ISENTROPIC link was added to more properly account for the nearly isentropic acceleration of helium from the supply stagnation conditions to the orifice flow conditions. This is sometimes necessary in NETFLOW simulations if there is little or no pressure drop due to friction between the supply vessel and the choke point in the flow path. This is certainly the case here since orifice or choke point is adjacent to the supply vessel exit. For simulations in which choking occurs at the receiver entrance after a long run of friction induced pressure drop, eliminating the ISENTROPIC link would produce no significant errors.

In simulating the tests, it was discovered that no significant frictional pressure drop occurs between the downstream side of the orifice and the receiver. Nevertheless the default Moody [14] friction model was used in the modeling. It was originally thought that heat transfer along the flow path was also negligible. As a result in Part I of this report the flow path was assumed to be adiabatic. It was later discovered that including the path heat transfer had an important effect on model predictions. This point is illustrated in Figures 10 and 11 which show predicted reservoir pressure and temperature with and without path heat transfer. This comparison is made for the TEST 700-3000PSI.

As a result of the observations made in Figures 10 and 11, it was decided that NETFLOW's default tube flow heat transfer correlation should be used in the modeling. This is a quasi-steady correlation developed by Dittus and Boelter [15] to describe forced convection heat transfer in fully-developed tube flow. In NETFLOW modeling the heat transfer is permitted to vary along the flow path according to the local Reynolds and Prandtl numbers.

The Abel-Noble real gas equation of state was used for all of the model predictions presented here. Real gas effects become important for tests in which the supply pressures exceed 3000 PSI. The Abel-Noble constants for NETFLOW's hydrogen and helium isotope mixture model were developed by Chenoweth [30] and have been shown to accurately reproduce the behavior of non ideal gas mixtures of helium and deuterium.

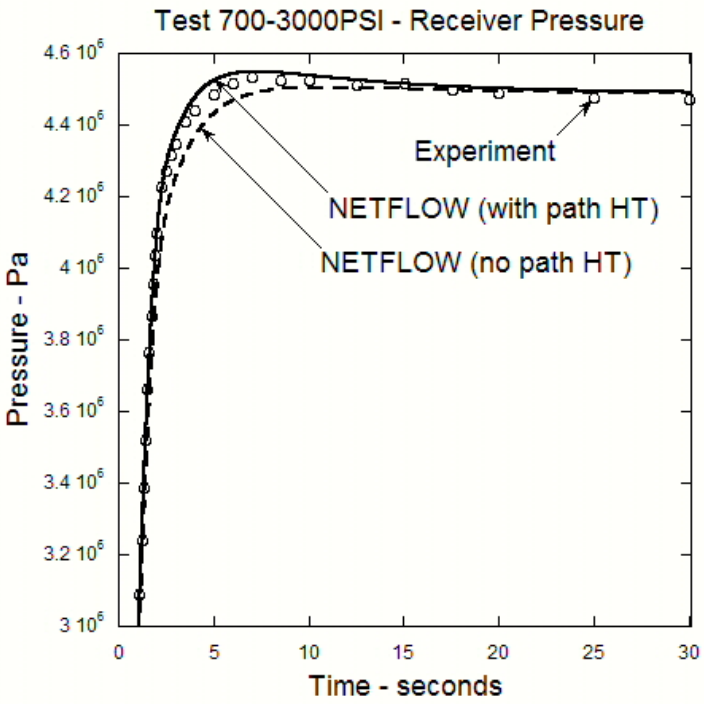

Figure 10. Influence of path heat transfer on receiver pressure transient.

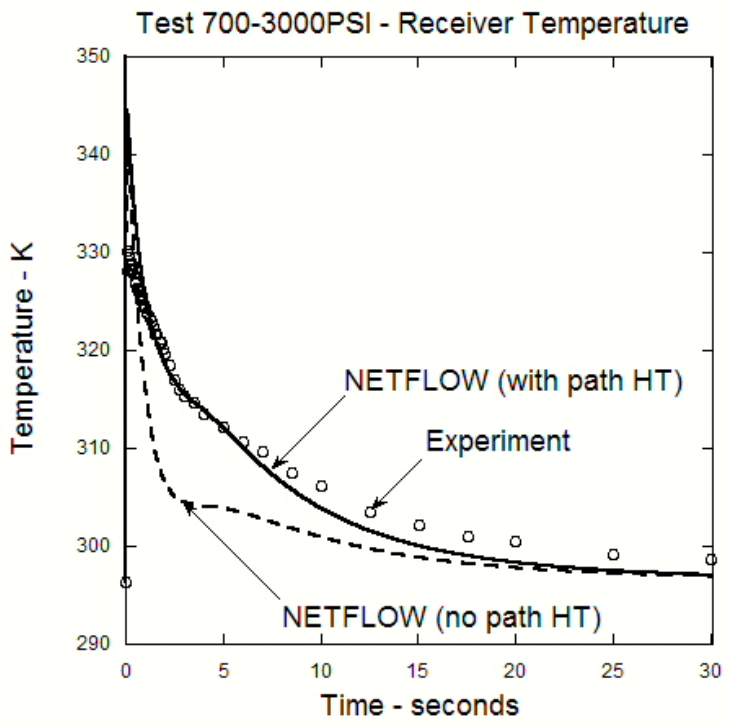

Figure 11. Influence of path heat transfer on receiver temperature transient.

5.3 Optimization of the NETFLOW Vessel Heat Transfer Correlations

Considerable effort was expended investigating many of the heat transfer models discussed in Chapter 3 and determining their applicability to supply-receiver flows. It proved to be relatively easy to capture the influence of heat transfer in the supply using well-established forms of the laminar and turbulent free convection correlations. Configuring and fitting heat transfer correlations for the receiver were more difficult.

The final form for forced convection heat transfer in receivers was taken to be

$$\mathrm{Nu} = C_1 \left[\mathrm{Re}_D \, \mathrm{Pr} \left(\frac{d}{D} \right)^2 \right]^{C_2} \tag{5.1}$$

where the Nusselt number, Nu is given by

$$\mathrm{Nu} = \frac{hD}{k} \tag{5.2}$$

the Reynolds number, Re_D is given by

$$\mathrm{Re}_D = \frac{\rho_i v_i D}{\mu} = \frac{\dot{m} D}{A_i \mu} \tag{5.3}$$

and the Prandtl number, Pr is given by

$$\mathrm{Pr} = \frac{C_p \mu}{k}. \tag{5.4}$$

and h is the heat transfer coefficient in Newton's law of cooling, D is the effective spherical diameter of the tank, d is the diameter of the inlet, k is the vessel gas thermal conductivity, μ is the vessel gas dynamic viscosity, ρ_i is the gas density at the inlet, v_i is the inlet velocity, $\dot{m}$ is the inlet mass flow rate, A_i is the inlet flow area and C_p is the vessel gas specific heat at constant pressure.

The final form for free convection heat transfer for both the supply and the receiver was taken to be

$$\mathrm{Nu} = c\mathrm{Ra}^n \tag{5.5}$$

The values for c and n in were assumed to vary depending on the mode of convective heat transfer, *i.e.*

laminar flow: $(\mathrm{Ra} \prec 1.24\mathrm{x}10^8)$: $\mathrm{c} = C_3$, n=.25 (5.6)

turbulent flow: $(\mathrm{Ra} \succ 1.24\mathrm{x}10^8)$: $\mathrm{c} = C_4$, n=.333 (5.7)

with Rayleigh number, Ra given by

$$\mathrm{Ra} = \mathrm{Gr}\,\mathrm{Pr} = \frac{g\beta(T - T_w)\rho^2 D^3}{\mu^2}\frac{C_p \mu}{k} \tag{5.8}$$

where Gr is the Grashof number, g is the gravitational constant and β, the volume expansivity is given by

$$\beta = -\frac{1}{\rho}\left(\frac{\partial \rho}{\partial T}\right)_P = \frac{1 - B\rho}{T} \tag{5.9}$$

for an Abel-Noble gas. The constant B in Equation (5.9) is the Abel-Noble constant for the gas or gas mixture. In the Rayleigh number definition T is the vessel mass averaged gas temperature, T_w is the wall temperature. The density ρ, dynamic viscosity μ, the specific heat at constant pressure C_p and the thermal conductivity, k are all evaluated at the vessel gas temperature and pressure.

In keeping with observations made for flat plate free convection correlations (see *e.g.* References [31,32]), the exponent *n* in Equations (5.6-5.7) was taken to be 1/4 for laminar flow and 1/3 for turbulent flow.

For vessels that act as supplies, interior flow velocities are negligible except for the small region just upstream of the exit. Hence the heat transfer is assumed to be governed solely by free convection. For receivers, multidimensional CFD calculations show (see *e.g.* Chapter 4) that during the initial injection the incoming jet stagnates against the opposite vessel wall and creates significant forced convection shear flows along the vessel wall. As pressure equilibrium is approached these flows diminish in strength and the dominant mode of heat transfer transitions to free convection. For vessels acting as receivers NETFLOW assumes the following model for heat transfer:

$$\mathrm{Nu} = \max(\mathrm{Nu}_{forced}, \mathrm{Nu}_{free}) \tag{5.10}$$

where Nu_{forced} is given by Equations (5.1) and Nu_{free} is given by Equations (5.5-5.7).

Once the vessel heat transfer Nusselt number is determined, NETFLOW computes the vessel heat transfer with Newton's law of cooling using the heat transfer coefficient

$$h = \frac{\mathrm{Nu}k}{D} \ . \tag{5.11}$$

where *D*, the characteristic dimension, is the diameter of an "equivalent" spherical vessel. For vessels that are not spherical, *D* is calculated from the tank volume, *V* using the following expression:

$$D = \left(\frac{6V}{\pi} \right)^{\frac{1}{3}} . \tag{5.12}$$

Having determined the final functional forms for the supply and receiver heat transfer correlations, the only remaining task was to determine values for the constants C_1, C_2, C_3 and C_4 in Equations (5.1), (5.6) and (5.7). This was accomplished by using HOPSPACK [33], a Hybrid Optimization Parallel Search PACKage developed at Sandia. HOPSPACK is a computer program that solves derivative-free optimization problems using an open source, C++ software framework. HOPSPACK utilizes an asynchronous pattern search solver that handles general optimization problems with linear and non linear constraints and continuous integer-valued variables.

HOPSPACK was coupled to NETFLOW using a Unix script. A special program was written to generate an objective function that characterized the difference between measured mass averaged temperatures and predicted mass average temperatures. Only the measured mass average temperatures from the high precision tests in Table 1 were used in the optimization problem. The data for the supply and the receiver was given

equal weighting in the optimization as was the importance of each of the five tests *(i.e.*, no test was assumed to be the most or least accurate). The objective function calculator computed an objective function, F_I for each of the five tests *(I=1,2,3,4,5*) using the following formula:

$$F_I = \sum_{J=1}^{JMAX_I} T_{D_{IJ}}^2 - T_{P_{IJ}}^2 \tag{5.13}$$

where *J* refers to the particular measured data point, $JMAX_I$, is the maximum number of data points in test *I*, $T_{D_{IJ}}$ is the measured mass average temperature of the J^{th} data point in test *I* and $T_{P_{IJ}}$ is the predicted mass average temperature corresponding to the time at which the measured temperature was evaluated. When the measured and predicted mass averaged times differed, the predicted temperatures were linearly interpolated from the adjacent prediction times.

The total objective function was computed by summing the objective functions from each test, *i.e.*

$$F = \sum_{I=1}^{5} F_I \tag{5.14}$$

The following procedure was used to determine the optimum values of C_1, C_2, C_3 and C_4 in Equations (5.1), (5.6) and (5.7):

1. Guess trial values for C_1, C_2, C_3 and C_4. Write these values to a file that NETFLOW will read the next time it is executed.

2. Run NETFLOW simulations for each of the five tests in Table 1 producing five sets of output files for predicted supply and receiver temperatures (*i.e.*, time in column one and corresponding predicted temperature in column two).

3. Execute the objective function evaluator program that reads the output files from step 2 and the data files for measured supply and receiver mass averaged temperature. Compute *F*. Print *F* to an output file.

4. Execute HOPSPACK which reads the file containing the current values for C_1, C_2, C_3 and C_4 and the corresponding objective function (*F* value). Determine new trial values for C_1, C_2, C_3 and C_4. Print the new trial values to a file that NETFLOW reads the next time it executes.

5. Go to step 2.

Steps 2-5 are executed for a maximum number of user-specified HOPSPACK executions or until it is determine that further variations in guesses for C_1, C_2, C_3 and C_4 fall below some user-specified tolerance. The only constraints placed on the range of C_1, C_2, C_3 and C_4 trial values were non negativity constraints.

HOPSPACK determined the following optimized values for C_1, C_2, C_3 and C_4:

$$C_1 = 6.694 \tag{5.15}$$

$$C_2 = .632 \tag{5.16}$$

$$C_3 = .9331 \tag{5.17}$$

$$C_4 = .168 \tag{5.18}$$

These constants together with Equations (5.1), (5.5), (5.6) and (5.7) constitute the new default vessel heat transfer correlations for NETFLOW. The Rayleigh number at which free convection transitions into forced convection for Equations (5.6) and (5.7) is increased from 1.24×10^8 to 2.21×10^8.

The next two sub chapters compare predictions made using these correlations to the measured data obtained from the tests in Tables 1 and 2.

5.4 NETFLOW Validation with High Precision Data Sets

Figures 12-23 compare predicted and measured supply and receiver pressure and temperature for Tests 700-300PSI, 700-3000PSI and 700-6000PSI. These tests demonstrate the influence of initial supply pressure level on the transfer between a 200 cc nominal supply and a 700 cc nominal receiver. Comparisons for Test 700-300PSI are shown in Figures 12-15; Comparisons for Test 700-3000PSI are shown in Figures 16-19 and comparisons for Test 700-6000PSI are shown in Figures 20-23. The data and predictions show that higher initial supply pressures result in larger transient temperature excursions for both the supply and the receiver. This expected and observed trend is well replicated by the NETFLOW models. Predicted temperature transients for the supply are in excellent agreement with the measurements. The timing and magnitude of the minimum supply temperature spike and the recovery back to ambient temperature are accurately reproduced by NETFLOW. Predictions for the receiver are improved from those previously documented in Part I [1] of this report. Predicted receiver peak temperatures are closer to measured values (although they are still over-predicted) and the predicted fall-off to ambient temperature is more inline with the measurements.

Figures 24-31 illustrate the influence of reducing the receiver size from a nominal 700cc to a nominal 90cc. Figure 24-27 show measured and predicted supply and receiver pressure and temperature transients for Test 90-3000PSI in which the nominal supply

pressure was 3000 PSI. Similar comparisons are made in Figures 28-31 for Test-90-6000PSI in which the nominal supply pressure was doubled to 6000 PSI. The influence of reduced receiver size is evident when Figures 16-19 from Test 700-3000PSI are compared to Figure 24-27 for Test 90-3000PSI; both tests were performed using a nominal supply pressure of 3000 PSI. It is evident from looking at the pressure transients that reducing the receiver size from 700 to 90 cc reduced the transfer time to pressure equilibrium from approximately 2 seconds to 0.5 seconds. A similar reduction in the time to pressure equilibrium can be seen by comparing results from the two 6000 PSI nominal supply pressures tests *i.e.*, Test 700-6000PSI (Figures 20-23) and Test 90-6000PSI (Figures 28-31). Reducing the receiver size reduces the pressure drop in the supply during transfer and results in a corresponding smaller drop in the supply transient temperature. Conversely, reducing the receiver size increases the pressure change in the receiver resulting in a correspondingly higher transient temperature spike. This behavior is observed in the experiments and is predicted by the modeling.

For all the high precision tests listed in Table 1 the measured transient temperature history in the supply is well-predicted by the model. Predictions for receiver temperature are less accurate although they have been improved significantly from those originally presented in Part I of this report [1]. The comparison with the least agreement between measured and predicted temperature is shown in Figure 31. This figure compares the receiver temperature transients for Test 90-6000PSI. Measured temperature levels are approximately 4-6K higher than predicted levels near the end of the transient as the receiver gas temperature returns to ambient levels. The impact on predicting the mass transfer will be discussed later in Sub Chapter 5.6.

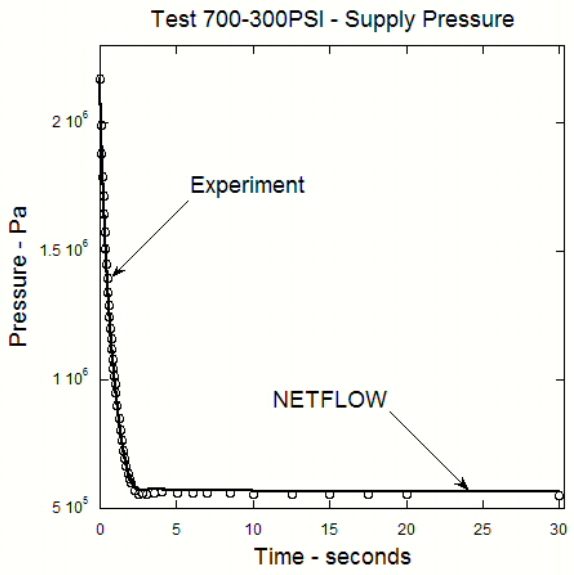

Figure 12. Predicted and measured supply pressure for Test 700-300 PSI.

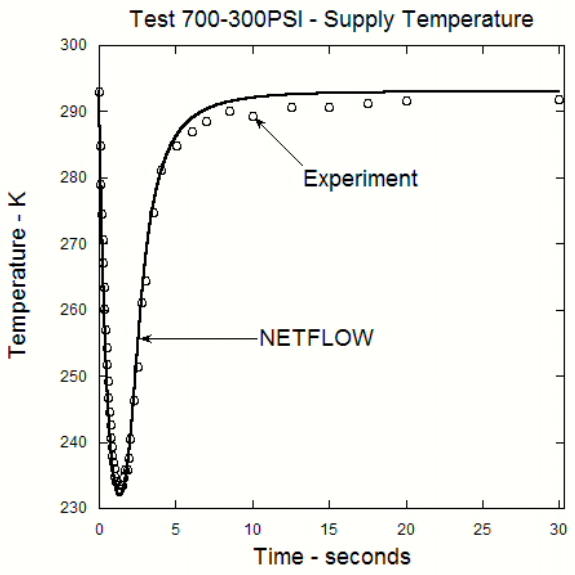

Figure 13. Predicted and measured supply temperature for Test 700-300 PSI.

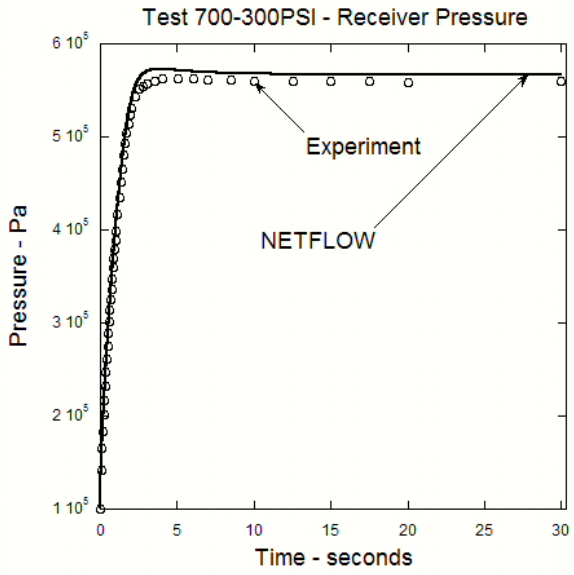

Figure 14. Predicted and measured receiver pressure for Test 700-300 PSI.

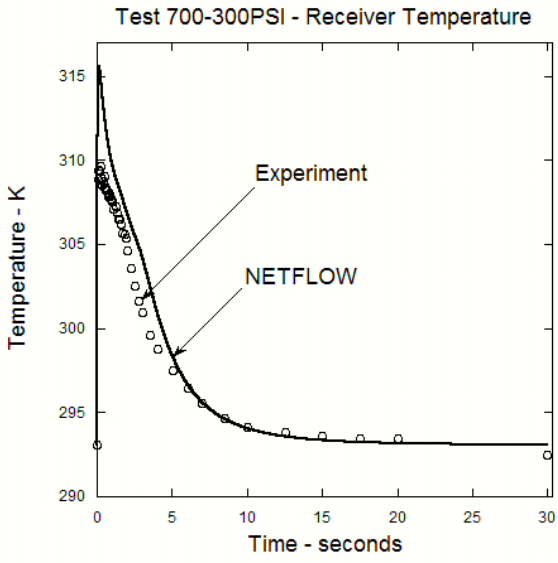

Figure 15. Predicted and measured receiver temperature for Test 700-300 PSI.

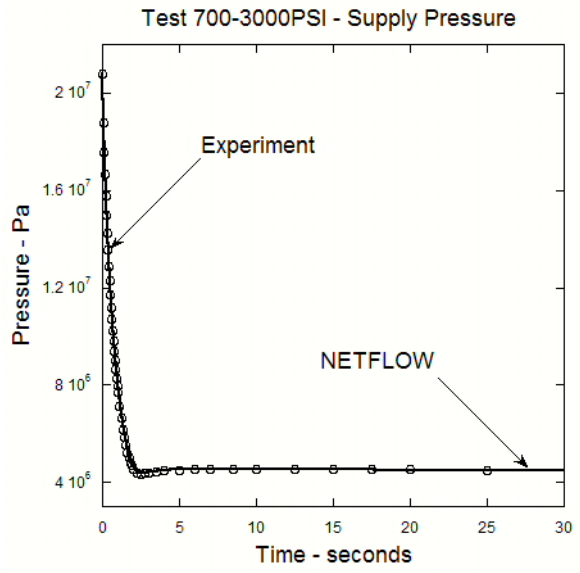

Figure 16. Predicted and measured supply pressure for Test 700-3000 PSI.

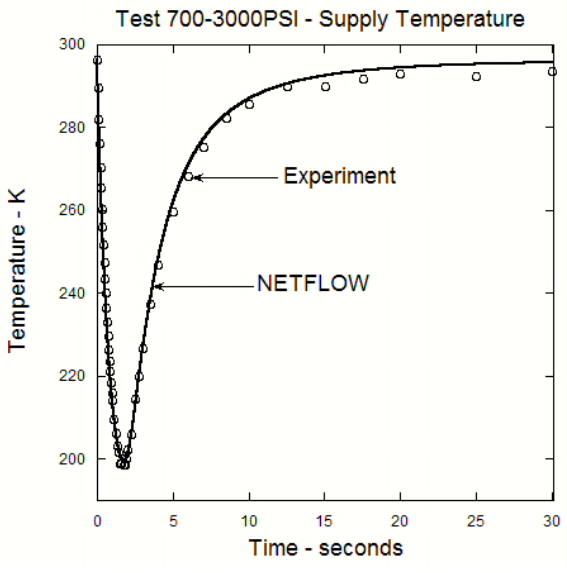

Figure 17. Predicted and measured supply temperature for Test 700-3000 PSI.

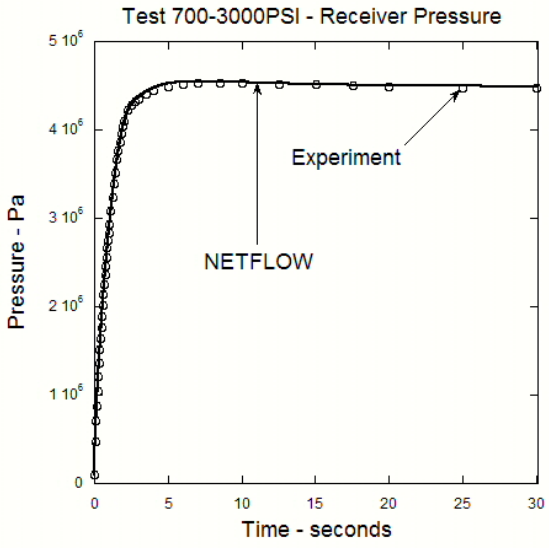

Figure 18. Predicted and measured receiver pressure for Test 700-3000 PSI.

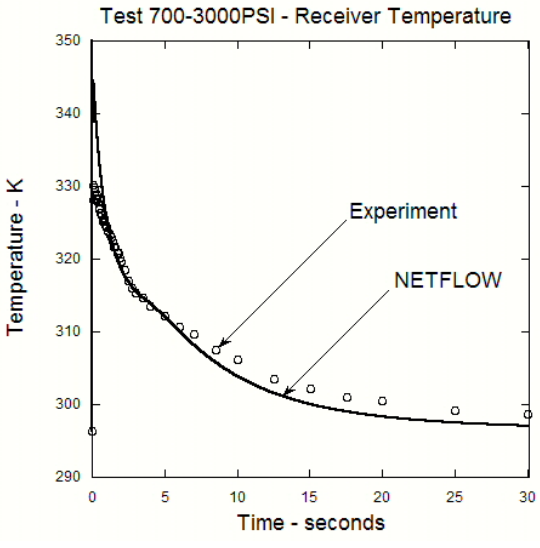

Figure 19. Predicted and measured receiver temperature for Test 700-3000 PSI.

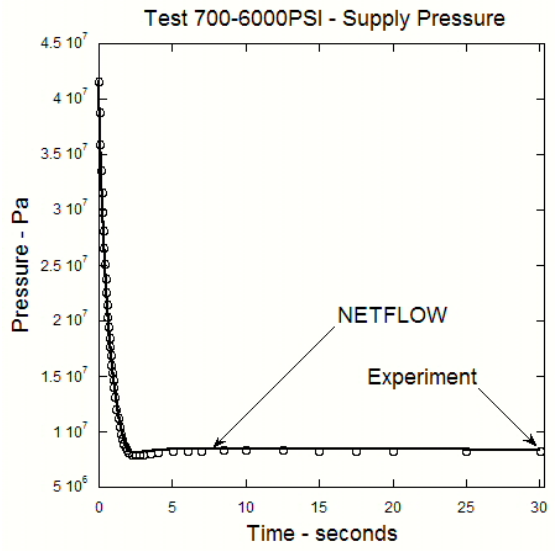

Figure 20. Predicted and measured supply pressure for Test 700-6000 PSI.

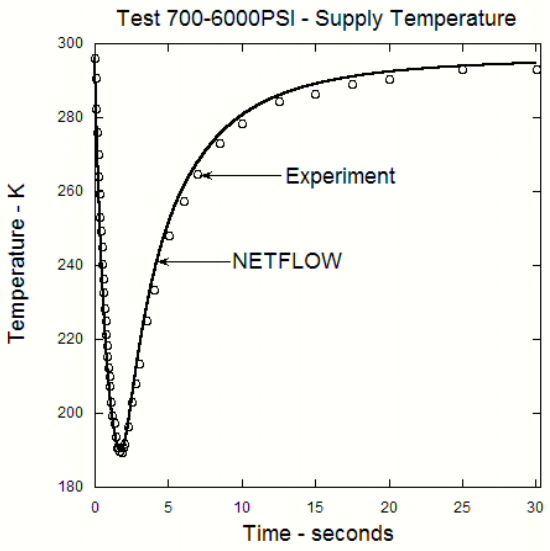

Figure 21. Predicted and measured supply temperature for Test 700-6000 PSI.

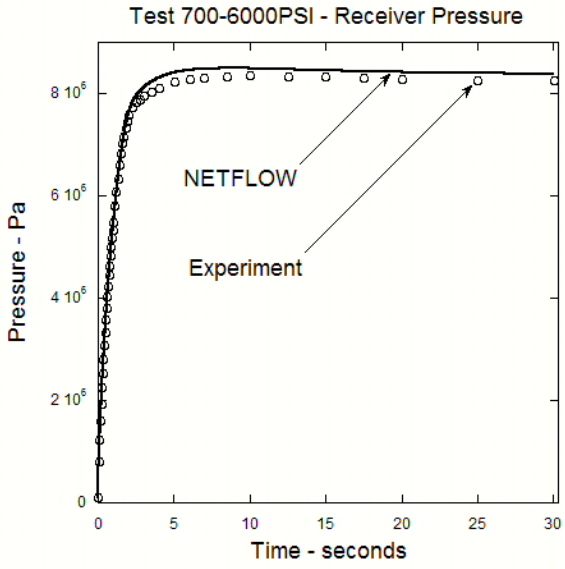

Figure 22. Predicted and measured receiver pressure for Test 700-6000 PSI.

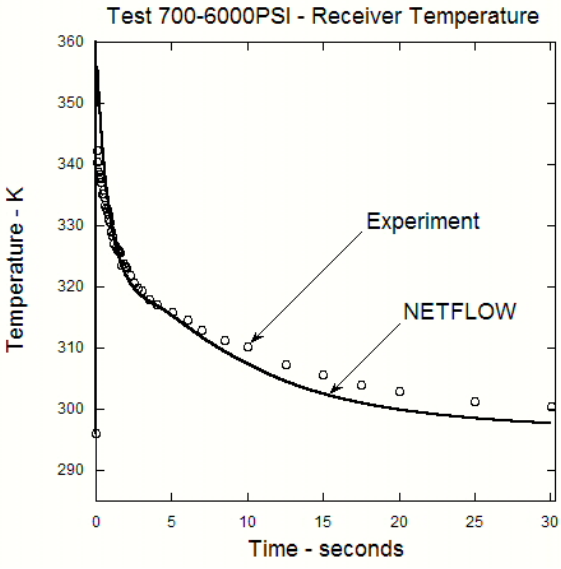

Figure 23. Predicted and measured receiver temperature for Test 700-6000 PSI.

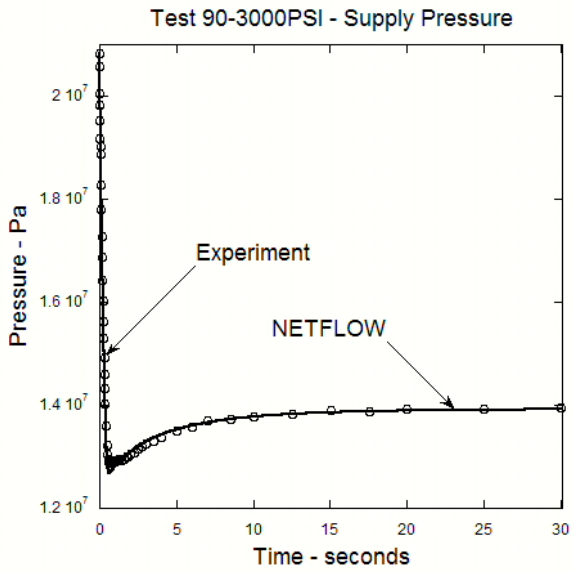

Figure 24. Predicted and measured supply pressure for Test 90-3000 PSI.

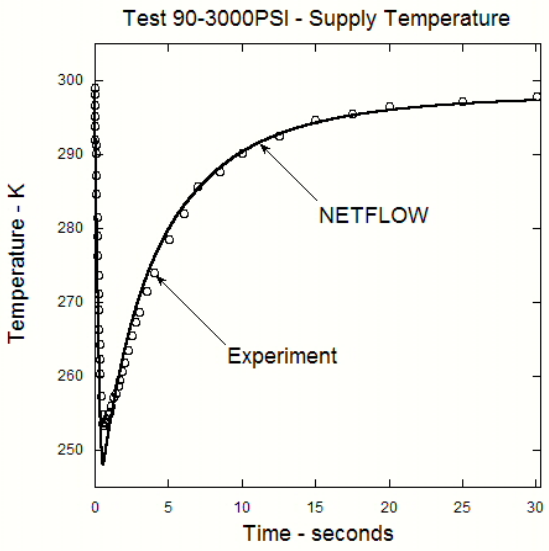

Figure 25. Predicted and measured supply temperature for Test 90-3000 PSI.

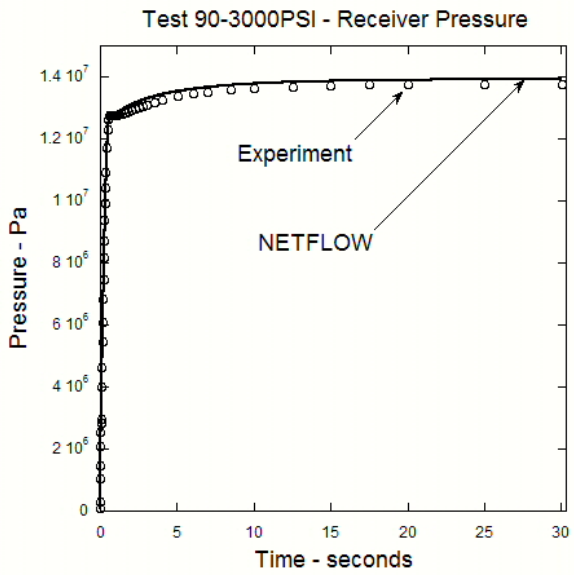

Figure 26. Predicted and measured receiver pressure for Test 90-3000 PSI.

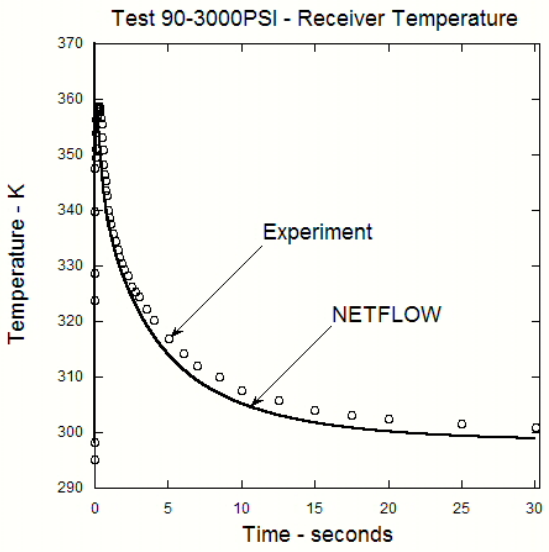

Figure 27. Predicted and measured receiver temperature for Test 90-3000 PSI.

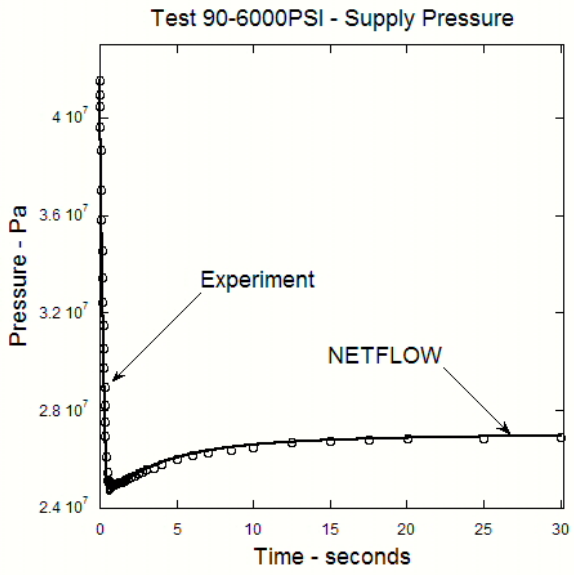

Figure 28. Predicted and measured supply pressure for Test 90-6000 PSI.

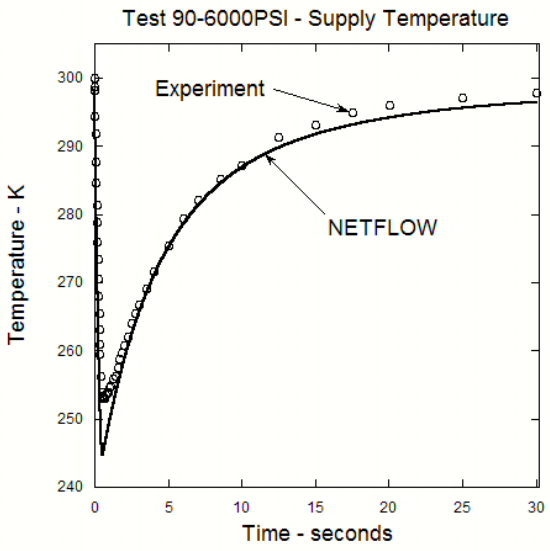

Figure 29. Predicted and measured supply temperature for Test 90-6000 PSI.

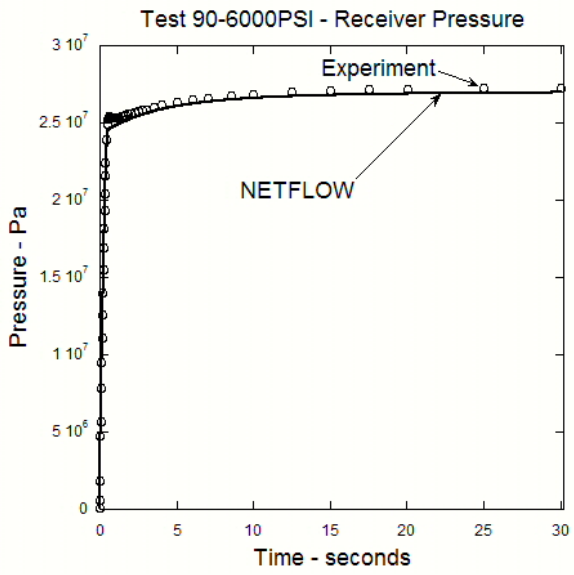

Figure 30. Predicted and measured receiver pressure for Test 90-6000 PSI.

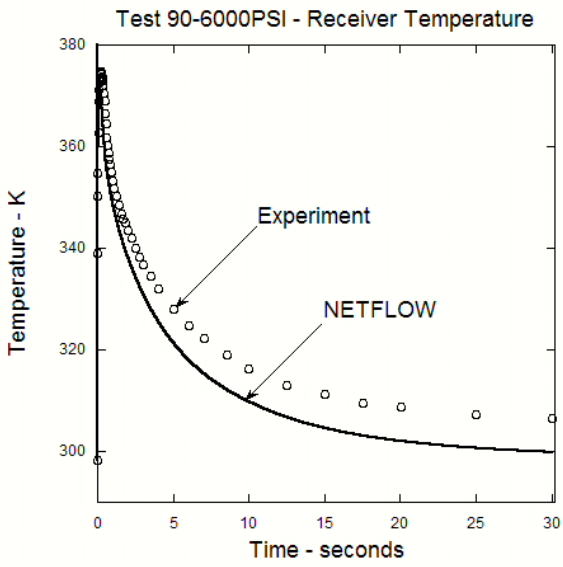

Figure 31. Predicted and measured receiver temperature for Test 90-6000 PSI.

5.5 Validation with the 13K Receiver Data Sets

In this chapter we examine the influence of large receivers (in this case 13000 cc nominal volume) on vessel heat transfer. Comparisons for measured and predicted supply and receiver transient pressure and temperature are made for the test conditions and geometry summarized in Table 2. For reasons discussed earlier these data sets are qualitative in nature but add insight to our understanding of vessel heat transfer, particularly for large receivers. In the two cases presented here the supply and receiver nominal volumes were 200 and 13000 cc respectively.

Figures 32-35 compare measured and predicted pressure and temperature transients for Test 13K-300PSI). This test is a low pressure ratio (350:203) transfer in which no choking occurs. (For choking to occur in this test the initial supply pressure would have to be increased to at least 410 psi while keeping the initial receiver pressure at 200 PSI). The measured supply pressure and temperatures were accurately reproduced by model. The scatter in the data for the receiver makes comparisons difficult but it appears that the predicted temperature is within data scatter and the predicted pressure is slight lower than the measured pressures. Reasons for data scatter are discussed in [1].

Figures 36-39 compare measured and predicted pressure and temperature transients for Test 13K-6000PSI. This test is for an extremely high pressure ratio (6000:Vacuum) transfer in which a large portion of the transfer takes place with choked flow at the orifice. With the exception of Test 13K-300PSI, choking was present in all previously discussed tests. However in this test, choked flow was present for a larger percentage of the time required to reach pressure equilibrium. The measured supply temperature and pressure were well-reproduced by the model. The greatest deviation between measurement and prediction occurred for the temperature recovery in the supply which appears to be more rapid for a portion of the time after the temperature drop spike. Quantitative agreement for the receiver pressure and temperature transients was not as good with the pressure and temperature being under predicted.

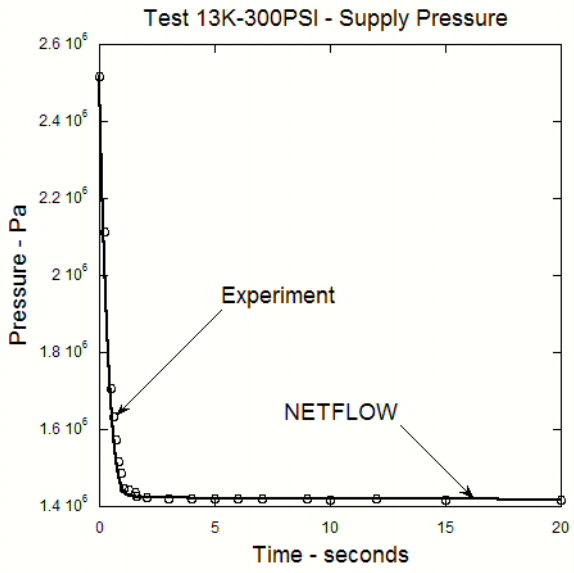

Figure 32. Predicted and measured supply pressure for Test 13K-300 PSI.

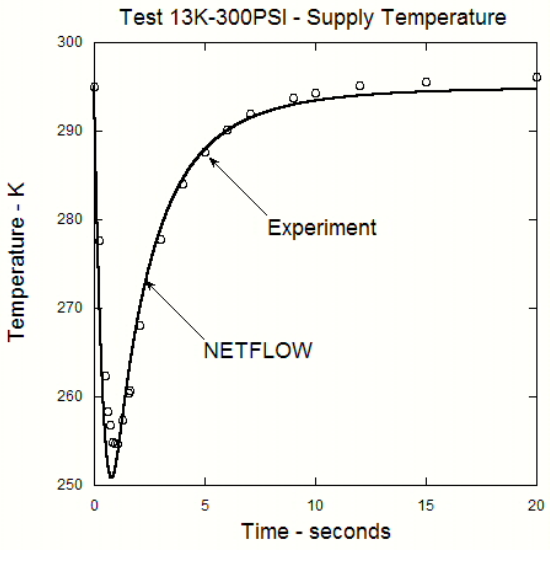

Figure 33. Predicted and measured supply temperature for Test 13K-300 PSI.

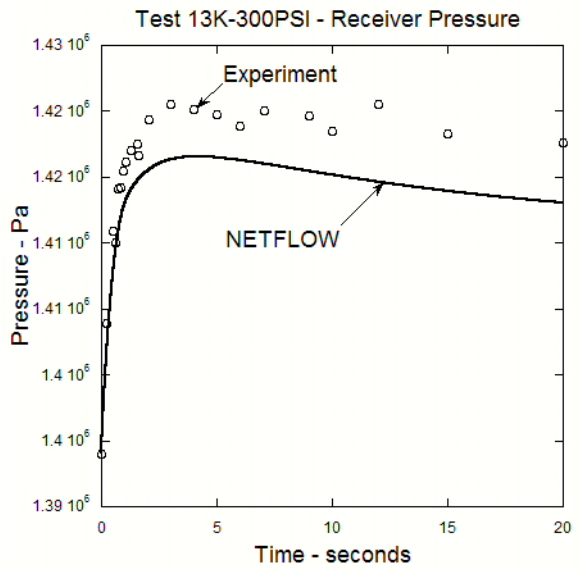

Figure 34. Predicted and measured receiver pressure for Test 13K-300 PSI.

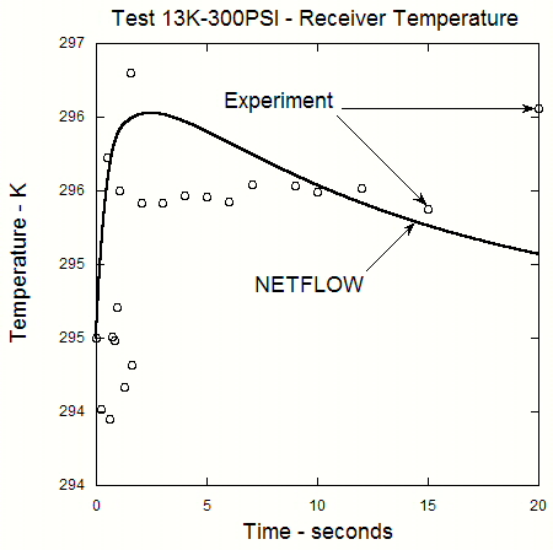

Figure 35. Predicted and measured receiver temperature for Test 13K-300 PSI.

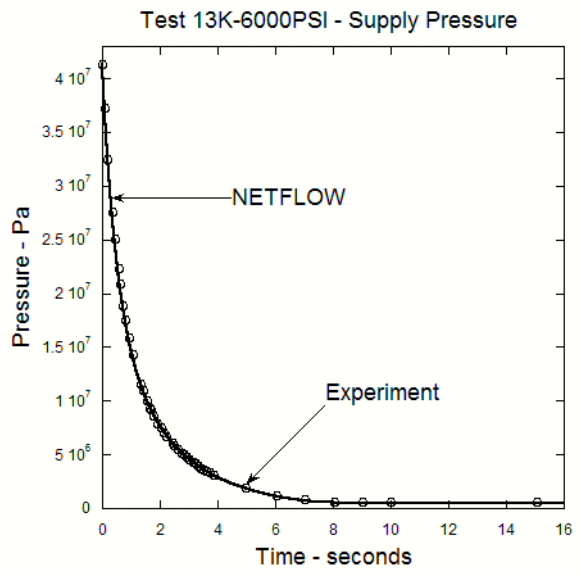

Figure 36. Predicted and measured supply pressure for Test 13K-6000 PSI.

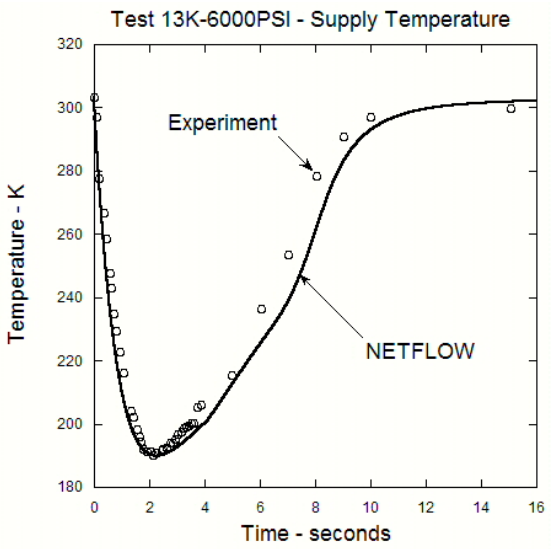

Figure 37. Predicted and measured supply temperature for Test 13K-6000 PSI.

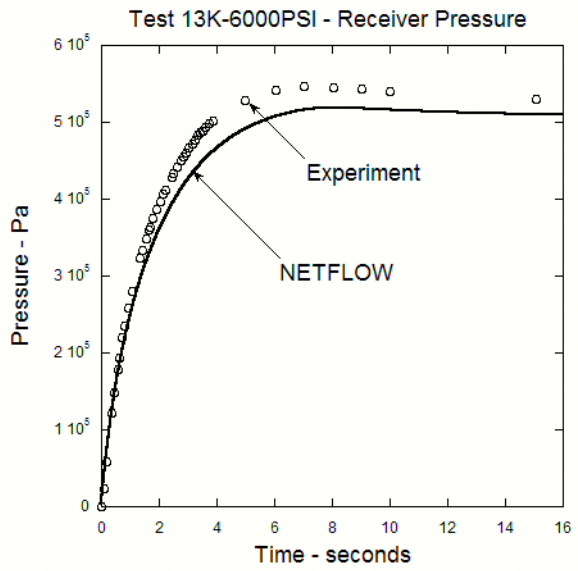

Figure 38. Predicted and measured receiver pressure for Test 13K-6000 PSI.

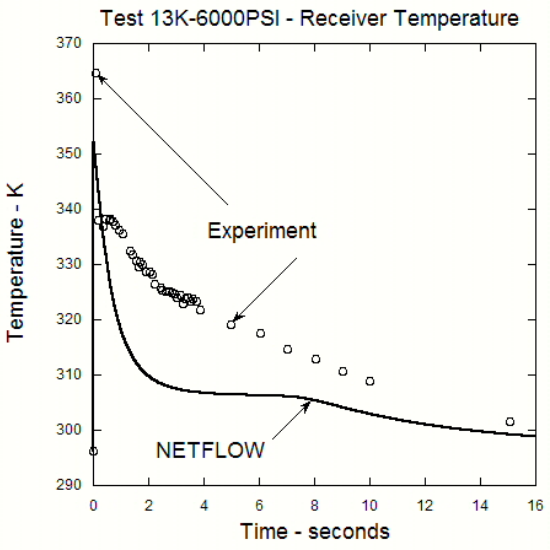

Figure 39. Predicted and measured receiver temperature for Test 13K-6000 PSI.

5.6 Measured and Predicted Mass Transfer

To this point NETFLOW predictions have been compared to measured supply and receiver pressure and temperature transients. The measured pressures and temperatures can be used to construct the mass inventories in the system as a function of time. This was in fact done as a data reduction step in order to compute the mass averaged supply and receiver temperature. As explained in Part I [1] the entire mass inventory upstream of the valve was measured and used to compute the mass averaged temperature upstream of the valve. Similarly the measured mass inventory downstream of the valve was used to compute the downstream mass averaged temperature. It is these measured temperatures that have been compared to NETFLOW-predicted supply and receiver temperatures.

In this chapter we directly compare computed mass inventories upstream and downstream of the valve to those directly measured in the experiment. This will provide us with some insight into how errors in predicting vessel pressures and temperatures translate into errors in predicting actual mass inventories. Accurately predicting mass inventories over time is the principal objective of gas transfer analysis.

Predicted and measured mass inventories are compared for two tests: Test 700-3000PSI and Test 90-6000PSI. The first test was selected since it is believed that this is the highest precision data set for which there was the smallest measured total mass deviation (less than 0.4%) over the series of individual transient PVT measurements. The second test was selected because it had the largest variation in predicted and measured receiver temperature near the end of the transfer (see Figure 31). The lower precision tests listed in Table 2 were not considered for this mass comparison.

Figure 40 shows measured and predicted mass inventories upstream and downstream of the valve for Test 700-3000PSI. Also shown in the figure is the total measured and predicted system mass as a function of time. The total system mass predicted by NETFLOW over time never changes since this is a closed system and conservation of mass is rigidly enforced. The total measured system mass increases by as much as 0.4% over the course of the measurements due to small experimental errors as explained in [1]. At time zero the predicted mass is 1.03% higher than the measured mass. This difference is solely due to the equations of state used to compute the initial masses from the initial measured temperature and pressure. In reducing the data the FILLUP [34] equation of state was used which is based on the work of Keeton [35]. The equation of state used by NETFLOW is based on the Able-Nobel real gas model developed by Chenoweth [30]. This means that the sum of NETFLOW-predicted masses upstream and downstream of the valve should never be better than 1.03%. At the end of the transfer the predicted total mass is approximately .99% greater than the measured total mass. The decrease in the deviation between predicted and measured total mass can be explained by the small amount of measured mass (~.4%) that was accumulated as a result of experimental errors. We can conclude that the small errors in predicting upstream and downstream masses are due in large part to the NETFLOW equation of state and not the errors predicting temperature and pressure which are apparent in Figures 13-16.

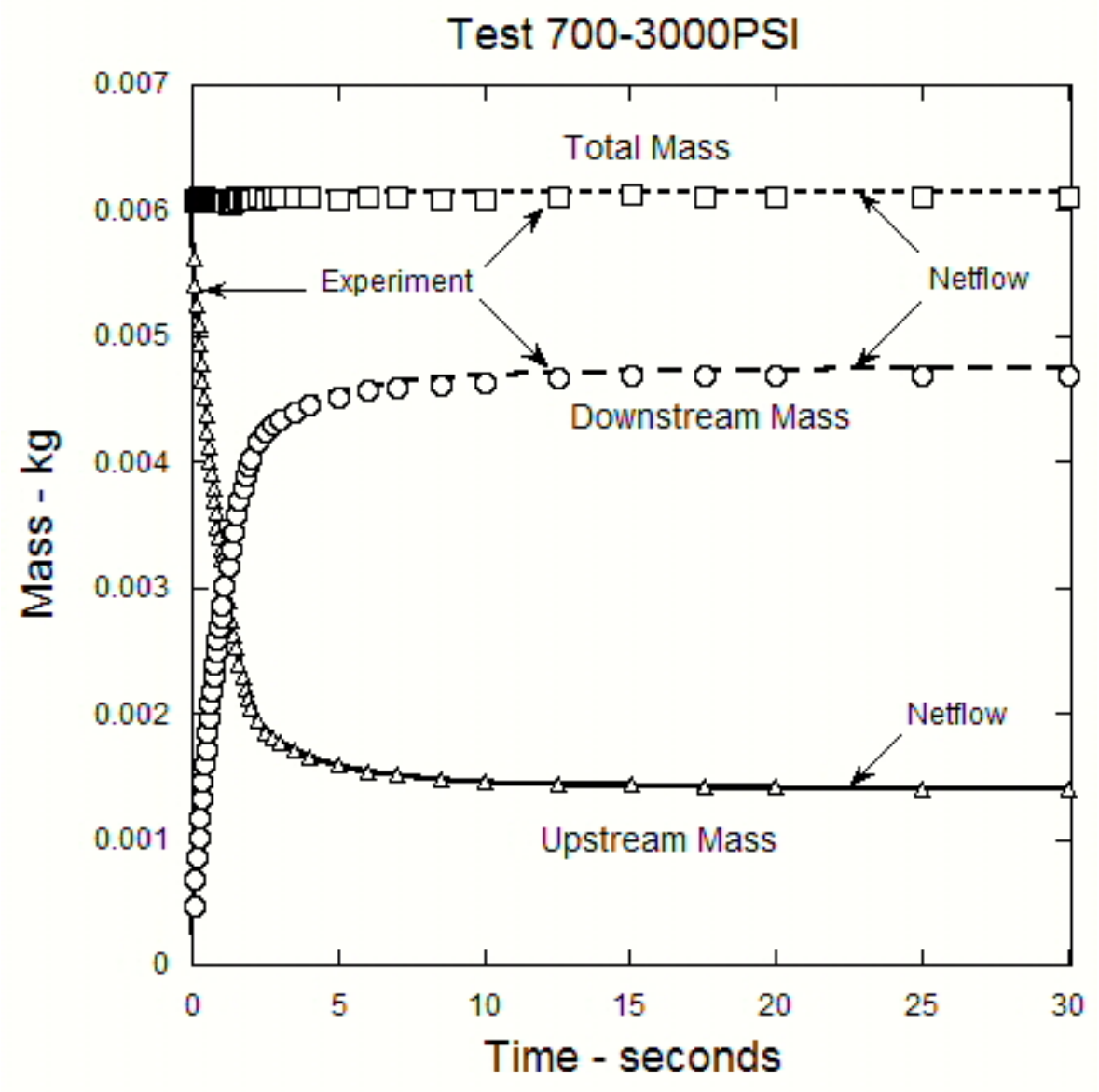

Figure 40. Measured and predicted masses upstream and downstream of the valve and total mass for Test 700-3000PSI.

Figure 41 shows measured and predicted mass inventories upstream and downstream of the valve for Test 90-6000PSI. Also shown are the total predicted and measured masses. At time zero the measured total mass computed using FILLUP is 1.4% lower than that computed by NETFLOW. The larger difference (compared to 1.03% for Test 700-3000PSI) is due to the increased supply pressure (from 3000 to 6000 PSI). It is apparent from Figure 41 that the predicted mass inventories upstream and downstream of the valve are slightly over predicted by NETFLOW. At the end of the transfer (30 seconds) the predicted mass upstream of the valve is .67% greater than the measured values. On the downstream side the predicted mass is 3.14% greater than the measurement. In this case

it appears that the larger error in predicted downstream mass inventory may be due to inherent errors in the equation of state and an inability to precisely predict the temperature in the receiver. The predicted final receiver temperature is 6 K lower than the measurement (see Figure 31). The decreased temperature would cause a corresponding increase in receiver gas density which along with the equation of state errors could result in the observed 3.14% mass error.

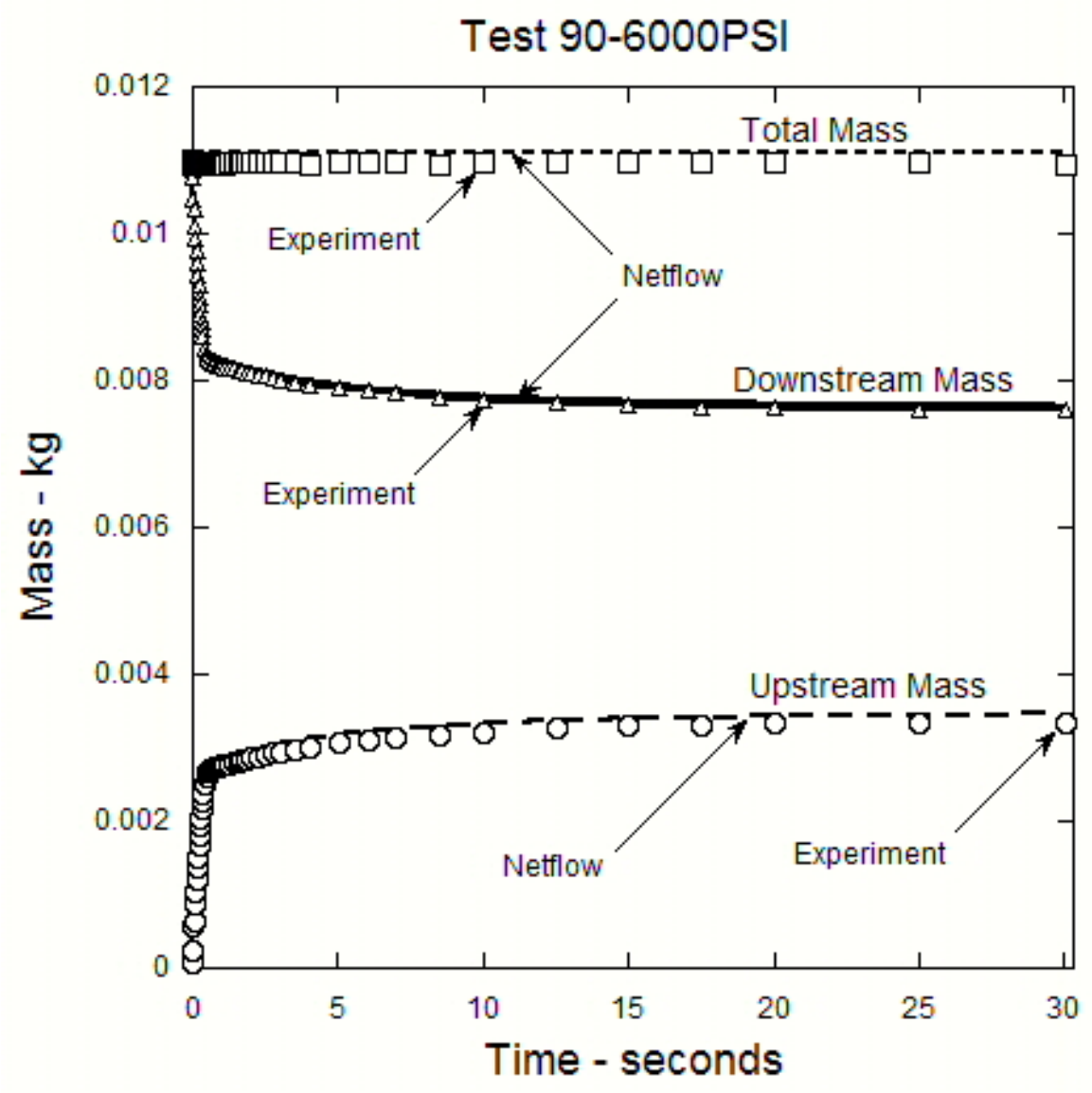

Figure 41. Measured and predicted masses upstream and downstream of the valve and total mass for Test 90-6000PSI.

6. MULTIDIMENSIONAL MODELING OF THE SUPPLY/RECEIVER TRANSFER

6.1 Introduction

In this chapter we validate CFD models against some of the transient PVT data obtained from the present work (Part I) and from similar work performed by Clark and Libkind [26]. The application of CFD to high pressure supply/receiver transfer problems is relatively new. It is only made possible through the advent of massively parallel computer software and hardware. These problems present significant computational challenges since they are by nature transient, three-dimensional, turbulent and compressible with large pressure ratios and regions of transonic flow. Furthermore they encompass geometries that vary several orders of magnitude in dimension, *(e.g.* relatively large vessels transferring gas through tiny holes).

As mentioned in Chapter 3, Sandia has recently completed a multi-year ASC V&V project to validate FUEGO and coupled FUEGO/NETFLOW compressible flow models. The calculations presented here are a result of that effort. While we have demonstrated the feasibility of applying CFD to gas transfer problems, there is still more work to be done. Our efforts have uncovered a number of computational issues that must be addressed by ASC code developers and modelers before CFD can fully replace network flow modeling as the go-to analysis tool for gas transfer problems.

In Chapter 6.2 we compare FUEGO stand-alone calculations to the data of Clark and Libkind [26]. The supply-to-receiver pressure ratio was relatively low, thus allowing both the supply and receiver volumes to be simulated with FUEGO. Often pressure ratios commonly encountered in applications that store and dispense gases are too large to model using FUEGO or any similar commercial code (*e.g.* CFX, FLUENT, FIDAP, etc.) without making simplifying approximations. The Mach numbers encountered upstream of shocks and expansion waves in the transonic flow of underexpanded receiver jets are large and result in either unstable calculations or prohibitively long computational times. These problems can be overcome by isolating the CFD regions from transonic flow. This is the motivation behind coupling NETFLOW to FUEGO. NETFLOW easily handles choking and unchoking of compressible flow in tubing permitting predominantly one-dimensional transonic flow to be computed by NETFLOW and multidimensional subsonic or near sonic flow to be calculated by FUEGO. Some geometry compromises may be necessary such as providing a larger than actual hole diameter for receiver inlets but the continuity of mass and energy flows into the receiver are not affected.

Chapters 6.3 through 6.6 present a series of mostly coupled FUEGO/NETFLOW calculations. Chapter 6.3 documents a supply simulation with FUEGO for TEST 700-3000PSI. In Chapter 6.4, supply blowdown calculations with FUEGO are compared to a Bird, Stewart and Lightfoot (BSL) analysis [36] for tank blowdown. This verification problem tests the NETFLOW “linking” or “coupling” mass flow boundary condition. A similar verification is performed in Chapter 6.5 for a constant pressure boundary

condition at the supply exit. Chapter 6.6 documents a supply simulation for TEST 700-300PSI.

6.2 FUEGO Simulation of Clark-Libkind Test

Clark and Libkind [26] conducted a transient PVT experiment for helium blowdown of a 201 cc supply vessel. Transient pressure and mass averaged temperature were measured as the vessel was evacuated through a .020 inch diameter orifice into a 14700 cc receiving vessel. Only the 201 cc vessel was instrumented for transient PVT. Conditions of the test are summarized below:

Ambient Temperature:	295K
Initial Supply Pressure:	13.68×10^6 Pa (1986 PSIA)
Initial Receiver Pressure:	6.84×10^6 Pa (992 PSIA)

Although a series of tubes and valves were used to connect the supply to the receiver, the predominant pressure loss in the flow path was the .020 inch diameter orifice. The relatively low pressure ratio (2:1) for the experiment and the fact that the helium could be modeled as an ideal gas made it possible to simulate this experiment using FUEGO. Figure 42 shows the computational mesh that was used. The flow path between the reservoir and the receiver was simulated using a smooth transition that was .020 inches in diameter. Figure 43 shows the FUEGO-computed temperature distribution in the supply at 2.0 seconds which is shortly after pressure equilibrium was attained in the transfer. As discussed in Chapter 4, gas velocities in the supply are expected to be extremely low and heat transfer is likely to be dominated by free convection. These observations are supported by the FUEGO calculations. Figure 43 is similar to Figure 6 in Chapter 4.3.

The computed supply pressure and mass averaged temperature are compared to the transient PVT measurements in Figures 44 and 45 respectively. The temperature data shown in Figure 45 shows that the minimum temperature achieved in the supply is 237 K or 58 K less than the wall/ambient temperature. For that temperature difference and the equilibrium pressure, the Rayleigh number (see *e.g.* Equation 5.8) in the supply is 3.7×10^8 which lies at the transition between laminar and turbulent free convection.

The two curves shown in Figures 44 and 45 are for laminar flow and turbulent flow. The SST turbulence model [37] was used to make the turbulent flow calculations. This model was recently added to FUEGO and utilizes the $\kappa - \omega$ turbulence formulation near the wall and the $\kappa - \varepsilon$ formulation away from the wall. One of the greatest advantages of the SST model is that special meshing constraints need not be imposed to avoid violating the law-of-the-wall considerations [37]. The default SST parameters were used in the calculation. It should be noted that the SST model is not specifically designed to model turbulent free convection and would be more appropriate for the early stages of reservoir fill-up when forced convection is likely to play a greater role. For this problem the model results for the supply are in good agreement with the data and are also in good agreement with the laminar results; agreement with the latter is expected since the computed Rayleigh number of 3.7×10^8 corresponds to transitional flow.

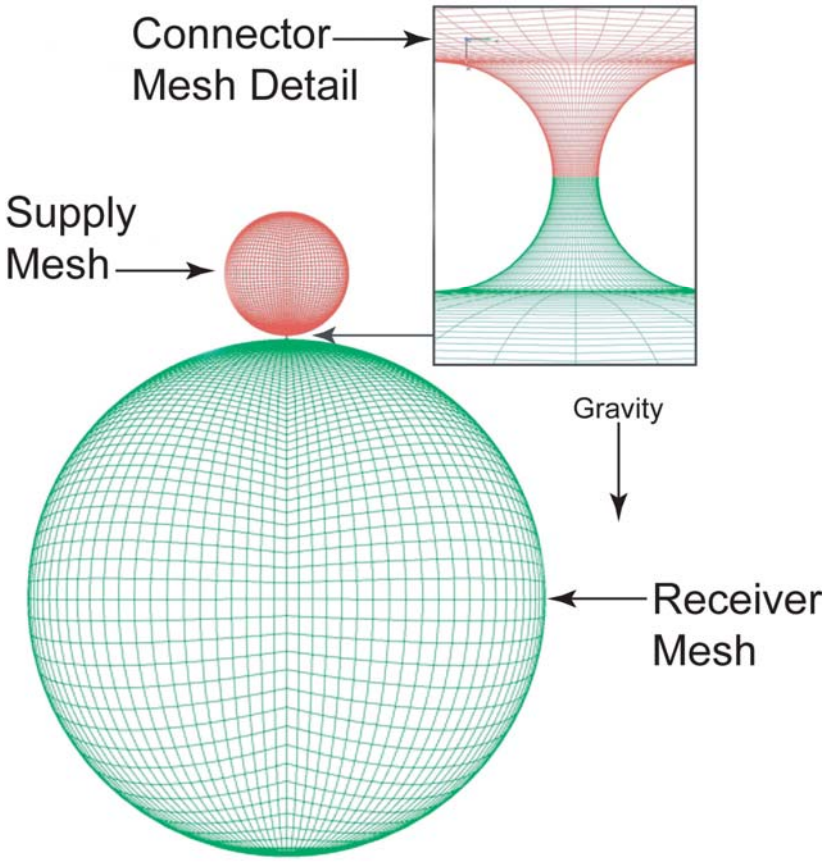

Figure 42. FUEGO mesh for the Clark-Libkind problem.

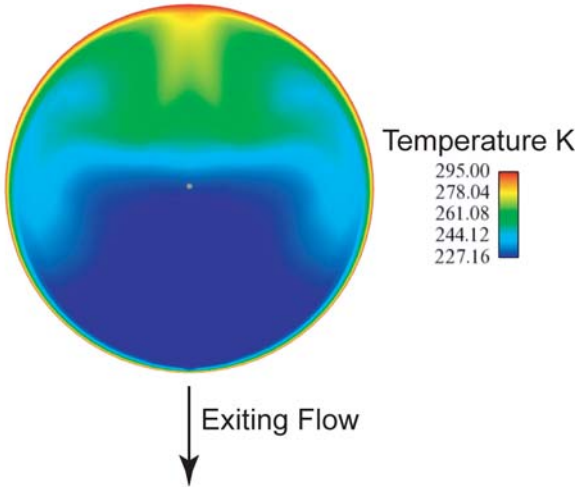

Figure 43. FUEGO-computed temperature distribution in the supply at t=2.0s.

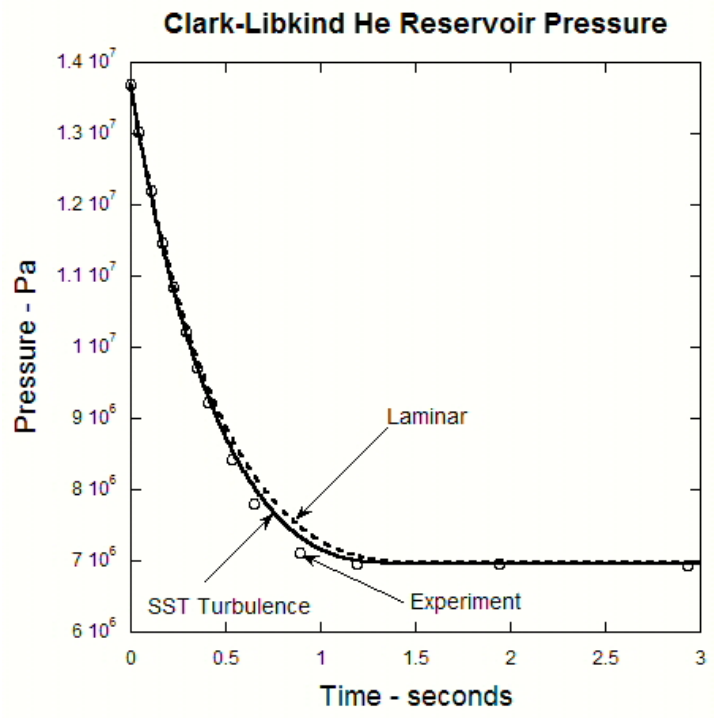

Figure 44. Measured and predicted supply pressure transient.

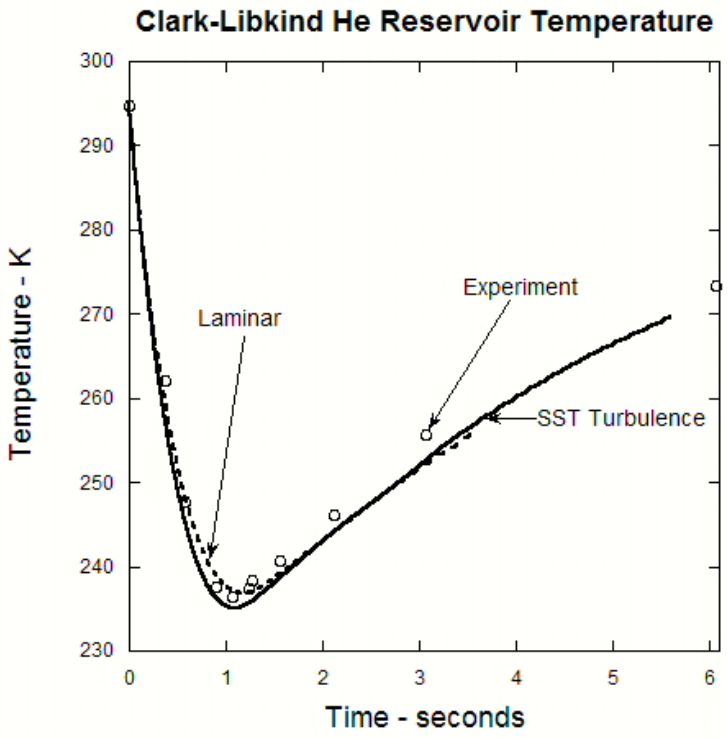

Figure 45. Measured and predicted supply temperature transient.

6.3 Coupled FUEGO/NETFLOW Simulation of Test 700-3000PSI

As mentioned in the introduction, development of compressible flow capabilities in FUEGO and the coupling of FUEGO to NETFLOW have enabled coupled simulations of mass, heat, and momentum transport in a complete gas transfer system consisting of a supply, a receiver, and the connecting piping to be made for the first time.

FUEGO/NETFLOW coupling occurs at a linking node in the NETFLOW network where velocity, temperature, and pressure computed in FUEGO are used as Dirichlet boundary conditions in NETFLOW. NETFLOW is used to compute the mass flow mass flow rate and the linking node and returns this value to FUEGO so that it can be used as a mass flow boundary condition. Coupling occurs at every time step in the transient simulation.

Since FUEGO is still limited to mildly compressible flow (Mach number of order 1), simulating the complex flow and heat transfer in a receiver for large pressure ratios requires additional development work. However it is now possible to simulate the complete transfer between a high pressure supply and a low pressure receiver using FUEGO to simulate the flow and heat transfer in the supply coupled with NETFLOW to simulate the flow and heat transfer in the connecting piping and the receiver. The results presented here are for such a configuration.

At a pressure of 3000 psi and ambient temperature there is a moderate departure from the ideal gas equation of state (EOS) (e.g., the density of helium is about 10% less than that predicted by the ideal gas EOS). To enable gas transport predictions at higher pressure where the ideal gas EOS is not accurate, the Abel-Noble EOS was implemented in FUEGO. This was accomplished using user-supplied subroutines.

Test 700-3000PSI was chosen for validation of the new predictive capabilities: (1) FUEGO compressible flow algorithm, (2) Abel-Noble EOS via user subroutines, and (3) FUEGO/NETFLOW coupling. In this Test, a 200 cc supply initially filled with helium at 3000 psi was connected via a 0.02” ID orifice, some short lengths of tubing, and a valve to a 700 cc receiver initially containing helium at 1 atm, all at ambient temperature initially. The volumes, initial pressures, and initial temperature stated in the last sentence are all approximate; see Appendix B in this report for detailed conditions. In the coupled simulation FUEGO was used to simulate the supply and NETFLOW was used to simulate the piping network and the receiver. The coupling between FUEGO and NETFLOW occurs at a linking node where the state of the gas (pressure and temperature) and the velocity are passed from FUEGO to NETFLOW where this information is used to compute the mass flow rate in the piping network and into the receiver. This mass flow rate is then passed back to FUEGO, completing the coupling. The coupling occurs at every time step in the transient simulation.

A sensitivity study was undertaken in which convergence and model parameters in FUEGO were varied, including the number of non-linear iterations, the maximum mesh CFL criterion, the maximum time step, under-relaxation factors, laminar vs. turbulent flow, and Abel-Noble vs. ideal gas EOS. Comparisons were made between the predicted

and measured time variation of the bulk (mass averaged) temperature in the supply; selected results are shown in Figure 46.

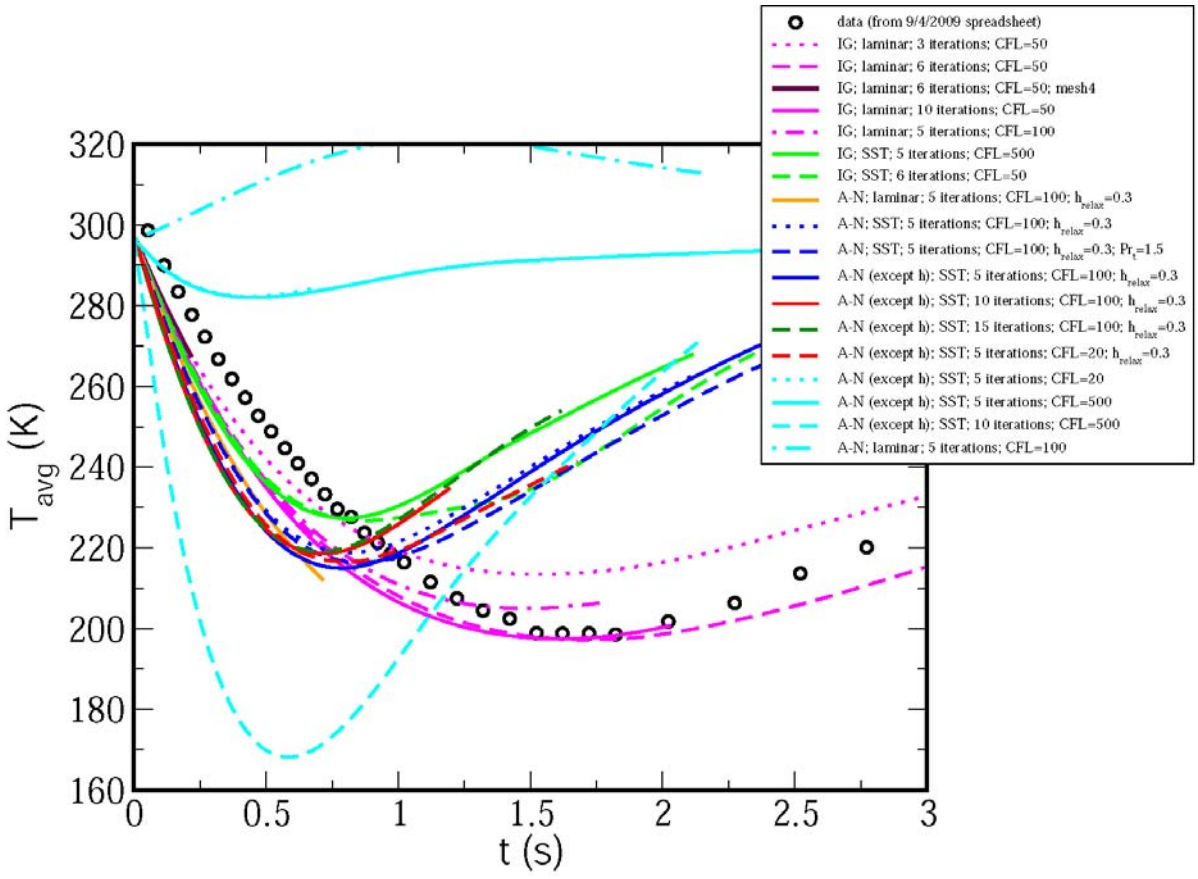

Figure 46. Predicted and measured bulk temperature in the supply for Test 700-3000PSI; initial temperature is 296.5 K.

Although there are obvious problems with a few of the results which will be discussed later, the initial assessment of the results is that the laminar model yielded bulk temperatures that tracked the data reasonably well (note the magenta curves in Figure 46) and the SST turbulence model gave results that appeared to have too much heat transfer (the predicted bulk temperature minimum value was larger than the measured value and occurred earlier in time; e.g., green and blue curves in Figure 46). Except for the flow in the immediate vicinity of the outlet, the flow in the supply is likely to be laminar initially, transitioning to turbulent buoyant convection at later time. The SST turbulence model is a recent implementation in FUEGO; this model is tuned for forced convection; research is necessary to assess and perhaps modify the turbulence parameters in this model for buoyant turbulent convection. Results showed that at least 5 to 6 nonlinear iterations were required for convergence for most of the CFL parameter values used in this study. A maximum mesh CFL criterion of 100 appeared to be adequate provided the equations were converging; use of a CFL parameter value of 500 resulted in poor convergence typically; little relaxation was required except for the energy equation when using the

Abel-Noble equation of state (e.g., note poor results of cyan curves which had no relaxation of energy equation).

All FUEGO/NETFLOW results show pressure in the supply decreasing faster than the experimental data initially, then leveling off and crossing the data and reaching an equilibrium pressure either equal to or greater than the data (cf. Figure 47). One exception is the result from the calculation with the Abel-Noble EOS and no relaxation of the energy equation as shown in Figure 47. Since NETFLOW can simulate the pressure transients within both supply and receiver for this problem (cf. Figures 16-19), the results of Figure 47 point to problems in either FUEGO (e.g., compressible flow algorithm and/or Abel-Noble EOS) or the FUEGO/NETFLOW coupling algorithm.

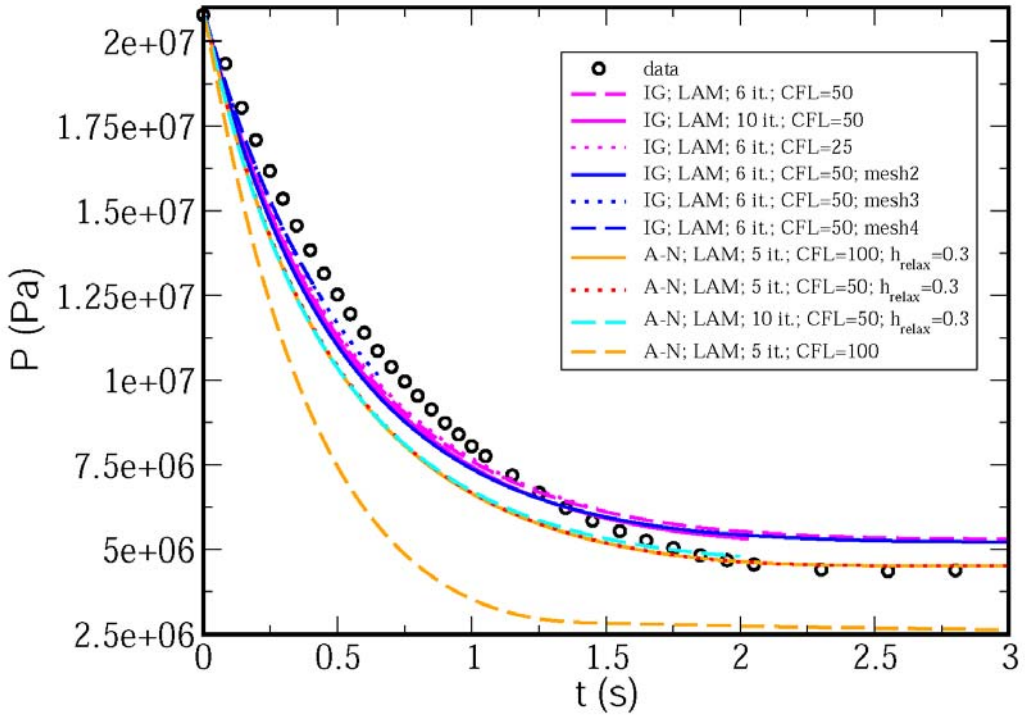

Figure 47. Predicted (at center of supply) and measured pressure in the supply for Test 700-3000PSI.

6.4 FUEGO Simulation of Blowdown of 3000 PSI Supply with Specified Mass Flow Rate Boundary Condition (BSL Verification Problem)

The unsatisfactory results shown above for the supply pressure (cf. Figure 47) and bulk temperature (cf. Figure 46) using coupled FUEGO/NETFLOW for Test 700-3000PSI in which FUEGO was used to simulate the gas transfer from the supply and NETFLOW was used to simulate the gas transfer through the piping and into the receiver led us to examine simpler problems to look for implementation and/or code errors. As noted above, standalone NETFLOW gave good results for the time histories of pressure and

temperature in the supply; it also did a good job for the time history of pressure in the receiver. Only the early time behavior of temperature in the receiver was not predicted well by standalone NETFLOW.

In this chapter we present results from using standalone FUEGO to simulate the 3000 psi supply blowdown for a specified outflow mass flow rate of 1 g/s at the outflow hole. Since we wanted to compare the FUEGO result with known analytical solutions (Bird et al., [36]) which are for isentropic flow conditions and ideal gas, we set the supply heat transfer to zero and used CANTERA for property evaluations. We quickly discovered that for the specified mass flow rate boundary condition, standalone FUEGO predicted the time histories of pressure (cf. Figure 48) and temperature (not shown) in the supply accurately provided the equations were not relaxed. Deviations from the analytical solution were noted when the energy equation was relaxed using a relaxation factor of 0.3. We also determined that coupled FUEGO/NETFLOW gave accurate solutions for this boundary condition (not shown in Figure 48). However, when we tried running FUEGO with Abel-Noble real gas equation of state (EOS), even when setting parameter b=0, which causes the Abel-Noble EOS to reduce to ideal gas, we found large deviations from the analytical solution (compare blue and black curves in Figure 48). This behavior occurred whether FUEGO was run standalone (cf. Figure 48) or coupled to NETFLOW. We had identified a bug in the implementation of the Abel-Noble EOS in FUEGO. The strange behavior shown by the cyan curves for the supply bulk temperature in Figure 46 and the dashed orange curve for the supply pressure in Figure 47, when no relaxation was applied to the energy equation and user subroutines for the Abel-Noble EOS were being used, may be related to this problem. To our knowledge this bug, which was identified in October 2009 by D. Glaze as being related to the reference temperature used in the algorithm for extracting temperature from enthalpy, has not been fixed.

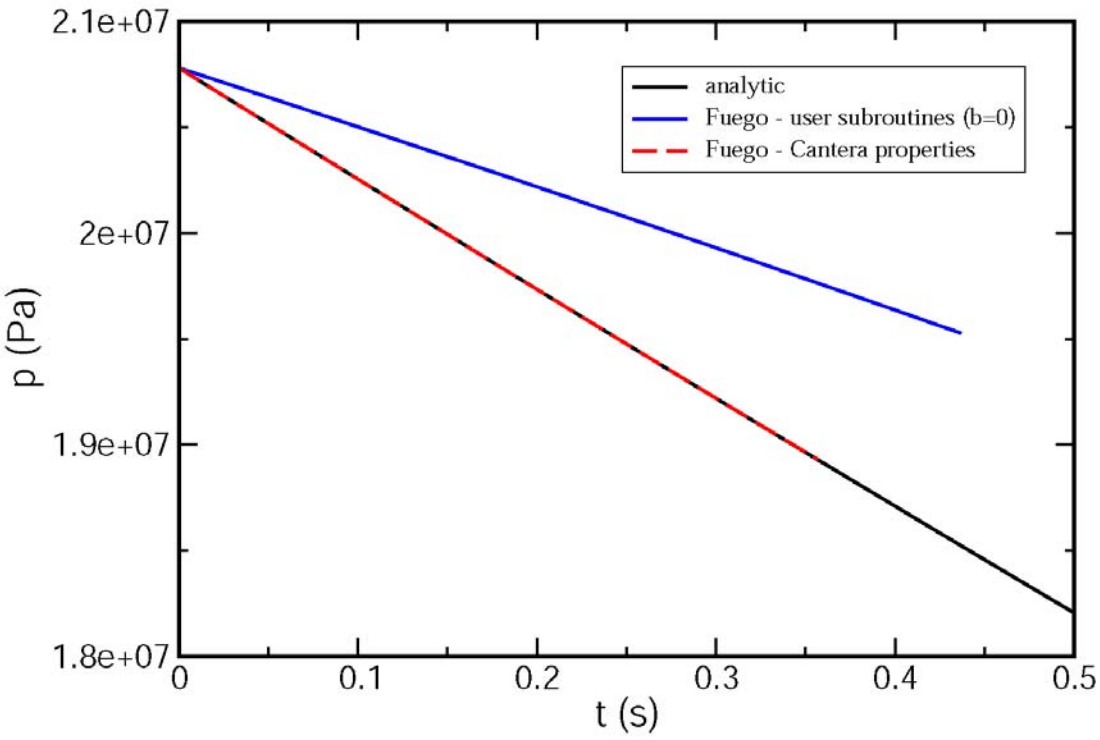

Figure 48. Pressure predicted (at center of supply) using standalone FUEGO for simulation of isentropic blowdown of 3000 psi vessel with specified outflow mass flow rate of 1 g/s; black curve is analytical solution (Winters) based on Bird et al. (1960) solution; red curve is ideal gas (CANTERA properties); blue curve (Abel-Noble properties with b=0, corresponding to ideal gas).

6.5 FUEGO Simulation of Blowdown of 3000 PSI Supply to 1 ATM Pressure Boundary Condition (BSL Verification Problem)

In the previous chapter a specified mass flow rate boundary condition in FUEGO was shown to yield the correct pressure transient when running FUEGO standalone; although not shown the same result was found in a FUEGO/NETFLOW coupled simulation which serves as verification of the coupling algorithm. We note that the Mach number at the opening for the specified mass flow rate boundary condition case discussed in the previous chapter was approximately 0.3 for the 1 g/s condition and 0.9 for the 3 g/s condition (not shown). In this chapter we present results from a coupled FUEGO/NETFLOW simulation of the 3000 psi supply blowdown to atmospheric pressure. Note that as far as FUEGO is concerned this is still a specified mass flow rate boundary condition; the network in NETFLOW includes a node with large volume at 1 atm. The results are compared with the analytical solution of Bird et al. [36] in Figure 49. The FUEGO/NETFLOW results are in excellent agreement with the analytical solution. We note that these results were generated with a single orifice in the NETFLOW network; the flow at the orifice was choked for the entire 2 seconds of the blowdown

shown in Figure 49. During the course of this study we determined that the proper method to use in coupling FUGEO and NETFLOW at the linking node was to take the state of the gas as computed by FUEGO and apply an isentropic expansion to stagnant conditions for use as the NETFLOW linking node boundary condition. Early results computed using the FUEGO solution at the linking node directly as the NETFLOW boundary condition without applying the isentropic expansion were unsatisfactory.

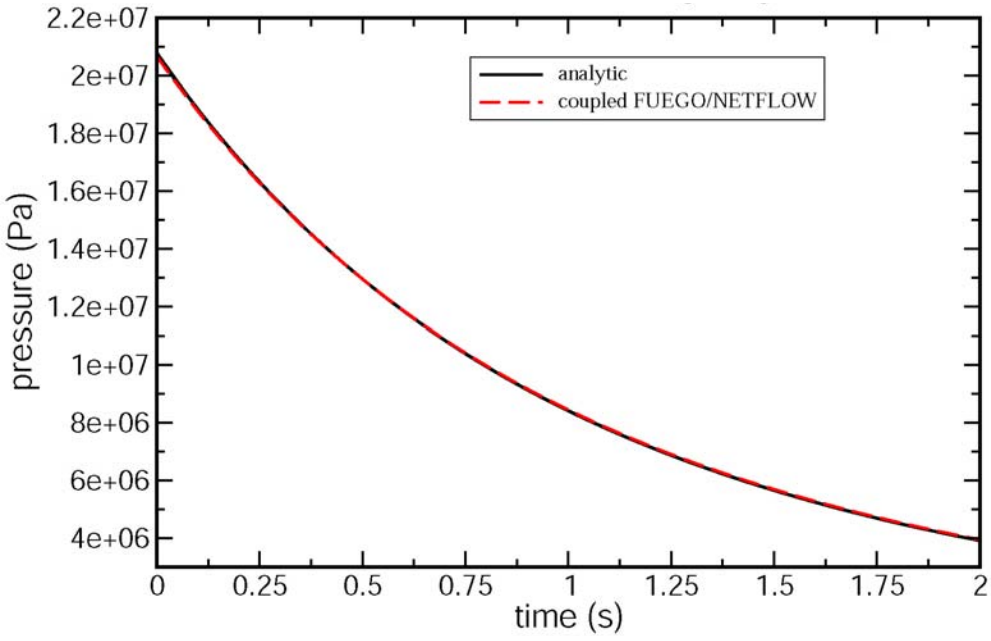

Figure 49. Pressure predicted (at center of supply) using FUEGO/NETFLOW for isentropic blowdown (initial pressure 3000 psi) to ambient pressure; ideal gas EOS in Fuego using CANTERA; black curve is analytical solution (Bird et al., 1960); dashed red curve is FUEGO/NETFLOW coupled solution result.

6.6 Coupled FUEGO/NETFLOW Simulation of Test 700-300PSI

At this point we decided to focus on the lower pressure case (300 psi initial supply pressure) and use the ideal gas EOS via Cantera properties in Fuego, thus avoiding problems associated with user subroutines and the Abel-Noble EOS. In Figures 50 and 51 we compare supply pressure and temperature, respectively, predicted by FUEGO in a coupled FUEGO/NETFLOW simulation with data from Test 700-300PSI and with a simulation where NETFLOW alone was used to simulate everything: supply, piping, and receiver. The agreement is quite good although the supply pressure predicted by coupled FUEGO/NETFLOW is slightly higher than the data and the NETFLOW result during the middle part of the blowdown (between 1 and 3 seconds in Figure 50). We note that the flow is choked for the first 1.25 seconds of the blowdown at the orifice in the NETFLOW network immediately downstream of the supply exit after which the flow is subsonic

throughout the system. The results of this simulation provide us with confidence that, at least for relatively low pressure transfer where the ideal gas EOS approximation is valid, the strategy and implementation for modeling a GTS network consisting of a supply, a receiver, and the interconnected piping, with FUEGO simulating the supply and NETFLOW simulating the receiver and the piping, is appropriate and validated. A listing of the FUGEO and NETFLOW input files for this case are given in Appendix H.

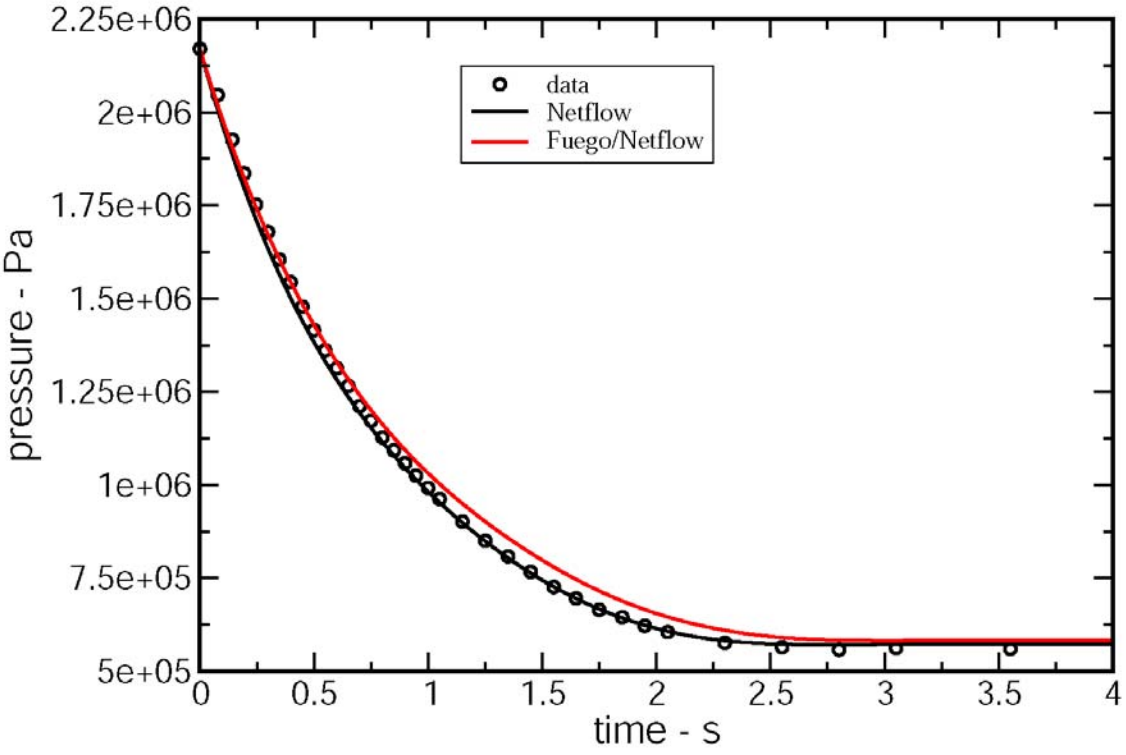

Figure 50. Predicted (with coupled FUEGO/NETFLOW and with NETFLOW alone) and measured pressure at the center of the supply for Test 700-300PSI.

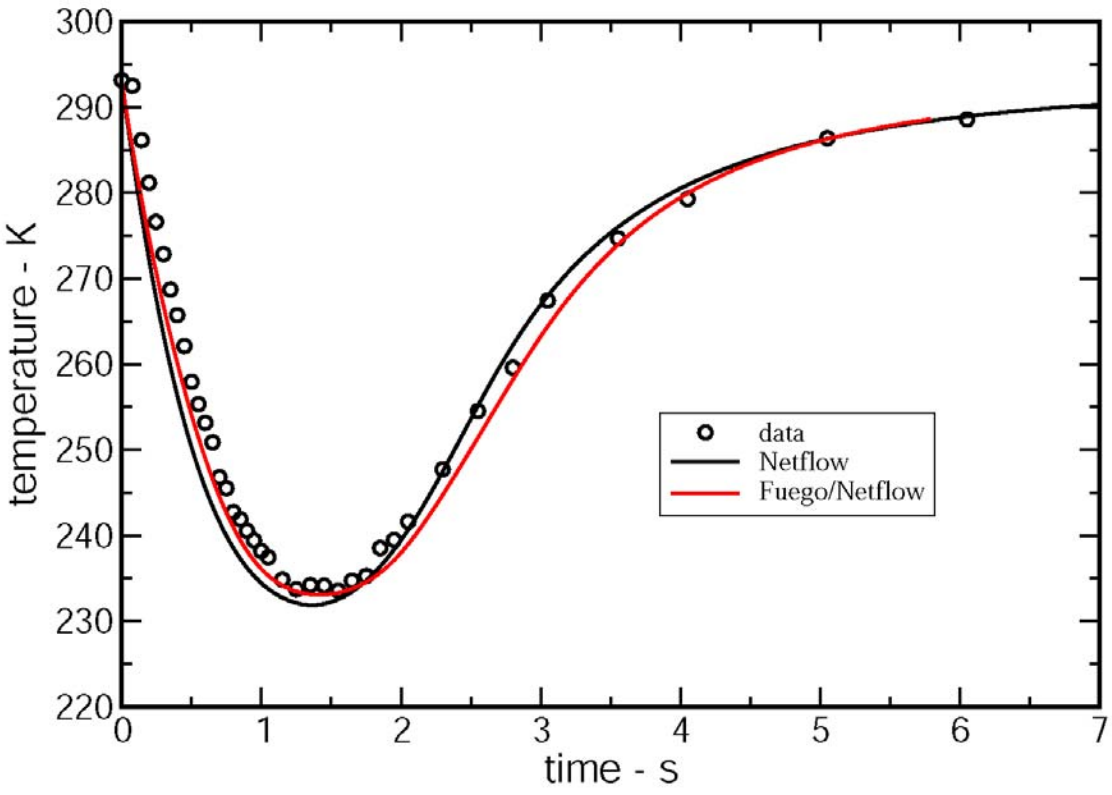

Figure 51. Predicted (with coupled FUEGO/NETFLOW and with NETFLOW alone) and measured bulk temperature in the supply for Test 700-300PSI.

7.0 SUMMARY AND CONCLUSIONS

In this chapter we provide a brief summary and conclusions. Recommendations for future work are also presented.

7.1 Summary and Conclusions

Data from transient PVT experiments discussed in Part I were utilized in this Part II Report to validate the NETFLOW computer model of gas transfer between a high pressure supply and a low pressure receiver. The transfer gas was helium, the supply volume was 200 cc, and the initial supply pressure varied from 300 psi to 6000 psi. The receiver pressure was 1 atm and the receiver volume varied from 90 cc to 13,000 cc.

The supply and receiver heat transfer correlations in NETFLOW were optimized using the transient PVT experimental data. This optimization resulted in very small changes to the presently existing free convection heat transfer correlation. The free convection correlation is the only correlation used in vessels that act as supplies. The correlation is also used to describe late-time heat transfer in vessels acting as receivers.

Significant changes were made to the receiver forced convection heat transfer correlation. This correlation is applicable to the receiver during the early stages of gas transfer and prior to the time when pressure equilibrium is achieved. With the present form of the correlation we were unable to reproduce measured temperature transients during the earliest part of the transfer even after optimizing the correlation with the data. However at later times as free convection became the dominate mechanism for heat transfer our NETFLOW models predicted measured temperatures.

A strategy for coupling the CFD code FUEGO with the network flow code NETFLOW was developed. This coupling takes advantages of the most useful features of each code. Modeling the three-dimensional space in the vessel using FUEGO permits the direct calculation of vessel heat transfer without relying on correlations which may be limited in their application. Use of NETFLOW to model the interconnecting tube provides a means of quickly and accurately modeling the pressure driven flow in the tubing while at the same time isolating the FUEGO computational domains from transonic flow.

FUEGO/NETFLOW coupling occurs at a linking node where velocity, temperature, and pressure computed in FUEGO are used as Dirichlet boundary conditions in NETFLOW. NETFLOW is used to compute the mass flow rate at the linking node, and returning this value to FUEGO so that it can be used as a mass flow boundary condition. Coupling occurs at every time step in the transient simulation.

The FUEGO/NETFLOW coupling algorithm was verified by comparing FUEGO and FUEGO/NETFLOW solutions to the analytical solution given in Bird et al. [36] for isentropic blowdown of a pressure vessel to ambient pressure or blowdown with a fixed mass flow rate boundary condition.

FUEGO/NETFLOW coupling was validated against an experiment using transient PVT data from the high precision Test 700-300PSI. FUEGO was used to model the supply space and NETFLOW was used to model the receiver and interconnecting tubing

Results from the above FUEGO/NETFLOW simulation of heat transfer in the supply were in excellent agreement with the data. Furthermore, these calculations demonstrated that the predominant mode of heat transfer in supplies is free convection.

Preliminary calculations for receiver heat transfer during Test 700-300PSI were made using FUEGO/NETFLOW. In this simulation NETFLOW was used to simulate the supply and interconnecting tubing and FUEGO was used to simulate the receiver. This simulation demonstrated the complex nature of the flow and heat transfer in the receiver at early time.

7.2 Recommendations for Future Work

1. Abel-Noble equation of state implementation bug in FUEGO.

The ideal gas EOS is not accurate for gas transfer at pressures exceeding 3000 psi. For problems of interest the Abel-Noble EOS enables accurate simulation of real gas effects. During the course of this work we identified a problem with the recent implementation of the Abel-Noble EOS via user subroutines in FUEGO. To our knowledge this bug, which was identified in October 2009 by D. Glaze as being related to the reference temperature used in the algorithm for extracting temperature from enthalpy, has not been fixed.

2. Simulation of high pressure receivers.

Once a high pressure equation of state is available in FUEGO, coupled FUEGO/NETFLOW can be validated against the remaining high precision transient PVT experiments. This is a necessary step to insure that the tool can be applied to systems in the 3000-6000 PSI pressure range.

3. SST turbulence model.

The SST turbulence model is a recent implementation in FUEGO. This model is tuned for forced convection; research is necessary to assess and perhaps modify the constants in this model for buoyant turbulent convection. This is likely to be important for modeling receiver flows.

4. Receiver flow and heat transfer modeling with coupled FUEGO/NETFLOW.

Limited work was done during this project on this very important aspect of the GTS heat transfer problem. Strategies must be tested for handling the high Mach number under-expanded jet that enters the receiver during the initial part of the transfer as well as the highly transient nature of the flow and heat transfer throughout the transfer process. The work on this problem discussed in this report shows the complexity of the transport.

Options to explore include (a) expand the receiver inlet hole size with a model of the under-expanded jet to enable compressible subsonic receiver calculations to be made with FUEGO; (b) use actual jet conditions entering the receiver and solve receiver flow and heat transfer problem with incompressible FUEGO and a time-dependent thermodynamic pressure option.

5. Coupled FUEGO/NETFLOW restart capability.

FUEGO/NETFLOW restart capability appeared to function as designed for cases in which FUEGO was being used to model the supply volume. In the closing weeks of this project it was discovered calculations cannot be restarted for cases in which FUEGO is modeling the receiver. This bug needs to be addressed.

6. Simulation of all vessels using FUEGO/NETFLOW.

It should now be possible to model an entire gas transfer system using coupled FUEGO/NETFLOW. However because of limitations mentioned above, this capability was not demonstrated for high pressure systems. The first step toward accomplishing this goal is to simulate all of the high pressure transient PVT tests using FUEGO to model both the supply and receiver. Once this is done the tool will be ready to model more complex systems.

REFERENCES

[1] S. F. Rice, N. J. Paradiso and T. G. Felver, W. S. Winters and G. H. Evans, "Transient PVT Measurements and Modeling Predictions for Vessel Heat Transfer – Part II," Sandia Technical Report, SAND2010-XXXX, Sandia National Laboratories, Livermore, CA, In preparation.

[2] W. S. Winters, "Implementation and Validation of the NETFLOW Porous Media Model, " Sandia Technical Report, SAND2009-6838, Sandia National Laboratories, Livermore, CA, December 2009.

[3] W. S. Winters, "TOPAZ-A Computer Code for Modeling Heat Transfer and Fluid Flow in Arbitrary Networks of Pipes, Flow Branches and Vessels, " SAND83-8253, Sandia National Laboratories, Livermore, CA, January, 1984.

[4] C. M. Allison, R. J. Wagner, L.J. Siefken and J. K Hororst, "The Development of RELAP5/SCDAPSIM/MOD4.0 for Reactor System Analysis and Simulation," *Proceedings of the 7th International Conference on Nuclear Option in Countries with Small and Medium Electricity Grids*", Dubrovnik, Croatia, Paper Ref. No. S-05.01, May 25-29, 2008.

[5] "RETRAN-02- A program for Transient Thermal-Hydraulic Analysis of Complex Fluid Flow Systems, Volume 1: Equations and Numerics," NP-1850-CCM, Volume 1 Research Project 889, Electric Power Research Institute, Palo Alto, CA, May 1981.

[6] W. S. Winters, "Dynamic Modeling of Solar Central Receivers," Sandia Technical Report, SAND81-8213, Sandia National Laboratories, Livermore, CA, July 1981.

[7] W. S. Winters, "DRAC- A User Friendly Computer Code for Modeling Transient Thermohydraulic Phenomena in Solar Receiver Tubing," Sandia Technical Report, SAND82-8744, Sandia National Laboratories, Livermore, CA, January 1983.

[8] W. S. Winters, "TOPAZ-The Transient One-Dimensional Pipe Flow Analyzer: User's Manual," Sandia Technical Report SAND85-8215, July, Sandia National Laboratories, Livermore, CA, 1985.

[9] W. S. Winters, "TOPAZ-The Transient One-Dimensional Pipe Flow Analyzer: Code Validation and Sample Problems," Sandia Technical Report SAND85-8236, Sandia National Laboratories, Livermore, CA, October, 1985.

[10] W. S. Winters, "TOPAZ-The Transient One-Dimensional Pipe Flow Analyzer: Equations and Numerics," Sandia Technical Report SAND85-8248, Sandia National Laboratories, Livermore, CA, December, 1985.

[11] W. S. Winters, "TOPAZ-The Transient One-Dimensional Pipe Flow Analyzer: An Update on Code Improvements and Increased Capabilities," Sandia Technical Report SAND87-8225, Sandia National Laboratories, Livermore, CA, September, 1987.

[12] W. S. Winters, "A New Approach to Modeling Fluid/Gas Flows in Networks," Sandia Technical Report, SAND2001-8422, Sandia National Laboratories, Livermore, CA, July 2001.

[13] L. R. Petzold, P. N. Brown, A. C. Hindmarsh, and C. W. Ulrich, "DDASKR – Differential Algebraic Solver Software," Center for Computational Science & Engineering, L-316, Lawrence Livermore National Laboratory, P.O. Box 808, a private communication with L. R. Petzold.

[14] L. F. Moody, "Friction Factors for Pipe Flow," *Trans. ASME, volume 66*, No. 8 p. 671, 1944.

[15] F. W. Dittus and L. M. K Boelter, *University of California (Berkeley) Pub. Eng. Volume 2*, p. 443, 1930.

[16] C. S. Landram, "Heat Transfer during Vessel Discharge: Mean and Fluctuating Gas Temperature," *Journal of Heat Transfer*, February 1973.

[17] S. C. Johnston and H. A. Dwyer, "Thermal Instabilities in Discharging Gas Reservoirs," *Journal of Heat Transfer*, August, 1976.

[18] S. Paolucci, "Heat Transfer During the Early Expansion of Gas in Pressurized Vessels," *International Journal of Heat and Mass Transfer, 28*, No. 8, pp. 1525-1537, 1985.

[19] R. Greif, T. Namba, and M. Nikanham, "Heat Transfer During Piston Compression Including Side Wall and Convection Effects," *International Journal of Heat and Mass Transfer*, **22**, pp. 901-907, 1978.

[20] R. D. Ulrich, D. P. Wirtz and R. H. Nunn, "Transient Heat Transfer in Closed Containers after Gas Injection," *Transactions of the ASME, Journal of Heat Transfer*, pp 461-463, August, 1969.

[21] W. C. Reynolds and W. M. Kays, "Blowdown and Charging Processes in a Single Gas Receiver with Heat Transfer," *Proc. On Heat Conduction Charts*, Annual Meeting of Heat Transfer Division of ASME, New York, N. Y., December 1-6, 1957.

[22] Lyons III, J. T., "Heat Transfer Considerations in a Pressure Vessel Being Charged," MS thesis, Mechanical Engineering, Naval Postgraduate School, Monterey, CA, June, 1969.

[23] Means, J. D., and Ulrich, R. D., "Transient Convective Heat Transfer During and After Gas Injection Into Containers," *J. Heat Transfer*, pp. 282-287, May, 1975.

[24] S. C. Johnston and H. A. Dwyer, "Bulk Gas Temperature Measurement During Vessel Discharge using Transient PVT," *Rev. Sci. Instruments*, **46,** No. 12, December 1975.

[25] M. Clement and C. B. Desormes, *J. Phys.* (Paris), **89**, p 321, 1819.

[26] G.L. Clark, "A Zero-Dimensional Model of Compressible Gas Flow in Networks of Pressure Vessels – Program TRIC," Sandia Technical Report SAND83-8226, Sandia National Laboratories, Livermore, CA, July, 1983.

[27] S. Charton, V. Blet and J.P. Corriou, "A Simplified Model for Real Gas Expansion Between Two Reservoirs Connected by a Thin Tube," *Chemical Engineering Science*, **51**, pp. 295-308, 1996.

[28] M. Monde, Y. Mitsutake, P. L. Woodfield and S. Maruyama, "Characteristics of Heat Transfer and Temperature Rise of Hydrogen during Rapid Hydrogen Filling at High Pressure," *Heat Transfer-Asian Research, Vol. 36*, No. 1, 2007.

[29] T. Terada, H. Yoshimura, Y. Tamura, H. Mitsuishi and S. Watanabe, "Thermal Behavior in Hydrogen Storage Tank for FCV on Fast Filling (2nd Report)," SAE Technical Paper 2008-01-0463, 2008 World Congress, Detroit, MI, April 14-17, 2008.

[30] D. R. Chenoweth, "Gas-Transfer Analysis Section H- Real Gas Results vis the van der Waals Equation of State and Virial Expansion Extension of its Limiting Abel-Noble Form," Sandia Technical Report SAND83-8229, Sandia National Laboratories, Livermore, CA, June, 1983.

[31] L. Burmeister, L., *Convection Heat Transfer, Second Edition*, John Wiley & Sons, Inc., NY,1993.

[32] Henkes, R., 1990, *Natural-Convection Boundary Layers*, PhD Thesis, Tech. U. of Delft.

[33] T. D. Plantenga, "HOPSPACK 2.0 User Manual," Sandia Technical Report SAND2009-6265, Sandia National Laboratories, Livermore, CA, October 2009.

[34] M. F. Hardwick, "FILLUP – An Equation-of-State Calculator for Mixtures of Hydrogen and Helium Isotopes," Version 1.0, Sandia National Laboratories, mfhardw@sandia.gov, March 2004.

[35] S. C. Keeton, Classified Sandia Report, SAND76-8240, Sandia National Laboratories, Livermore, California, July 1976.

[36] Bird, R. B., Stewart, W. E., and Lightfoot, E. N., *Transport Phenomena*, John Wiley & Sons, Inc., pp. 480-482, 1960.

[37] F. R. Menter, M. Kuntz and R. Langtry, "Ten Years of Industrial Experience with the SST Turbulence Model," *Turbulence, Heat and Mass Transfer*, K. Hanjalic, Y. Nagauno and M Tummers (Editors), Begell House, Inc., 2003.

[38] W. S. Winters, "Modeling Vessel Fillup and Blowdown," Sandia Technical Report, SAND2009-0100, Sandia National Laboratories, Livermore, CA, January 2009.

APPENDIX A

```
! 04_29_09_200-700_300psi
! Netflow stand alone simulation of GTS Test
! Initial supply pressure=2.170452E+06 Pa
! Initial receiver pressure=9.997315E+04 Pa
! Effective supply volume=189.87 cc
! Effective receiver volume=657.67 cc
! Initial temperature 293.05 K

NODE=1 !SUPPLY
  VOLUME=189.87E-6
  HEAT TRANSFER=COMBINED
NODE=2 !RECEIVER
  VOLUME = 657.67E-6
  HEAT TRANSFER=COMBINED
PATH=1 !ISENTROPIC ORIFICE
  TYPE=ISENTROPIC
  UPSTREAM NODE=1
  DOWNSTREAM NODE=3
  DIAMETER=5.08E-4 !0.02 INCH DIA
  LENGTH=.0001
PATH=2 !NPT ADAPTOR
  TYPE=TUBE
  UPSTREAM NODE=3
  DOWNSTREAM NODE=4
  DIAMETER=1.5875E-2  !0.625 INCH DIA
  LENGTH=9.525E-3     !0.375 INCH LENGTH
  HEAT TRANSFER=DITTUS_BOELTER
PATH=3 !THIN WALL PORT CONNECTOR
  TYPE=TUBE
  UPSTREAM NODE=4
  DOWNSTREAM NODE=5
  DIAMETER=7.63E-3   !0.300 INCH DIA
  LENGTH=2.667E-2     !1.05 INCH LENGTH
  HEAT TRANSFER=DITTUS_BOELTER
PATH=4 !ADAPTORS VALVE & INTERNALS
  TYPE=TUBE
  UPSTREAM NODE=5
  DOWNSTREAM NODE=6
  DIAMETER=6.35E-3   !.25 INCH DIA
  LENGTH=5.900E-2    !2.323 INCH LENGTH
  HEAT TRANSFER=DITTUS_BOELTER
PATH=5 !BALL VALVE
  TYPE=TUBE
  UPSTREAM NODE=6
  DOWNSTREAM NODE=7
  DIAMETER=4.7499E-3   !.187 INCH DIA
  LENGTH=1.27E-2       !.500 INCH LENGTH
  TOPEN=0.0
  DTOPEN=.001
  HEAT TRANSFER=DITTUS_BOELTER
PATH=6 !ADAPTORS VALVE & INTERNALS
  UPSTREAM NODE=7
  DOWNSTREAM NODE=8
  DIAMETER=6.35E-3 !0.25 INCH DIA
```

```
  LENGTH=6.223E-2  !2.45 INCH LENGTH
  HEAT TRANSFER=DITTUS_BOELTER
PATH=7 !THIN WALL PORT
  UPSTREAM NODE=8
  DOWNSTREAM NODE=9
  DIAMETER=7.62E-3 !0.3 INCH DIA
  LENGTH=2.667E-2  !1.05 INCH LENGTH
  HEAT TRANSFER=DITTUS_BOELTER
PATH=8 !ADAPTOR
  UPSTREAM NODE=9
  DOWNSTREAM NODE=10
  DIAMETER=1.5875E-2 !0.625 INCH DIA
  LENGTH=1.4275E-2  !0.562 INCH LENGTH
  HEAT TRANSFER=DITTUS_BOELTER
PIPE=1 !INTEGRAL TUBE
  NUMP=2
  UPSTREAM NODE=10
  DOWNSTREAM NODE=2
  DIAMETER=2.54E-3 !0.100 INCH DIA
  LENGTH=3.4925E-2 !1.375 INCH LENGTH
  HEAT TRANSFER=DITTUS_BOELTER
SPECIES=1
  MIXTURE=ABELNOBLE
  NAMES=HE4
REGION=1
  LOCATIONS=1,3:6
  TEMPERATURE=293.05
  TWALL=293.05
  PRESSURE=2.170452E+06
  CONCENTRATIONS=1.0
REGION=2
  LOCATIONS=7:10,11,2
  TEMPERATURE=293.05
  TWALL=293.05
  PRESSURE=9.997315E+04
  CONCENTRATIONS=1.0
MODEL=DASKR
  DATA DUMP=NO
  SOLVE_ENERGY=YES
  INITIAL TIME STEP = .000000001
  PRINT INTERVAL = .001
  TMAX = 30.
  DTMAX=.001
  S_ATOL=1.0E-5
  S_RTOL=1.0E-5
  M_ATOL=1.0E-5
  M_RTOL=1.0E-5
  E_ATOL=1.0E-5
  E_RTOL=1.0E-5
OUTPUT=1
  NUMBER=1
  TYPE=NODE
  PROPERTY=PRESSURE
OUTPUT=2
  NUMBER=1
  TYPE=NODE
  PROPERTY=TEMPERATURE
```

```
OUTPUT=3
  NUMBER=2
  TYPE=NODE
  PROPERTY=PRESSURE
OUTPUT=4
  NUMBER=2
  TYPE=NODE
  PROPERTY=TEMPERATURE
OUTPUT=5 ! ORIFICE MACH NUMBER
  NUMBER=1
  TYPE=PATH
  PROPERTY=MACH NUMBER
OUTPUT=6 ! ORIFICE MDOT
  NUMBER=1
  TYPE=PATH
  PROPERTY=MDOT
OUTPUT=7 ! RECEIVER INLET MACH NUMBER
  NUMBER=10
  TYPE=PATH
  PROPERTY=MACH NUMBER
OUTPUT=8 ! RECEIVER INLET MDOT
  NUMBER=10
  TYPE=PATH
  PROPERTY=MDOT
OUTPUT=9 ! SUPPLY NUSSELT NUMBER
  NUMBER=1
  TYPE=NODE
  PROPERTY=NUSSELT NUMBER
OUTPUT=10 ! RECEIVER NUSSELT NUMBER
  NUMBER=2
  TYPE=NODE
  PROPERTY=NUSSELT NUMBER
OUTPUT=11 ! SUPPLY HDATA
  NUMBER=1
  TYPE=NODE
  PROPERTY=HDATA
OUTPUT=12 ! RECEIVER HDATA
  NUMBER=2
  TYPE=NODE
  PROPERTY=HDATA
OUTPUT=13 ! SUPPLY MASS
  NUMBER=1
  TYPE=NODE
  PROPERTY=MASS
OUTPUT=14 ! RECEIVER MASS
  NUMBER=2
  TYPE=NODE
  PROPERTY=MASS
```

APPENDIX B

```
! 07_09_09_200-700_3000psi
! Netflow stand alone simulation of GTS Test
! Initial supply pressure=2.078752E+07 Pa
! Initial receiver pressure=9.997315E+04 Pa
! Effective supply volume=189.71 cc (-.11578)
! Effective receiver volume=657.67 cc (+.117981)
! Initial temperature 296.35

NODE=1 !SUPPLY
  VOLUME=189.59422E-6
  HEAT TRANSFER=COMBINED
NODE=2 !RECEIVER
  VOLUME = 657.787981E-6
  HEAT TRANSFER=COMBINED
PATH=1 !ISENTROPIC ORIFICE
  TYPE=ISENTROPIC
  UPSTREAM NODE=1
  DOWNSTREAM NODE=3
  DIAMETER=5.08E-4 !0.02 INCH DIA
  LENGTH=.0001
PATH=2 !NPT ADAPTOR
  TYPE=TUBE
  UPSTREAM NODE=3
  DOWNSTREAM NODE=4
  DIAMETER=1.5875E-2  !0.625 INCH DIA
  LENGTH=9.525E-3     !0.375 INCH LENGTH
  HEAT TRANSFER=DITTUS_BOELTER
PATH=3 !THIN WALL PORT CONNECTOR
  TYPE=TUBE
  UPSTREAM NODE=4
  DOWNSTREAM NODE=5
  DIAMETER=7.63E-3   !0.300 INCH DIA
  LENGTH=2.667E-2     !1.05 INCH LENGTH
  HEAT TRANSFER=DITTUS_BOELTER
PATH=4 !ADAPTORS VALVE & INTERNALS
  TYPE=TUBE
  UPSTREAM NODE=5
  DOWNSTREAM NODE=6
  DIAMETER=6.35E-3   !.25 INCH DIA
  LENGTH=5.900E-2    !2.323 INCH LENGTH
  HEAT TRANSFER=DITTUS_BOELTER
PATH=5 !BALL VALVE
  TYPE=TUBE
  UPSTREAM NODE=6
  DOWNSTREAM NODE=7
  DIAMETER=4.7499E-3   !.187 INCH DIA
  LENGTH=1.27E-2       !.500 INCH LENGTH
  TOPEN=0.0
  DTOPEN=.001
  HEAT TRANSFER=DITTUS_BOELTER
PATH=6 !ADAPTORS VALVE & INTERNALS
  UPSTREAM NODE=7
  DOWNSTREAM NODE=8
```

```
  DIAMETER=6.35E-3 !0.25 INCH DIA
  LENGTH=6.223E-2  !2.45 INCH LENGTH
  HEAT TRANSFER=DITTUS_BOELTER
PATH=7 !THIN WALL PORT
  UPSTREAM NODE=8
  DOWNSTREAM NODE=9
  DIAMETER=7.62E-3 !0.3 INCH DIA
  LENGTH=2.667E-2  !1.05 INCH LENGTH
  HEAT TRANSFER=DITTUS_BOELTER
PATH=8 !ADAPTOR
  UPSTREAM NODE=9
  DOWNSTREAM NODE=10
  DIAMETER=1.5875E-2 !0.625 INCH DIA
  LENGTH=1.4275E-2  !0.562 INCH LENGTH
  HEAT TRANSFER=DITTUS_BOELTER
PIPE=1 !INTEGRAL TUBE
  NUMP=2
  UPSTREAM NODE=10
  DOWNSTREAM NODE=2
  DIAMETER=2.54E-3 !0.100 INCH DIA
  LENGTH=3.4925E-2 !1.375 INCH LENGTH
  HEAT TRANSFER=DITTUS_BOELTER
SPECIES=1
  MIXTURE=ABELNOBLE
  NAMES=HE4
REGION=1
  LOCATIONS=1,3:6
  TEMPERATURE=296.35
  TWALL=296.35
  PRESSURE=2.078752E+07
  CONCENTRATIONS=1.0
REGION=2
  LOCATIONS=7:10,11,2
  TEMPERATURE=296.35
  TWALL=296.35
  PRESSURE=9.997315E+04
  CONCENTRATIONS=1.0
MODEL=DASKR
  DATA DUMP=NO
  SOLVE_ENERGY=YES
  INITIAL TIME STEP = .000000001
  PRINT INTERVAL = .001
  TMAX = 30.0
  DTMAX=.001
  S_ATOL=1.0E-5
  S_RTOL=1.0E-5
  M_ATOL=1.0E-5
  M_RTOL=1.0E-5
  E_ATOL=1.0E-5
  E_RTOL=1.0E-5
OUTPUT=1
  NUMBER=1
  TYPE=NODE
  PROPERTY=PRESSURE
OUTPUT=2
  NUMBER=1
  TYPE=NODE
```

```
  PROPERTY=TEMPERATURE
OUTPUT=3
  NUMBER=2
  TYPE=NODE
  PROPERTY=PRESSURE
OUTPUT=4
  NUMBER=2
  TYPE=NODE
  PROPERTY=TEMPERATURE
OUTPUT=5 ! ORIFICE MACH NUMBER
  NUMBER=1
  TYPE=PATH
  PROPERTY=MACH NUMBER
OUTPUT=6 ! ORIFICE MDOT
  NUMBER=1
  TYPE=PATH
  PROPERTY=MDOT
OUTPUT=7 ! RECEIVER INLET MACH NUMBER
  NUMBER=10
  TYPE=PATH
  PROPERTY=MACH NUMBER
OUTPUT=8 ! RECEIVER INLET MDOT
  NUMBER=10
  TYPE=PATH
  PROPERTY=MDOT
OUTPUT=9 ! SUPPLY NUSSELT NUMBER
  NUMBER=1
  TYPE=NODE
  PROPERTY=NUSSELT NUMBER
OUTPUT=10 ! RECEIVER NUSSELT NUMBER
  NUMBER=2
  TYPE=NODE
  PROPERTY=NUSSELT NUMBER
OUTPUT=11 ! SUPPLY HDATA
  NUMBER=1
  TYPE=NODE
  PROPERTY=HDATA
OUTPUT=12 ! RECEIVER HDATA
  NUMBER=2
  TYPE=NODE
  PROPERTY=HDATA
OUTPUT=13 ! SUPPLY MASS
  NUMBER=1
  TYPE=NODE
  PROPERTY=MASS
OUTPUT=14 ! RECEIVER MASS
  NUMBER=2
  TYPE=NODE
  PROPERTY=MASS
```

APPENDIX C

```
! 08_06_09_200-700_6000psi
! Netflow stand alone simulation of GTS Test
! Initial supply pressure=4.150609E+07 Pa
! Initial receiver pressure=9.652580E+04 Pa
! Effective supply volume=190.53 cc
! Effective receiver volume=657.67 cc
! Initial temperature 296.15

NODE=1 !SUPPLY
  VOLUME=190.53E-6
  HEAT TRANSFER=COMBINED
NODE=2 !RECEIVER
  VOLUME = 657.67E-6
  HEAT TRANSFER=COMBINED
PATH=1 !ISENTROPIC ORIFICE
  TYPE=ISENTROPIC
  UPSTREAM NODE=1
  DOWNSTREAM NODE=3
  DIAMETER=5.08E-4 !0.02 INCH DIA
  LENGTH=.0001
PATH=2 !NPT ADAPTOR
  TYPE=TUBE
  UPSTREAM NODE=3
  DOWNSTREAM NODE=4
  DIAMETER=1.5875E-2  !0.625 INCH DIA
  LENGTH=9.525E-3     !0.375 INCH LENGTH
PATH=3 !THICK WALL PORT CONNECTOR
  TYPE=TUBE
  UPSTREAM NODE=4
  DOWNSTREAM NODE=5
  DIAMETER=6.35E-3   !0.250 INCH DIA
  LENGTH=2.667E-2     !1.05 INCH LENGTH
PATH=4 !ADAPTORS VALVE & INTERNALS
  TYPE=TUBE
  UPSTREAM NODE=5
  DOWNSTREAM NODE=6
  DIAMETER=6.35E-3   !.25 INCH DIA
  LENGTH=5.900E-2    !2.323 INCH LENGTH
PATH=5 !BALL VALVE
  TYPE=TUBE
  UPSTREAM NODE=6
  DOWNSTREAM NODE=7
  DIAMETER=4.7499E-3   !.187 INCH DIA
  LENGTH=1.27E-2       !.500 INCH LENGTH
  TOPEN=0.0
  DTOPEN=.001
PATH=6 !ADAPTORS VALVE & INTERNALS
  UPSTREAM NODE=7
  DOWNSTREAM NODE=8
  DIAMETER=6.35E-3 !0.25 INCH DIA
  LENGTH=6.223E-2  !2.45 INCH LENGTH
PATH=7 !THIN WALL PORT
  UPSTREAM NODE=8
```

```
  DOWNSTREAM NODE=9
  DIAMETER=7.62E-3 !0.3 INCH DIA
  LENGTH=2.667E-2  !1.05 INCH LENGTH
PATH=8 !ADAPTOR
  UPSTREAM NODE=9
  DOWNSTREAM NODE=10
  DIAMETER=1.5875E-2 !0.625 INCH DIA
  LENGTH=1.4275E-2  !0.562 INCH LENGTH
PIPE=1 !INTEGRAL TUBE
  NUMP=2
  UPSTREAM NODE=10
  DOWNSTREAM NODE=2
  DIAMETER=2.54E-3 !0.100 INCH DIA
  LENGTH=3.4925E-2 !1.375 INCH LENGTH
SPECIES=1
  MIXTURE=ABELNOBLE
  NAMES=HE4
REGION=1
  LOCATIONS=1,3:6
  TEMPERATURE=296.15
  TWALL=296.15
  PRESSURE=4.150609E+07
  CONCENTRATIONS=1.0
REGION=2
  LOCATIONS=7:10,11,2
  TEMPERATURE=296.15
  TWALL=296.15
  PRESSURE=9.652580E+04
  CONCENTRATIONS=1.0
MODEL=DASKR
  DATA DUMP=NO
  SOLVE_ENERGY=YES
  INITIAL TIME STEP = .000000001
  PRINT INTERVAL = .001
  TMAX = 30.
  DTMAX=.001
  S_ATOL=1.0E-5
  S_RTOL=1.0E-5
  M_ATOL=1.0E-5
  M_RTOL=1.0E-5
  E_ATOL=1.0E-5
  E_RTOL=1.0E-5
OUTPUT=1
  NUMBER=1
  TYPE=NODE
  PROPERTY=PRESSURE
OUTPUT=2
  NUMBER=1
  TYPE=NODE
  PROPERTY=TEMPERATURE
OUTPUT=3
  NUMBER=2
  TYPE=NODE
  PROPERTY=PRESSURE
OUTPUT=4
  NUMBER=2
  TYPE=NODE
```

```
  PROPERTY=TEMPERATURE
OUTPUT=5 ! ORIFICE MACH NUMBER
  NUMBER=1
  TYPE=PATH
  PROPERTY=MACH NUMBER
OUTPUT=6 ! ORIFICE MDOT
  NUMBER=1
  TYPE=PATH
  PROPERTY=MDOT
OUTPUT=7 ! RECEIVER INLET MACH NUMBER
  NUMBER=10
  TYPE=PATH
  PROPERTY=MACH NUMBER
OUTPUT=8 ! RECEIVER INLET MDOT
  NUMBER=10
  TYPE=PATH
  PROPERTY=MDOT
OUTPUT=9 ! SUPPLY NUSSELT NUMBER
  NUMBER=1
  TYPE=NODE
  PROPERTY=NUSSELT NUMBER
OUTPUT=10 ! RECEIVER NUSSELT NUMBER
  NUMBER=2
  TYPE=NODE
  PROPERTY=NUSSELT NUMBER
```

APPENDIX D

```
! 08_24_09_200-90_3000psi
! Netflow stand alone simulation of GTS Test
! Initial supply pressure=2.082199E+07 Pa
! Initial receiver pressure=9.997315E+04 Pa
! Effective supply volume=189.71 cc
! Effective receiver volume=83.17 cc
! Initial temperature 298.15

NODE=1 !SUPPLY
  VOLUME=189.71E-6
  HEAT TRANSFER=COMBINED
NODE=2 !RECEIVER
  VOLUME = 83.17E-6
  HEAT TRANSFER=COMBINED
PATH=1 !ISENTROPIC ORIFICE
  TYPE=ISENTROPIC
  UPSTREAM NODE=1
  DOWNSTREAM NODE=3
  DIAMETER=5.08E-4 !0.02 INCH DIA
  LENGTH=.0001
PATH=2 !NPT ADAPTOR
  TYPE=TUBE
  UPSTREAM NODE=3
  DOWNSTREAM NODE=4
  DIAMETER=1.5875E-2  !0.625 INCH DIA
  LENGTH=9.525E-3     !0.375 INCH LENGTH
PATH=3 !THIN WALL PORT CONNECTOR
  TYPE=TUBE
  UPSTREAM NODE=4
  DOWNSTREAM NODE=5
  DIAMETER=7.63E-3   !0.300 INCH DIA
  LENGTH=2.667E-2     !1.05 INCH LENGTH
PATH=4 !ADAPTORS VALVE & INTERNALS
  TYPE=TUBE
  UPSTREAM NODE=5
  DOWNSTREAM NODE=6
  DIAMETER=6.35E-3   !.25 INCH DIA
  LENGTH=5.900E-2    !2.323 INCH LENGTH
PATH=5 !BALL VALVE
  TYPE=TUBE
  UPSTREAM NODE=6
  DOWNSTREAM NODE=7
  DIAMETER=4.7499E-3   !.187 INCH DIA
  LENGTH=1.27E-2       !.500 INCH LENGTH
  TOPEN=0.0
  DTOPEN=.001
PATH=6 !ADAPTORS VALVE & INTERNALS
  UPSTREAM NODE=7
  DOWNSTREAM NODE=8
  DIAMETER=6.35E-3 !0.25 INCH DIA
  LENGTH=6.223E-2  !2.45 INCH LENGTH
PATH=7 !THICK WALL PORT
  UPSTREAM NODE=8
```

```
  DOWNSTREAM NODE=9
  DIAMETER=6.35E-3 !0.25 INCH DIA
  LENGTH=2.667E-2  !1.05 INCH LENGTH
PATH=8 !ADAPTOR
  UPSTREAM NODE=9
  DOWNSTREAM NODE=10
  DIAMETER=1.5875E-2 !0.625 INCH DIA
  LENGTH=1.4275E-2  !0.562 INCH LENGTH
PIPE=1 !INTEGRAL TUBE
  NUMP=2
  UPSTREAM NODE=10
  DOWNSTREAM NODE=2
  DIAMETER=2.54E-3 !0.100 INCH DIA
  LENGTH=2.4765E-2 !.975 INCH LENGTH
SPECIES=1
  MIXTURE=ABELNOBLE
  NAMES=HE4
REGION=1
  LOCATIONS=1,3:6
  TEMPERATURE=298.15
  TWALL=298.15
  PRESSURE=2.082199E+07
  CONCENTRATIONS=1.0
REGION=2
  LOCATIONS=7:10,11,2
  TEMPERATURE=298.15
  TWALL=298.15
  PRESSURE=9.997315E+04
  CONCENTRATIONS=1.0
MODEL=DASKR
  DATA DUMP=NO
  SOLVE_ENERGY=YES
  INITIAL TIME STEP = .000000001
  PRINT INTERVAL = .001
  TMAX = 30.
  DTMAX=.001
  S_ATOL=1.0E-5
  S_RTOL=1.0E-5
  M_ATOL=1.0E-5
  M_RTOL=1.0E-5
  E_ATOL=1.0E-5
  E_RTOL=1.0E-5
OUTPUT=1
  NUMBER=1
  TYPE=NODE
  PROPERTY=PRESSURE
OUTPUT=2
  NUMBER=1
  TYPE=NODE
  PROPERTY=TEMPERATURE
OUTPUT=3
  NUMBER=2
  TYPE=NODE
  PROPERTY=PRESSURE
OUTPUT=4
  NUMBER=2
  TYPE=NODE
```

```
  PROPERTY=TEMPERATURE
OUTPUT=5 ! ORIFICE MACH NUMBER
  NUMBER=1
  TYPE=PATH
  PROPERTY=MACH NUMBER
OUTPUT=6 ! ORIFICE MDOT
  NUMBER=1
  TYPE=PATH
  PROPERTY=MDOT
OUTPUT=7 ! RECEIVER INLET MACH NUMBER
  NUMBER=10
  TYPE=PATH
  PROPERTY=MACH NUMBER
OUTPUT=8 ! SUPPLY NUSSELT NUMBER
  NUMBER=1
  TYPE=NODE
  PROPERTY=NUSSELT NUMBER
OUTPUT=9 ! RECEIVER NUSSELT NUMBER
  NUMBER=2
  TYPE=NODE
  PROPERTY=NUSSELT NUMBER
```

APPENDIX E

```
! 08_16_09_200-90_6000psi
! Netflow stand alone simulation of GTS Test
! Initial supply pressure=4.150609E+07 Pa
! Initial receiver pressure=1.013521E5 Pa
! Effective supply volume=190.53 cc
! Effective receiver volume=83.01 cc
! Initial temperature 298.15

NODE=1 !SUPPLY
  VOLUME=190.53E-6
  HEAT TRANSFER=COMBINED
NODE=2 !RECEIVER
  VOLUME = 83.01E-6
  HEAT TRANSFER=COMBINED
PATH=1 !ISENTROPIC ORIFICE
  TYPE=ISENTROPIC
  UPSTREAM NODE=1
  DOWNSTREAM NODE=3
  DIAMETER=5.08E-4 !0.02 INCH DIA
  LENGTH=.0001
PATH=2 !NPT ADAPTOR
  TYPE=TUBE
  UPSTREAM NODE=3
  DOWNSTREAM NODE=4
  DIAMETER=1.5875E-2  !0.625 INCH DIA
  LENGTH=9.525E-3     !0.375 INCH LENGTH
PATH=3 !THIN WALL PORT CONNECTOR
  TYPE=TUBE
  UPSTREAM NODE=4
  DOWNSTREAM NODE=5
  DIAMETER=7.63E-3   !0.300 INCH DIA
  LENGTH=2.667E-2     !1.05 INCH LENGTH
PATH=4 !ADAPTORS VALVE & INTERNALS
  TYPE=TUBE
  UPSTREAM NODE=5
  DOWNSTREAM NODE=6
  DIAMETER=6.35E-3   !.25 INCH DIA
  LENGTH=5.900E-2    !2.323 INCH LENGTH
PATH=5 !BALL VALVE
  TYPE=TUBE
  UPSTREAM NODE=6
  DOWNSTREAM NODE=7
  DIAMETER=4.7499E-3   !.187 INCH DIA
  LENGTH=1.27E-2       !.500 INCH LENGTH
  TOPEN=0.0
  DTOPEN=.001
PATH=6 !ADAPTORS VALVE & INTERNALS
  UPSTREAM NODE=7
  DOWNSTREAM NODE=8
  DIAMETER=6.35E-3 !0.25 INCH DIA
  LENGTH=6.223E-2  !2.45 INCH LENGTH
PATH=7 !THICK WALL PORT
  UPSTREAM NODE=8
```

```
  DOWNSTREAM NODE=9
  DIAMETER=6.35E-3 !0.25 INCH DIA
  LENGTH=2.667E-2  !1.05 INCH LENGTH
PATH=8 !ADAPTOR
  UPSTREAM NODE=9
  DOWNSTREAM NODE=10
  DIAMETER=1.5875E-2 !0.625 INCH DIA
  LENGTH=1.4275E-2  !0.562 INCH LENGTH
PIPE=1 !INTEGRAL TUBE
  NUMP=2
  UPSTREAM NODE=10
  DOWNSTREAM NODE=2
  DIAMETER=2.54E-3 !0.100 INCH DIA
  LENGTH=2.4765E-2 !.975 INCH LENGTH
SPECIES=1
  MIXTURE=ABELNOBLE
  NAMES=HE4
REGION=1
  LOCATIONS=1,3:6
  TEMPERATURE=298.15
  TWALL=298.15
  PRESSURE=4.150609E+07
  CONCENTRATIONS=1.0
REGION=2
  LOCATIONS=7:10,11,2
  TEMPERATURE=298.15
  TWALL=298.15
  PRESSURE=1.013521E5
  CONCENTRATIONS=1.0
MODEL=DASKR
  DATA DUMP=NO
  SOLVE_ENERGY=YES
  INITIAL TIME STEP = .000000001
  PRINT INTERVAL = .001
  TMAX = 30.
  DTMAX=.001
  S_ATOL=1.0E-5
  S_RTOL=1.0E-5
  M_ATOL=1.0E-5
  M_RTOL=1.0E-5
  E_ATOL=1.0E-5
  E_RTOL=1.0E-5
OUTPUT=1
  NUMBER=1
  TYPE=NODE
  PROPERTY=PRESSURE
OUTPUT=2
  NUMBER=1
  TYPE=NODE
  PROPERTY=TEMPERATURE
OUTPUT=3
  NUMBER=2
  TYPE=NODE
  PROPERTY=PRESSURE
OUTPUT=4
  NUMBER=2
  TYPE=NODE
```

```
  PROPERTY=TEMPERATURE
OUTPUT=5 ! ORIFICE MACH NUMBER
  NUMBER=1
  TYPE=PATH
  PROPERTY=MACH NUMBER
OUTPUT=6 ! ORIFICE MDOT
  NUMBER=1
  TYPE=PATH
  PROPERTY=MDOT
OUTPUT=7 ! RECEIVER INLET MACH NUMBER
  NUMBER=10
  TYPE=PATH
  PROPERTY=MACH NUMBER
OUTPUT=8 ! RECEIVER INLET MDOT
  NUMBER=10
  TYPE=PATH
  PROPERTY=MDOT
OUTPUT=9 ! SUPPLY NUSSELT NUMBER
  NUMBER=1
  TYPE=NODE
  PROPERTY=NUSSELT NUMBER
OUTPUT=10 ! RECEIVER NUSSELT NUMBER
  NUMBER=2
  TYPE=NODE
  PROPERTY=NUSSELT NUMBER
```

APPENDIX F

```
! 10_22_07_200-13k_300psi
! Netflow stand alone simulation of GTS Test
! Initial supply pressure= 2.517255E+06 Pa
! Initial receiver pressure=1.399038E+06 Pa
! Effective supply volume=189.87 cc
! Effective receiver volume=12908.58 cc
! Initial temperature 295.

NODE=1 !SUPPLY
  VOLUME=189.87E-6
  HEAT TRANSFER=COMBINED
NODE=2 !RECEIVER
  VOLUME = 12908.58E-6
  HEAT TRANSFER=COMBINED
PATH=1 !ISENTROPIC ORIFICE
  TYPE=ISENTROPIC
  UPSTREAM NODE=1
  DOWNSTREAM NODE=3
  DIAMETER=5.08E-4 !0.02 INCH DIA
  LENGTH=.0001
PATH=2 !SUPPLY TUBE
  TYPE=TUBE
  UPSTREAM NODE=3
  DOWNSTREAM NODE=4
  DIAMETER=1.5875E-2  !0..25 INCH DIA
  LENGTH=9.525E-3     !2.25 INCH LENGTH
PATH=3 !1/4" BALL VALVE
  TYPE=TUBE
  UPSTREAM NODE=4
  DOWNSTREAM NODE=5
  DIAMETER=6.35E-3   !.25 INCH DIA
  LENGTH=3.81E-2       !1.5 INCH LENGTH
  TOPEN=0.0
  DTOPEN=.001
PATH=4 !RECEIVER TUBE
  UPSTREAM NODE=5
  DOWNSTREAM NODE=6
  DIAMETER=6.35E-3 !0.25 INCH DIA
  LENGTH=6.35E-2   !2.5 INCH LENGTH
PIPE=1 !INTEGRAL TUBE
  NUMP=2
  UPSTREAM NODE=6
  DOWNSTREAM NODE=2
  DIAMETER=9.525E-3 !0.375 INCH DIA
  LENGTH=5.08E-2    !2.0 INCH LENGTH
SPECIES=1
  MIXTURE=ABELNOBLE
  NAMES=HE4
REGION=1
  LOCATIONS=1,3:4
  TEMPERATURE=295.
  TWALL=295.
  PRESSURE=2.517255E+06
```

```
  CONCENTRATIONS=1.0
REGION=2
  LOCATIONS=5:6,7,2
  TEMPERATURE=295.
  TWALL=295.
  PRESSURE=1.399038E+06
  CONCENTRATIONS=1.0
MODEL=DASKR
  DATA DUMP=NO
  SOLVE_ENERGY=YES
  INITIAL TIME STEP = .000000001
  PRINT INTERVAL = .001
  TMAX = 30.
  DTMAX=.001
  S_ATOL=0.0E-6
  S_RTOL=1.0E-6
  M_ATOL=0.0E-6
  M_RTOL=1.0E-6
  E_ATOL=0.0E-6
  E_RTOL=1.0E-6
OUTPUT=1
  NUMBER=1
  TYPE=NODE
  PROPERTY=PRESSURE
OUTPUT=2
  NUMBER=1
  TYPE=NODE
  PROPERTY=TEMPERATURE
OUTPUT=3
  NUMBER=2
  TYPE=NODE
  PROPERTY=PRESSURE
OUTPUT=4
  NUMBER=2
  TYPE=NODE
  PROPERTY=TEMPERATURE
OUTPUT=5 ! ORIFICE MACH NUMBER
  NUMBER=1
  TYPE=PATH
  PROPERTY=MACH NUMBER
OUTPUT=6 ! ORIFICE MDOT
  NUMBER=1
  TYPE=PATH
  PROPERTY=MDOT
OUTPUT=7 ! RECEIVER INLET MACH NUMBER
  NUMBER=6
  TYPE=PATH
  PROPERTY=MACH NUMBER
OUTPUT=8 ! SUPPLY NUSSELT NUMBER
  NUMBER=1
  TYPE=NODE
  PROPERTY=NUSSELT NUMBER
OUTPUT=9 ! RECEIVER NUSSELT NUMBER
  NUMBER=2
  TYPE=NODE
  PROPERTY=NUSSELT NUMBER
```

APPENDIX G

```
! 09_07_07_200-13k_6000psi
! Netflow stand alone simulation of GTS Test
! Initial supply pressure= 4.136820E+07 Pa
! Initial receiver pressure=6.894700E+2 Pa
! Effective supply volume=190.55 cc
! Effective receiver volume=12908.58 cc
! Initial supply temperature 303.15
! Initial receiver temperature 296.15
! Initial conditions altered slightly from the test to enable starting.

NODE=1 !SUPPLY
  VOLUME=190.55E-6
  HEAT TRANSFER=CONSTANT
NODE=2 !RECEIVER
  VOLUME = 12908.58E-6
  HEAT TRANSFER=CONSTANT
PATH=1 !ISENTROPIC ORIFICE
  TYPE=ISENTROPIC
  UPSTREAM NODE=1
  DOWNSTREAM NODE=3
  DIAMETER=5.08E-4 !0.02 INCH DIA
  LENGTH=.0001
PATH=2 !SUPPLY TUBE
  TYPE=TUBE
  UPSTREAM NODE=3
  DOWNSTREAM NODE=4
  DIAMETER=1.5875E-2  !0..25 INCH DIA
  LENGTH=9.525E-3     !2.25 INCH LENGTH
PATH=3 !1/4" BALL VALVE
  TYPE=TUBE
  UPSTREAM NODE=4
  DOWNSTREAM NODE=5
  DIAMETER=6.35E-3   !.25 INCH DIA
  LENGTH=3.81E-2       !1.5 INCH LENGTH
!  TOPEN=0.0
!  DTOPEN=.001
PATH=4 !RECEIVER TUBE
  UPSTREAM NODE=5
  DOWNSTREAM NODE=6
  DIAMETER=6.35E-3 !0.25 INCH DIA
  LENGTH=6.35E-2   !2.5 INCH LENGTH
PIPE=1 !INTEGRAL TUBE
  NUMP=2
  UPSTREAM NODE=6
  DOWNSTREAM NODE=2
  DIAMETER=9.525E-3 !0.375 INCH DIA
  LENGTH=5.08E-2    !2.0 INCH LENGTH
SPECIES=1
  MIXTURE=ABELNOBLE
  NAMES=HE4
REGION=1
!  LOCATIONS=1,3:4
  LOCATIONS=1
```

```
  TEMPERATURE=303.15
  TWALL=303.15
  PRESSURE=4.136820E+07
  CONCENTRATIONS=1.0
REGION=2
!  LOCATIONS=5:6,7,2
  LOCATIONS=3:6,7,2
  TEMPERATURE=296.15
  TWALL=296.15
!  PRESSURE=6.894700E+3
  PRESSURE=4.0E+3
  CONCENTRATIONS=1.0
MODEL=DASKR
  DATA DUMP=NO
  SOLVE_ENERGY=YES
  INITIAL TIME STEP = .000000001
  PRINT INTERVAL = .001
  TMAX = 30.
  DTMAX=.001
  S_ATOL=0.0E-6
  S_RTOL=1.0E-6
  M_ATOL=0.0E-6
  M_RTOL=1.0E-6
  E_ATOL=0.0E-6
  E_RTOL=1.0E-6
OUTPUT=1
  NUMBER=1
  TYPE=NODE
  PROPERTY=PRESSURE
OUTPUT=2
  NUMBER=1
  TYPE=NODE
  PROPERTY=TEMPERATURE
OUTPUT=3
  NUMBER=2
  TYPE=NODE
  PROPERTY=PRESSURE
OUTPUT=4
  NUMBER=2
  TYPE=NODE
  PROPERTY=TEMPERATURE
OUTPUT=5 ! ORIFICE MACH NUMBER
  NUMBER=1
  TYPE=PATH
  PROPERTY=MACH NUMBER
OUTPUT=6 ! ORIFICE MDOT
  NUMBER=1
  TYPE=PATH
  PROPERTY=MDOT
OUTPUT=7 ! RECEIVER INLET MACH NUMBER
  NUMBER=6
  TYPE=PATH
  PROPERTY=MACH NUMBER
OUTPUT=8 ! SUPPLY NUSSELT NUMBER
  NUMBER=1
  TYPE=NODE
  PROPERTY=NUSSELT NUMBER
```

```
OUTPUT=9 ! RECEIVER NUSSELT NUMBER
  NUMBER=2
  TYPE=NODE
  PROPERTY=NUSSELT NUMBER
```

APPENDIX H

FUEGO Input File:

```
BEGIN SIERRA FUEGO

# FUEGO supply calculation using ideal gas helium via CANTERA.
# 300 psi.

  TITLE Coupled FUEGO/NETFLOW simulation: supply>network-and-receiver

  RESTART = auto

$=====================================================================
$
$  Assign material properties to element blocks here.
$
$=====================================================================

  BEGIN FINITE ELEMENT MODEL coupling

#    Database Name = mesh300-s1_mod.g

    Database Name = MESH-128/mesh300-s1_mod.par

    Database Type = EXODUSII

    BEGIN PARAMETERS FOR BLOCK block_1

      MATERIAL HE

    END   PARAMETERS FOR BLOCK block_1

  END FINITE ELEMENT MODEL coupling

$=====================================================================
$
$  Define a material property set here.
$
$=====================================================================

  BEGIN PROPERTY SPECIFICATION FOR FUEGO MATERIAL HE

    CANTERA XML FILE = He.xml

    DATUM PRESSURE             = 0.0
    REFERENCE PRESSURE         = 1.0    $ (in atm); set to 0.0 for the
compressible flow option.
    REFERENCE TEMPERATURE      = 293.05  $ Kelvin
    REFERENCE MASS_FRACTION HE = 1.0

  END PROPERTY SPECIFICATION FOR FUEGO MATERIAL HE
```

```
$=====================================================================
$
$  Define the global constants here
$
$=====================================================================

  BEGIN GLOBAL CONSTANTS const

    Ideal Gas Constant = 8.3134e7  $ units of ergs/mole-K

    GRAVITY VECTOR = 0.0, -980.0, 0.0  $ units of cm/s^2

  END GLOBAL CONSTANTS const

  BEGIN GLOBAL CONSTANTS turb

    K-E TURBULENCE MODEL PARAMETER ALPHA =      0.5555555
    K-E TURBULENCE MODEL PARAMETER SIGMA_K =    2.0
    K-E TURBULENCE MODEL PARAMETER SIGMA_W =    2.0
    K-E TURBULENCE MODEL PARAMETER BETA =       0.075
    K-E TURBULENCE MODEL PARAMETER BETA_P =     0.09
    K-E TURBULENCE MODEL PARAMETER AMU =        0.31
    K-E TURBULENCE MODEL PARAMETER ALPHA_KE =   0.44
    K-E TURBULENCE MODEL PARAMETER SIGMA_K_KE = 1.0
    K-E TURBULENCE MODEL PARAMETER SIGMA_W_KE = 1.168
    K-E TURBULENCE MODEL PARAMETER BETA_KE =    0.0828

    TURBULENCE MODEL PRANDTL NUMBER = 0.9

  END GLOBAL CONSTANTS turb

$=====================================================================
$
$  Define the linear solver parameters here.
$
$=====================================================================

  BEGIN aztec EQUATION SOLVER continuity

    SOLUTION METHOD = gmres
    PRECONDITIONING METHOD = dd-ilut
    PRECONDITIONING STEPS = 1
    RESTART ITERATIONS = 100
    MAXIMUM ITERATIONS = 250
    RESIDUAL NORM SCALING  = R0
    RESIDUAL NORM TOLERANCE = 1.0e-8
    Param-Real AZ_ilut_fill value 3.0

  END aztec EQUATION SOLVER continuity

  BEGIN aztec EQUATION SOLVER scalar

    SOLUTION METHOD = gmres
    PRECONDITIONING METHOD = dd-ilut
    PRECONDITIONING STEPS = 1
    RESTART ITERATIONS = 50
    MAXIMUM ITERATIONS = 50
```

```
    RESIDUAL NORM SCALING  = R0
    RESIDUAL NORM TOLERANCE = 1.0e-8
    BC ENFORCEMENT = EXACT
    Param-Real AZ_ilut_fill value 3.0

  END aztec EQUATION SOLVER scalar

$=====================================================================
$
$  Begin the Fuego procedure (integration of equations).
$
$=====================================================================

  BEGIN FUEGO PROCEDURE fuego_procedure

$=====================================================================
$
$  Define the parameters for time integration over an interval here
$  as done through solver controls.
$
$=====================================================================

   begin solution control description

      use system main

      begin system main

         begin transient mytransient

            advance supply_region

         end transient mytransient

      end system main

      begin parameters for transient mytransient

         start time = 0.0
         initial deltat = 1E-7
         termination time = 10.0

         begin parameters for fuego region supply_region

            transient step type is automatic
            cfl limit               = 50.
            maximum time step       = 1.0e-4
            time step change factor = 1.2

         end   parameters for fuego region supply_region

      end parameters for transient mytransient

   end solution control description

$=====================================================================
$
```

```
$  Begin the Fuego region (evauation of equations within a time step).
$
$=====================================================================

    BEGIN FUEGO REGION supply_region

$=====================================================================
$
$  Select the math model configuration for this run.
$
$=====================================================================

      BEGIN SOLUTION OPTIONS

        # turn on equations as needed

        ACTIVATE EQUATION Continuity
        ACTIVATE EQUATION X_Momentum
        ACTIVATE EQUATION Y_Momentum
        ACTIVATE EQUATION Z_Momentum
        ACTIVATE EQUATION Enthalpy

        ACTIVATE ACOUSTIC COMPRESSIBILITY ALGORITHM

        PROJECTION METHOD = fourth_order SMOOTHING WITH timestep
SCALING

        # specify the nonlinear iterations for the system

        MINIMUM NUMBER OF NONLINEAR ITERATIONS = 1
        MAXIMUM NUMBER OF NONLINEAR ITERATIONS = 6

        # attach solvers to the equations

        USE EQUATION SOLVER continuity FOR EQUATION Continuity
        USE EQUATION SOLVER scalar     FOR EQUATION X_Momentum
        USE EQUATION SOLVER scalar     FOR EQUATION Y_Momentum
        USE EQUATION SOLVER scalar     FOR EQUATION Z_Momentum
        USE EQUATION SOLVER scalar     FOR EQUATION Enthalpy

        # set upwinding

        UPWIND METHOD IS UPW
        FIRST ORDER UPWIND FACTOR = 1.0

        UPWIND METHOD IS UPW FOR EQUATION X_Momentum
        UPWIND METHOD IS UPW FOR EQUATION Y_Momentum
        UPWIND METHOD IS UPW FOR EQUATION Z_Momentum

        HYBRID UPWIND FACTOR = 1.0
        HYBRID UPWIND FACTOR = 1.0 FOR EQUATION X_Momentum
        HYBRID UPWIND FACTOR = 1.0 FOR EQUATION Y_Momentum
        HYBRID UPWIND FACTOR = 1.0 FOR EQUATION Z_Momentum

        # set under-relaxation

        UNDER RELAX Momentum by 1.0
```

```
        UNDER RELAX pressure by 1.0
        UNDER RELAX enthalpy by 1.0

        BEGIN TURBULENCE MODEL SPECIFICATION

          TURBULENCE MODEL = LAM

        END TURBULENCE MODEL SPECIFICATION

        BEGIN BUOYANCY MODEL SPECIFICATION buoyancy_model

          BUOYANCY REFERENCE TEMPERATURE = 293.05
          buoyancy REFERENCE MASS_FRACTION HE  = 1.0
          BUOYANCY MODEL = BUOYANT

        END BUOYANCY MODEL SPECIFICATION buoyancy_model

      END SOLUTION OPTIONS

      MINIMUM TEMPERATURE ALLOWED FROM TEMPERATURE EXTRACTION = 100.0

$=====================================================================
$
$  Select the mesh, defined at the Domain level.
$
$=====================================================================

      USE FINITE ELEMENT MODEL coupling

$=====================================================================
$
$ Begin the definition of the contents of the plot file for this
region.
$
$=====================================================================

      Begin Results Output Label output

        Database Name = results/coupling.e

        At Step 0, Increment = 200

        TITLE FUEGO Supply - NETFLOW network and receiver

        NODAL Variables = pressure AS pressure
        NODAL Variables = density AS density
        NODAL Variables = x_velocity AS x_vel
        NODAL Variables = y_velocity AS y_vel
        NODAL Variables = z_velocity AS z_vel
        NODAL Variables = temperature AS temperature
        NODAL Variables = heat_flux AS heat_flux
        NODAL Variables = viscosity AS viscosity

      End Results Output Label output

$=====================================================================
$
```

```
$  Begin the definition of the restart file.
$
$=====================================================================

      Begin Restart Data restart

        Input Database Name = restart/coupling.rsin
        Output Database Name = restart/coupling.rsout

        At Step 0, Increment = 200

      End Restart Data restart

$=====================================================================
$
$  Set the initial condition for this region.
$
$=====================================================================

      Begin Initial Condition Block Supply

        volume is block_1

        pressure                =  2.170452e7 $ units of dynes/cm**2
        x_velocity              =   0.0
        y_velocity              =   0.0
        z_velocity              =   0.0
        temperature             = 293.05     $ units of degrees K

      End Initial Condition Block Supply

$=====================================================================
$
$  Define the boundary conditions for this region.
$
$=====================================================================

$ NETFLOW link at supply opening

      BEGIN NETWORK BOUNDARY CONDITION ON SURFACE surface_1

         NETWORK LABEL link1

      END NETWORK BOUNDARY CONDITION ON SURFACE surface_1

$  Supply walls - isothermal

      begin wall boundary condition on surface surface_2

        x_velocity          =   0.0
        y_velocity          =   0.0
        z_velocity          =   0.0
        temperature         = 293.05

      end wall boundary condition on surface surface_2

    END FUEGO REGION supply_region
```

```
  END FUEGO PROCEDURE fuego_procedure

END SIERRA FUEGO
```

NETFLOW Input File:

```
! 04_29_09_200-700_300psi
! Fuego Supply Simulation coupled to Netflow
! Initial supply pressure=2.170452E+06 Pa
! Initial receiver pressure=9.997315E+04 Pa
! Effective supply volume=189.87 cc
! Effective receiver volume=657.67 cc
! Initial temperature 293.05 K

!NODE=1 !SUPPLY
!  VOLUME=189.87E-6
!  HEAT TRANSFER=COMBINED
NODE=2 !RECEIVER
  VOLUME = 657.67E-6
  HEAT TRANSFER=COMBINED
LINK=1
  LOCATION=1
  NAME=link1
PATH=1 !ISENTROPIC ORIFICE
  TYPE=ISENTROPIC
  UPSTREAM NODE=1
  DOWNSTREAM NODE=3
  DIAMETER=5.08E-4 !0.02 INCH DIA
  LENGTH=.0001
PATH=2 !NPT ADAPTOR
  TYPE=TUBE
  UPSTREAM NODE=3
  DOWNSTREAM NODE=4
  DIAMETER=1.5875E-2  !0.625 INCH DIA
  LENGTH=9.525E-3     !0.375 INCH LENGTH
  HEAT TRANSFER=DITTUS_BOELTER
PATH=3 !THIN WALL PORT CONNECTOR
  TYPE=TUBE
  UPSTREAM NODE=4
  DOWNSTREAM NODE=5
  DIAMETER=7.63E-3   !0.300 INCH DIA
  LENGTH=2.667E-2     !1.05 INCH LENGTH
  HEAT TRANSFER=DITTUS_BOELTER
PATH=4 !ADAPTORS VALVE & INTERNALS
  TYPE=TUBE
  UPSTREAM NODE=5
  DOWNSTREAM NODE=6
  DIAMETER=6.35E-3   !.25 INCH DIA
  LENGTH=5.900E-2    !2.323 INCH LENGTH
```

```
  HEAT TRANSFER=DITTUS_BOELTER
PATH=5 !BALL VALVE
  TYPE=TUBE
  UPSTREAM NODE=6
  DOWNSTREAM NODE=7
  DIAMETER=4.7499E-3   !.187 INCH DIA
  LENGTH=1.27E-2       !.500 INCH LENGTH
  TOPEN=0.0
  DTOPEN=.01
  HEAT TRANSFER=DITTUS_BOELTER
PATH=6 !ADAPTORS VALVE & INTERNALS
  UPSTREAM NODE=7
  DOWNSTREAM NODE=8
  DIAMETER=6.35E-3 !0.25 INCH DIA
  LENGTH=6.223E-2  !2.45 INCH LENGTH
  HEAT TRANSFER=DITTUS_BOELTER
PATH=7 !THIN WALL PORT
  UPSTREAM NODE=8
  DOWNSTREAM NODE=9
  DIAMETER=7.62E-3 !0.3 INCH DIA
  LENGTH=2.667E-2  !1.05 INCH LENGTH
  HEAT TRANSFER=DITTUS_BOELTER
PATH=8 !ADAPTOR
  UPSTREAM NODE=9
  DOWNSTREAM NODE=10
  DIAMETER=1.5875E-2 !0.625 INCH DIA
  LENGTH=1.4275E-2  !0.562 INCH LENGTH
  HEAT TRANSFER=DITTUS_BOELTER
PIPE=1 !INTEGRAL TUBE
  NUMP=2
  UPSTREAM NODE=10
  DOWNSTREAM NODE=2
  DIAMETER=2.54E-3 !0.100 INCH DIA
  LENGTH=3.4925E-2 !1.375 INCH LENGTH
  HEAT TRANSFER=DITTUS_BOELTER
SPECIES=1
  MIXTURE=ABELNOBLE
  NAMES=HE4
REGION=1
  LOCATIONS=1,3:6
  TEMPERATURE=293.05
  TWALL=293.05
  PRESSURE=2.170452E+06
  CONCENTRATIONS=1.0
REGION=2
  LOCATIONS=7:11,2
  TEMPERATURE=293.05
  TWALL=293.05
  PRESSURE=9.997315E+04
  CONCENTRATIONS=1.0
MODEL=DASKR
  DATA DUMP=NO
  SOLVE_ENERGY=YES
  INITIAL TIME STEP = .000000001
  PRINT INTERVAL = .001
  TMAX = 30.
  DTMAX=.001
```

```
  S_ATOL=1.0E-5
  S_RTOL=1.0E-5
  M_ATOL=1.0E-5
  M_RTOL=1.0E-5
  E_ATOL=1.0E-5
  E_RTOL=1.0E-5
OUTPUT=1 !LINK NODE PRESSURE
  NUMBER=1
  TYPE=NODE
  PROPERTY=PRESSURE
OUTPUT=2 !LINK NODE TEMPERATURE
  NUMBER=1
  TYPE=NODE
  PROPERTY=TEMPERATURE
OUTPUT=3 !RECEIVER PRESSURE
  NUMBER=2
  TYPE=NODE
  PROPERTY=PRESSURE
OUTPUT=4 !RECEIVER TEMPERATURE
  NUMBER=2
  TYPE=NODE
  PROPERTY=TEMPERATURE
OUTPUT=5 ! ISENTROPIC ORIFICE MACH NUMBER
  NUMBER=1
  TYPE=PATH
  PROPERTY=MACH NUMBER
OUTPUT=6 ! ORIFICE MDOT
  NUMBER=1
  TYPE=PATH
  PROPERTY=MDOT
```

DISTRIBUTION

1	MS9001	C. D. Moen	08005 (electronic)
1	MS9035	P. A. Spence	08224
1	MS9035	C. A. LaJeunesse	08224
1	MS9035	A. H. Leung	08224
1	MS9035	B. E. Oden	08224 (electronic)
1	MS9035	N. J. Paradiso	08224
1	MS9035	S. F. Rice	08224
1	MS9054	R. W. Carling	08300
1	MS9153	M. F. Hardwick	08220 (electronic)
1	MS9154	J. L. Bowie	08237 (electronic)
1	MS9154	R. A. Van Cleave	08237 (electronic)
1	MS9154	J. P. Chan	08244 (electronic)
1	MS9154	C. W. Pretzel	08244 (electronic)
1	MS9161	S. K. Griffiths	08300 (electronic)
1	MS9161	A. E. Pontau	08360 (electronic)
1	MS9161	R. H. Nilson	08365 (electronic)
1	MS9292	M. P. Kanouff	08365 (electronic)
1	MS9409	Ralph Greif	08365
1	MS9409	N. R. Fornaciari	08365 (electronic)
1	MS9409	D. E. Dedrick	08365 (electronic)
1	MS9409	S. C. James	08365 (electronic)
3	MS9409	G. H. Evans	08365
1	MS9409	W. G. Houf	08365 (electronic)
1	MS9409	J. A. Templeton	08365 (electronic)
1	MS9409	G. J. Wagner	08365 (electronic)
3	MS9409	W. S. Winters	08365
1	MS9661	A. D. Shugard	08224
1	MS9661	S. Stieper	08224 (electronic)
1	MS9661	L. Thai	08224 (electronic)
1	MS9661	P. Van Blarigan	08224 (electronic)
1	MS9661	T. G. Felver	08224
1	MS0899	Technical Library	09536 (electronic)